GENERAL ATOMIC™

GA-A13353
UC-77

HTGR FUELS AND CORE DEVELOPMENT PROGRAM

QUARTERLY PROGRESS REPORT FOR THE PERIOD ENDING FEBRUARY 28, 1975

Prepared under
Contract AT(04-3)-167
Project Agreement No. 17
for the
San Francisco Operations Office
U.S. Energy Research and Development Administration

GENERAL ATOMIC PROJECT 0317 DATE PUBLISHED - MARCH 31, 1975

DISCLAIMER

QUARTERLY REPORT SERIES

GA-4072-December, 1962, through February, 1963
GA-4350-March, 1963, through May, 1963
GA-4569-June, 1963, through August, 1963
GA-4937-September, 1963, through November, 1963
GA-5104-December, 1963, through February, 1964
GA-5366-March, 1964, through May, 1964
GA-5618-June, 1964, through August, 1964
GA-5866-September, 1964, through November, 1964
GA-6113-December, 1964, through February, 1965
GA-6418-March, 1965, through May, 1965
GA-6671-June, 1965, through August, 1965
GA-6869-September, 1965, through November, 1965
GA-7010-December, 1965, through February, 1966
GA-7181-March, 1966, through May, 1966
GA-7396-June, 1966, through August, 1966
GA-7553-September, 1966, through November, 1966
GA-7801-December, 1966, through February, 1967
GA-7981-March, 1967, through May, 1967
GA-8200-June, 1967, through August, 1967
GA-8356-September, 1967, through November, 1967
GA-8530-December, 1967, through February, 1968
GA-8662-March, 1968, through May, 1968
GA-8860-June, 1968, through August, 1968
GA-9090-September, 1968, through November, 1968
GA-9227-December, 1968, through February, 1969
GA-9372-March, 1969, through May, 1969
GA-9660-June, 1969, through August, 1969
GA-9815-September, 1969, through November, 1969
GA-9944-December, 1969, through February, 1970
GA-10088-March, 1970, through May, 1970
GA-10288-June, 1970, through August, 1970
GA-10399-September, 1970, through November, 1970
GA-10501-December, 1970, through February, 1971
GA-10661-March, 1971, through May, 1971
Gulf-GA-A10784-June, 1971, through August, 1971
Gulf-GA-A10930-September, 1971, through November, 1971
Gulf-GA-A10999-December, 1971, through February, 1972
Gulf-GA-A12150-March, 1972, through May, 1972
Gulf-GA-A12222-June, 1972, through August, 1972
Gulf-GA-A12422-September, 1972, through November, 1972
Gulf-GA-A12515-December, 1972, through February, 1973
Gulf-GA-12599-March, 1973, through May, 1973
Gulf-GA-A12725-June, 1973, through August, 1973
Gulf-GA-A12818-September, 1973, through November, 1973
GA-A12916-December, 1973, through February, 1974
GA-A13030-March, 1974, through May, 1974
GA-A13126-June, 1974, through August, 1974
GA-A13253-September, 1974, through November, 1974

ABSTRACT

This publication continues the quarterly report series on the HTGR Fuels and Core Development Program. The Program covers items of the base technology of the High-Temperature Gas-Cooled Reactor (HTGR) system. The development of the HTGR system will, in part, meet the greater national objective of more effective and efficient utilization of our national resources. The work reported here includes studies of reactions between core materials and coolant impurities, basic fission product transport mechanisms, core graphite development and testing, the development and testing of recyclable fuel systems, and physics and fuel management studies. Materials studies include irradiation capsule tests of both fuel and graphite. Experimental procedures and results are discussed and, where appropriate, the data are presented in tables, graphs, and photographs. More detailed descriptions of experimental work are presented in topical reports; these are listed at the end of the report.

INTRODUCTION

This report covers the work performed by the General Atomic Company under U.S. Atomic Energy Commission Contract AT(04-3)-167, Project Agreement No. 17. This Project Agreement calls for support of basic technology associated with the fuels and core of the gas-cooled, nuclear power reactor systems. The program is based on the concept of the High-Temperature Gas-Cooled Reactor (HTGR) developed by the General Atomic Company.

Large HTGR systems will be placed in operation starting in the early 1980's following the operation of the 330-MW(e) prototype in 1975. Characteristics of these advanced systems include:

1. A single-phase gas coolant allowing generation of high-temperature, high-pressure steam with consequent high-efficiency energy conversion and low thermal discharge.

2. A prestressed concrete reactor vessel (PCRV) offering advantages in field construction, primary system integrity, and stressed member inspectability.

3. Graphite core material assuring high-temperature structural strength, large temperature safety margins, and good neutron economy.

4. Thorium fuel cycle leading to U-233 fuel which allows good utilization of nuclear resources and minimum demands on separative work.

CONTENTS

FIGURES

TABLES

TASK 4 (189a 13114)

FISSION PRODUCT MECHANISMS

FISSION GAS RELEASE STUDIES

Fission gas release (Kr-85m R/B) data have been measured for (1) intact and failed TRISO coated particles with weak-acid-resin (WAR) UC_2 kernels, (2) intact and failed TRISO coated particles with melted UC_2 (VSM) kernels, and (3) intact and failed BISO coated particles with VSM kernels. The failed particles were made by laser-drilling pinholes into the coatings of otherwise intact particles. Both unirradiated and irradiated (up to 58% burnup) particles were tested. The main purpose of this work was to provide R/B data as a function of burnup for failed reference UC_2 VSM particles and alternate reference UC_2 WAR particles.

Fission gas release (R/B) data are important for use in calculating the inventory of fission product gaseous (krypton and xenon) nuclides in the primary coolant of HTGR systems. An important input parameter in the calculation is the core average R/B,* which is derived as follows:

$$\overline{R/B} = (1 - F)\ (R/B)_{ii} + F(R/B)_{if} \quad ,$$

where $\overline{R/B}$ = core average R/B,

F = fraction of fissions that occurs in fuel particles with failed coatings,

$(R/B)_{ii}$ = R/B for the i^{th} nuclide for coated fuel particles with intact coatings, and

$(R/B)_{if}$ = R/B for the i^{th} nuclide for coated fuel particles with failed coatings.

*R/B is the ratio of release rate to birth rate at steady state.

The first term, $(1 - F)\ (R/B)_{ii}$, represents the average gaseous release contribution from intact (or as-manufactured) fuel over the lifetime of the fuel. The second term, $F(R/B)_{if}$, represents the average gaseous release from fuel particles with failed coatings.

At the beginning of life, the fraction of failed fuel is small and the fission gas inventory will be controlled by the fuel contamination level. Later in fuel life, the fission gas inventory will likely be controlled by release from particles with failed coatings.

Experimental

The fuel particle samples utilized in this study are described in Table 4-1. Samples of the WAR particles were irradiated (up to 58% FIMA burnup) in fuel test element FTE-14 and in capsule P13P. Samples of the VSM particles were irradiated (up to 58% FIMA burnup) in fuel test elements FTE-1 and -2 and in capsule P13P.

The WAR particle samples irradiated in FTE-14 were in the form of loose particles. The sample irradiated in P13P (identification No. ID-28) was in the form of a fuel rod. This rod was burned in order to obtain the WAR particles. In the burning operation, the outer PyC coating of the WAR particles was burned off. The rod contained TRISO coated inert particles, and these particles were separated from the burned-back WAR particles utilizing radiographic (X-ray) techniques. All the VSM particles were irradiated in the form of loose particles.

Intact particle samples were selected. Sample sizes were about 50 particles for each unirradiated sample and about 20 particles for each irradiated sample. All the particles in each sample were radiographed to eliminate defective and failed particles and to eliminate inert particles from the burned-back sample of WAR particles.

Particle samples were failed by utilization of a laser technique to introduce pinholes in the coatings. The laser beam was accurately focused

TABLE 4-1
DESCRIPTION OF FUEL PARTICLES

Batch Number	Kernel		Coating									
				Buffer		Inner Isotropic PyC		SiC		Outer Isotropic PyC		
	Type	Diameter (μm)	Type	Thickness (μm)	Density (g/cm^3)	Thickness (μm)	Density (g/cm^3)	Thickness (μm)	Density (g/cm^3)	Thickness (μm)	Density (g/cm^3)
OR-1694	Resin	394	TRISO	46	1.2	20	2.01	20.7	3.24	39.3	1.91
4161-00-023	VSM	137	TRISO	56	1.16	19	1.85	20	3.20	23	1.84
4000-300	VSM	100	BISO	49	1.35	--	--	--	--	74	1.85

to drill pinholes approximately 10 μm in diameter. The intensity of the laser beam was adjusted so that the pinhole penetrated into the buffer layer but not into the kernel.

During the laser-drilling of irradiated particles, the particles were contained in a sealed compartment, which had a window for the beam to enter. The compartment was purged with helium, which flowed into an ionization chamber. A burst of radioactive gas (mainly Kr-85) showed that the laser beam had penetrated the coating. Some particles did not give bursts on laser-failing and some coatings cracked after laser-failing. These particles were eliminated. Particles were retained in the sample only if they showed bursts on laser-failing and if the particles remained intact except for the pinhole.

Fission gas release (R/B) measurements were performed using a standard procedure, which involves irradiating fuel particle samples in a TRIGA reactor, trapping the released fission gases, and gamma-counting the traps. The gamma-counting and calculations are done by use of a Sigma II analyzer-computer. The test yields a direct measure of the R/B value at 1100°C for 4.4-hr Kr-85m, which is taken to be the reference noble gas nuclide.

The particle sample is placed inside of a special graphite crucible (about 3 in. long by 0.75 in. o.d. with a wall thickness of about 0.2 in.). The crucible is inserted into a King furnace mounted in the TRIGA Mark I reactor. The furnace is purged with helium, and the crucible is heated to 1100°C. With helium sweeping through the furnace, the sample is irradiated for one-half hour at a power level sufficient to yield about 10^{14} fissions per fuel rod. During the irradiation period, the sweep gas, which contains the fission gases escaping from the crucible, is purged into a liquid-nitrogen-cooled charcoal trap. After irradiation, the trap is removed and gamma-counted using a lithium-drifted germanium detector in conjunction with the Sigma II analyzer-computer. About 2 days after irradiation, the fuel sample is gamma-counted to determine the activity of I-131 (or another suitable nuclide) for use in calculating the total number of fissions.

The R/B value for Kr-85m (or other noble gas nuclide) is calculated using appropriate codes stored in the Sigma II computer. In the calculation, the measured value (in cpm) for the trap is compared to that for a trap run with a known uranium standard in the reactor. A correction is applied in the R/B calculation for unirradiated fuel particles because during the one-half hour irradiation the level of Kr-85m in the sweep gas does not reach equilibrium.* Input data for the calculation include the cpm value for Kr-85m, appropriate standardization factors, and the cpm value for I-131 (from counting the particle sample). (If the U-235 content of the particle sample is known, an R/B value can be calculated on the basis of the reactor flux level, without waiting for the particle sample to be counted.)

Results and Discussion

The R/B data obtained for the VSM particles are given in Table 4-2. The R/B values for the intact particles varied over a considerable range ($\leq 10^{-5}$ to 1.2×10^{-3}). The data indicate little, if any, effect of burnup on R/B for the intact particles.

The R/B values for three intact VSM samples, especially the value for the sample irradiated in P13P, were unusually high. This suggests that defective or failed particles were present in the samples although this was not shown by radiography. (Radiography is not always a positive means for identifying failed particles.) It could be that some particles failed during the TRIGA R/B test.

The R/B values for the laser-failed VSM particles are in the range of 0.0026 to 0.0097, the overall average value being 5.5×10^{-3}. The values are virtually independent of burnup. The results (for the laser-failed VSM particles) are in good accord with earlier studies (Ref. 4-1) of the fission gas release behavior of failed particles. The earlier studies found that an $(R/B)_f$ for Kr-85m at 1100°C of 5×10^{-3} is supported by in-pile reactor and capsule data and laboratory results. The earlier study found no effect of burnup (up to 54% FIMA) on R/B for laser-failed particles.

*Tests have shown that a steady-state correction is not required for fuel particles previously irradiated to several percent burnup.

TABLE 4-2

FISSION GAS RELEASE FROM COATED VSM PARTICLES

Irradiation Test Number	Identification Number	Design Irradiation Temperature (°C)	Burnup (% FIMA)	Coating Type	Kr-85m R/B at 1100°C	
					Intact Particles	Laser-Failed Particles
	4161-00-023	--	0	TRISO	3.3×10^{-4}	4.8×10^{-3}
FTE-2	72P[a]	1050	8	BISO	$\leq 10^{-5}$	3.5×10^{-3} 9.7×10^{-3} 6.6×10^{-3} avg
FTE-1	71P[a]	1050	21	BISO	2.9×10^{-4}	3.2×10^{-3} 2.7×10^{-3} 2.6×10^{-3} 8.1×10^{-3} 4.2×10^{-3} avg
FTE-1	77P[a]	1050	30	BISO	$\leq 10^{-5}$	7.3×10^{-3} 3.7×10^{-3} 6.3×10^{-3} 5.7×10^{-3} avg
P13P	E1319(U48)[b]	1050	58	TRISO	1.2×10^{-3}	4.5×10^{-3} 6.8×10^{-3} 5.6×10^{-3} avg

[a] Particles from batch number 4000-300 (see Table 4-1).

[b] Particles from batch number 4161-00-023.

Each R/B value in the last column of Table 4-2 is for a separate sample of laser-failed particles (i.e., none of the values is a repeat measurement for the same sample). Several samples were prepared for each burnup for use in this and other studies, and an R/B measurement was performed on each sample.

The R/B data for the resin particles are given in Table 4-3. The sample irradiated in FTE-14 (identification No. TS6-6) showed relatively high R/B values for both intact and laser-failed particles. Examination of the laser-failed sample after the TRIGA R/B test showed exposed kernels, indicating that the particles were defective, which would explain the high R/B values. The R/B values for this sample are considered nonrepresentative.

The average R/B value for the laser-failed resin particles is 3.4×10^{-2} (neglecting sample TS6-6). This value is higher by a factor of six than the average value (5.5×10^{-3}) for the laser-failed VSM particles. Thus, as expected, the resin kernels in failed particles are less retentive than the more dense VSM kernels. This reflects the porous nature of the resin kernels.

Neglecting sample TS6-6, the results indicate that the increase in R/B with burnup for the intact and failed resin particles is no more than a factor of about two.

It is worthwhile to add some comments on laser-failed particles. On the basis of an earlier study (Ref. 4-1), laser-failed particles are taken to be representative of failed particles in fuel rods. This seems reasonable when one considers that the normal mode of particle failure is the formation of coating cracks, which could develop, for example, as a result of internal gas pressure buildup. Cracks in the coating of loose particles can open up, whereas cracks in the coatings of particles in rods are constrained by the matrix material and cannot open up. Similarly, the pinholes in laser-failed particles cannot open up. As shown by the earlier study (Ref. 4-1), R/B values for loose (unconstrained) failed particles are higher than those for constrained particles.

TABLE 4-3

FISSION GAS RELEASE FROM COATED RESIN PARTICLES

Irradiation Test Number	Identification Number[a]	Design Irradiation Temperature (°C)	Burnup (% FIMA)	Kr-85m R/B at 1100°C	
				Intact Particles	Laser-Failed Particles
--	OR-1694	--	0	7.4×10^{-5}	1.8×10^{-2}
FTE-14	TS2-6	975	26	7.5×10^{-5}	3.7×10^{-2}
FTE-14	TS6-6	1250	29	9.0×10^{-3}	11.0×10^{-2}[b]
P13P	1D-28[c]	1050	58	1.4×10^{-4}	4.6×10^{-2}

[a] All particles were from batch number OR-1694 (see Table 4-1).

[b] Examination of sample after TRIGA test showed exposed kernels.

[c] Particle sample obtained from burn-back of irradiated fuel rod.

TRANSPORT CODE DEVELOPMENT

In the previous quarterly report the existence of numerical stability problems in TRAFIC was mentioned. In some cases the solution of the (5x5) nonlinear system did not converge. In other cases it occasionally converged to an incorrect solution. The effort in the current quarter has been spent in locating the causes of these problems and in implementing some automatic correction procedures. Some of the problems and their corrections are:

1. The solution tended to oscillate about a slope discontinuity in the vapor pressure adsorption isotherm. This was fixed by inserting an automated sequence of improved first guesses on either side of the "knee."

2. The (5x5) vector iteration stopped prematurely owing to a false convergence signal. This was fixed by partially normalizing the components and by establishing a criterion for both the vector norm and the components themselves. Note that an earlier atempt to normalize all five of the vector components caused an oscillatory divergence.

3. If the first guess was sufficiently inaccurate (after a large power change), the iteration would sometimes converge to a physically meaningless but mathematically correct solution. This was fixed by re-invoking the false guess correction scheme in VECTIT to prevent extrapolation across forbidden boundaries.

4. If all the above corrections fail to work the time step length is reduced automatically.

5. An option has been added to halve the time steps and to calculate more accurate release values using Simpson's rule to integrate the mass flux.

The above changes have been successful in that TRAFIC now gives reasonable results for both cesium and strontium release in a full core survey calculation. However, these changes must be viewed as short-term expediencies. The TRAFIC code now contains a complicated and inefficient sequence of trial and error corrections. The running time has more than doubled.

Work is now in progress to clean up the code, to improve the calculational efficiency, and to obtain a better understanding of the numerical characteristics of the model. One objective is to arrive at a more rational first guess for the iteration, thus avoiding the need for all the false guess corrections. Hopefully this effort will lead to a much more efficient solution procedure.

ANALYSIS OF TRANSPORT MECHANISMS

As was indicated in the previous Quarterly Progress Report (Ref. 4-2), cesium transport in graphite is a complex process that seems to involve at least two phenomena: (1) a rapid surface diffusion across the graphite, and (2) a slow diffusion into the bulk of the graphite. These impressions continue to be strengthened by diffusion experiments of the type described in an earlier Quarterly Progress Report (Ref. 4-3). A more direct approach has also been taken to measure directly the degree of diffusion involved in the slow process.

The experiments involve the loading of a sample of graphite with cesium, followed by a depletion that removes the surface-sorbed cesium. The loading is done in a niobium crucible with a slip cover, so that control of evacuation and atmosphere is possible but the escape of cesium is very slow. The crucible contains a source in the form of a charloaded highly sorptive graphite sleeve containing Cs-134 and a small rod of reference graphite. The sleeve is about 11 times heavier than the rod. This arrangement permits long-time successive annealings of sample rods using the same source, with minimum depletion of the source. The activity of the rod after such annealing represents the sum of surface and bulk sorption.

In the depletion step, the rod is surrounded by a sleeve and plugs of virgin charloaded graphite and annealed under conditions mild enough to remove only the surface-sorbed cesium. The remaining activity then represents the bulk-sorbed metal.

The success of this approach depends on achieving conditions during the depletion phase that effectively separate the two types of sorbed cesium. Ideal separation is, of course, not to be expected. It appears that annealing at 860°C for 2 hr is quite effective, although no attempt has been made as yet to optimize conditions. A second anneal under the same conditions causes no significant depletion. Loading at 860°C for much longer times leads to only minimal residue after the depletion, showing that bulk sorption is extremely slow at this temperature. Hence bulk desorption can also be assumed to be extremely slow. On the other hand, surface sorption is well completed in 2 hr at this temperature.

If loading is conducted at 1100°C, the total sorbed cesium increases with time. Depletion removes approximately the same amount independently of loading time, whereas the remainder (i.e., the bulk-sorbed material) increases with loading time.

The surface-sorbed amount seems quite constant between the two temperatures, which is to be expected since the sorption of both source and sample are affected by the temperature in the same way.

The slow sorption is probably best interpreted in terms of diffusion into an assembly of uniform spheres of unknown radius, from which $D' = D/r^2$ can be obtained. The first indications are that D' is on the order of 10^{-9} at 1100°C.

FISSION PRODUCT DATA REVIEW

A considerable amount of experimental data exists on the transport of gaseous and metallic fission products, including release, diffusion, and

vaporization data. These data have been accumulated over many years as a result of measurements in the United States and abroad and are scattered in a variety of documents.

The data are being collected, critically reviewed, and evaluated (1) to assure that the data are being utilized to maximum advantage, (2) to serve as a backup for reference fission product transport data used in reactor analyses, (3) to update the transport data, and (4) to determine the adequacy of the data and the specific need for additional work.

An important step in this work has been the establishment of a reference data file, which consists of an orderly arrangement of available data and reports pertaining to gaseous and metal fission product transport. Methods for indexing the reports, for ease of retrieval, are being considered. New data are continually being added to the file.

This file has already been utilized in preparation of (1) a topical report entitled "Strontium Transport Data Report for HTGR Systems" (Ref. 4-4), and (2) fission product transport data uncertainties for use in the Accident Initiation and Progression Analysis (AIPA) study under the ERDA Safety Program.

LITHIUM DETERMINATION METHOD

An important source of tritium in HTGR systems is neutron activation of Li-6 and Li-7 present as impurities in graphite and fuel rod matrix materials. Accordingly, it is important to determine the lithium content of reference graphite and matrix materials in order to predict tritium production levels.

An analytical method has been developed for the determination of lithium in graphite at levels below about 0.05 ppm, which heretofore has been the limit of detectability in methods available at GA. The developed method involves oxidation of the graphite with perchloric acid under

reflux. The resultant solution is analyzed for lithium on an atomic absorption spectrophotometer. A reagent blank is run in exactly the same manner as the sample. Interferences are not likely to be found in reactor-grade graphite. A deuterium background correction to eliminate unwanted background absorption had no effect. The method can be used to determine lithium in graphite at concentrations as low as 10 ppb. Details of the apparatus and methods are presented below.

Apparatus

The apparatus consists of the following:

1. Dissolution apparatus, consisting of (1) quartz Erlenmeyer reaction flask (250 ml), (2) pyrex soxlet extractor (accommodation volume about 50 ml), (3) pyrex air condenser, (4) hot plate, and (5) support stand and clamps.

2. Hood, perchloric acid with safety window.

3. Quartz beaker (150 ml) with speedy-vap.

4. Atomic absorption spectrophotometer.

5. Analytical balance.

The reagents used include:

1. Stock lithium standard solution (100 ppm Li). Dissolve 0.9940 g $LiNO_3$ in deionized water and dilute to 1000-ml volume.

2. Lithium standard solution (1 ppm Li). Pipet 10 ml of the stock solution into a 1000-ml volumetric flask and dilute to volume with deionized water.

3. Perchloric acid, reagent grade, assay 70%.

4. Nitric acid, fuming reagent grade, assay 90%.

To prepare standard solutions, 0, 1, 5, 10, 25, and 50 ml of lithium standard solution are pipetted into 100-ml volumetric flasks and diluted to volume with deionized water. Concentrations are 0, 10, 50, 100, 250, and 500 ppb, respectively.

Procedure

The procedure followed is:

1. Weigh 10 g of sample into a 250-ml Erlenmeyer flask.

2. Add 10 ml fuming nitric acid and 100 ml perchloric acid.

3. Assemble dissolution apparatus, place assembly on hot plate, and secure to a support stand.

4. Set the hot plate dial to achieve 140° to 150°C. Increase the temperature after the first hour to a maximum temperature of 180° to 190°C.

5. Add more (10 to 20 ml) perchloric acid as needed, along with an occasional drop of fuming nitric acid, until all graphite is destroyed. Oxidation of the graphite is complete when the solution is completely clear.

6. Turn off hot plate when the acid level in the extractor is approaching the top of the siphon arm.

7. When at ambient, carefully remove extractor portion and discard acid. All lithium remains in the reaction flask.

8. Transfer contents of flask to 150-ml quartz beaker and rinse with deionized water. Cover with speedy-vap. Run blank on all reagents.

9. Evaporate smaple solution and blank solution down to near dryness.

10. Transfer with deionized water to 10-ml volumetric flask.

The atomic absorption is determined as follows:

1. Utilize wavelength 335.1 nm (visible).

2. Aspirate standards, record absorbance readings, and plot concentration (ppb versus absorbance).

3. Aspirate blank and sample solutions, dilute sample solutions as necessary, and record absorbance readings.

4. Subtract blank absorbance readings from sample absorbance readings and determine concentration of lithium (ppb) in sample solution from standard curve.

The lithium content is calculated as follows:

$$\text{ng/g (or ppb) Li} = \frac{(A) \cdot (B) \cdot (C)}{D} ,$$

where A = volume of sample solution, ml
B = lithium concentration as read from standard curve, ppb or ng/ml
C = dilution factor, if any, or 1
D = sample weight, g

The accuracy of the method is being determined.

Precautions that should be taken are:

1. Operator should not physically expose himself to the dissolution apparatus while sample is being heated.

2. The addition of more acid should be made only after turning off the hot plate and cooling for 15 min.

3. The sample must not be allowed to go to dryness prior to complete dissolution.

4. No plastic or organic material should be in the hood work area.

TRITIUM PERMEATION RATE THROUGH STEAM GENERATOR MATERIALS

Measurements were completed during this quarter on the permeability of tritium through T-22 steel utilizing three more helium-tritium mixtures. The experimental data are shown in Table 4-4. The results, including those obtained during the last quarter, are summarized in Table 4-5. The least-square relationships of P versus 1/T, shown in Table 4-5, are plotted in Fig. 4-1.

Because the tritium primary source used for the preparation of the tritium-helium mixtures used in these studies contains hydrogen, it was not possible to vary the tritium activities and the hydrogen concentrations of these mixtures independently so that the effect of each of these two variables on tritium permeation rate could be evaluated separately. However, the tritium permeation rate should be dependent upon the tritium atom concentration on the surface of the metal sample, and the tritium atom concentration can be shown to be proportional to $P_{HT}/\sqrt{P_{H_2}}$ (P_{HT} and P_{H_2} are the partial presures of HT and H_2, respectively, in the tritium-helium mixture) by considering the two simultaneous equilibriums $HT \rightleftharpoons H + T$ and $HH \rightleftharpoons H + H$ on the metal sample surface. Therefore, the tritium permeation rate should vary with the $P_{HT}/\sqrt{P_{H_2}}$ value of the tritium-helium mixture. In Table 4-6 the relative values of $P_{HT}/\sqrt{P_{H_2}}$ are compared with the relative values of observed tritium permeation rates at 300° and 500°C for the four tritium-helium mixtures studied.

TABLE 4-4

TRITIUM PERMEATION RATE THROUGH T-22

Source specific activity = 3.62×10^{-5} μCi/cm^3, equivalent to p_{HT} = 2.14×10^{-8} torr. Impurity contents: H_2 = 50 ppm, O_2 = 4.9 ppm, CO < 1 ppm, CH_4 < 1 ppm, H_2O = 4.0 ppm.

Run Number[a]	Temperature (°C)	Permeation Rate (μCi-mm/cm^2-hr)
1	300	1.49×10^{-6}
2	300	1.39×10^{-6}
3	300	1.25×10^{-6}
4	350	5.17×10^{-6}
5	350	6.04×10^{-6}
6	350	8.21×10^{-6}
7	399	1.77×10^{-5}
8	399	1.87×10^{-5}
9	399	1.74×10^{-5}
10	446	2.68×10^{-5}
11	446	2.81×10^{-5}
12	446	3.00×10^{-5}
13	504	5.22×10^{-5}
14	504	5.39×10^{-5}
15	504	5.56×10^{-5}
16	292	9.43×10^{-7}
17	292	9.15×10^{-7}
18	400	7.78×10^{-6}
19	400	8.37×10^{-6}
20	400	7.97×10^{-6}
21	505	3.60×10^{-5}
22	505	3.70×10^{-5}
23	337	4.74×10^{-6}
24	337	5.21×10^{-6}

TABLE 4-4 (Continued)

Source specific activity = 6.14×10^{-3} $\mu Ci/cm^3$, equivalent to p_{HT} = 3.63×10^{-6} torr. Impurity contents: H_2 = 6500 ppm, O_2 = 2.7 ppm, CO < 1, CH_4 < 1 ppm, H_2O = 4.0 ppm.

Run Number[a]	Temperature (°C)	Permeation Rate (μCi-mm/cm^2-hr)
1	491	3.00×10^{-3}
2	491	2.80×10^{-3}
3	298	4.92×10^{-4}
4	298	3.95×10^{-4}
5	345	5.50×10^{-4}
6	345	7.00×10^{-4}
7	408	1.72×10^{-3}
8	408	1.64×10^{-3}
9	494	7.02×10^{-3}
10	494	6.03×10^{-3}
11	448	3.63×10^{-3}
12	448	3.40×10^{-3}
13	375	1.72×10^{-3}
14	375	1.65×10^{-3}
15	375	1.67×10^{-3}
16	300	6.07×10^{-4}
17	300	6.27×10^{-4}

TABLE 4-4 (Continued)

Source specific activity = 2.10×10^{-4} μCi/cm^3, equivalent to $p_{HT} = 1.24 \times 10^{-7}$ torr. Impurity contents: H_2 = 230 ppm, O_2 = 6 ppm, CO < 1 ppm, CH_4 < 1 ppm, H_2O = 4 ppm.

Run Number[a]	Temperature (°C)	Permeation Rate (μCi-mm/cm^2-hr)
1	352	2.00×10^{-5}
2	352	2.10×10^{-5}
3	352	2.00×10^{-5}
4	405	3.07×10^{-5}
5	405	2.93×10^{-5}
6	405	2.92×10^{-5}
7	446	5.54×10^{-5}
8	446	5.42×10^{-5}
9	446	5.22×10^{-5}
10	505	1.52×10^{-4}
11	505	1.69×10^{-4}
12	505	1.70×10^{-4}
13	337	6.80×10^{-6}
14	337	6.80×10^{-6}
15	337	5.93×10^{-6}

[a]Run number represents sequence of experiments.

TABLE 4-5
SUMMARY OF TRITIUM PERMEATION RATE THROUGH T-22

Tritium-Helium Mixture	Specific Activity (μCi/std cm^3)	Partial Pressure of Gaseous Impurities[a] (μatm)					Temp Range (°C)	Number of Data Points	Least Square Relationship Between Permeation Rate P (μCi-mm/cm^2-hr) and Temperature (°K)
		H_2	O_2	H_2O	CH_4	CO			
1	3.62×10^{-5}	50	4.9	4.0	<1	<1	292-505	24	$P = 1.05 \exp(-7690/T)$
2	2.10×10^{-4}	230	6.0	4.0	<1	<1	337-505	15	$P = 2.04 \exp(-7450/T)$
3	8.45×10^{-4}	610	28	4.6	<1	<1	304-508	20	$P = 6.09 \exp(-7380/T)$
4	6.14×10^{-3}	6500	2.7	4.0	<1	<1	300-494	17	$P = 3.41 \exp(-5070/T)$

[a] Total pressure of helium-tritium mixture was 1 atm in each case.

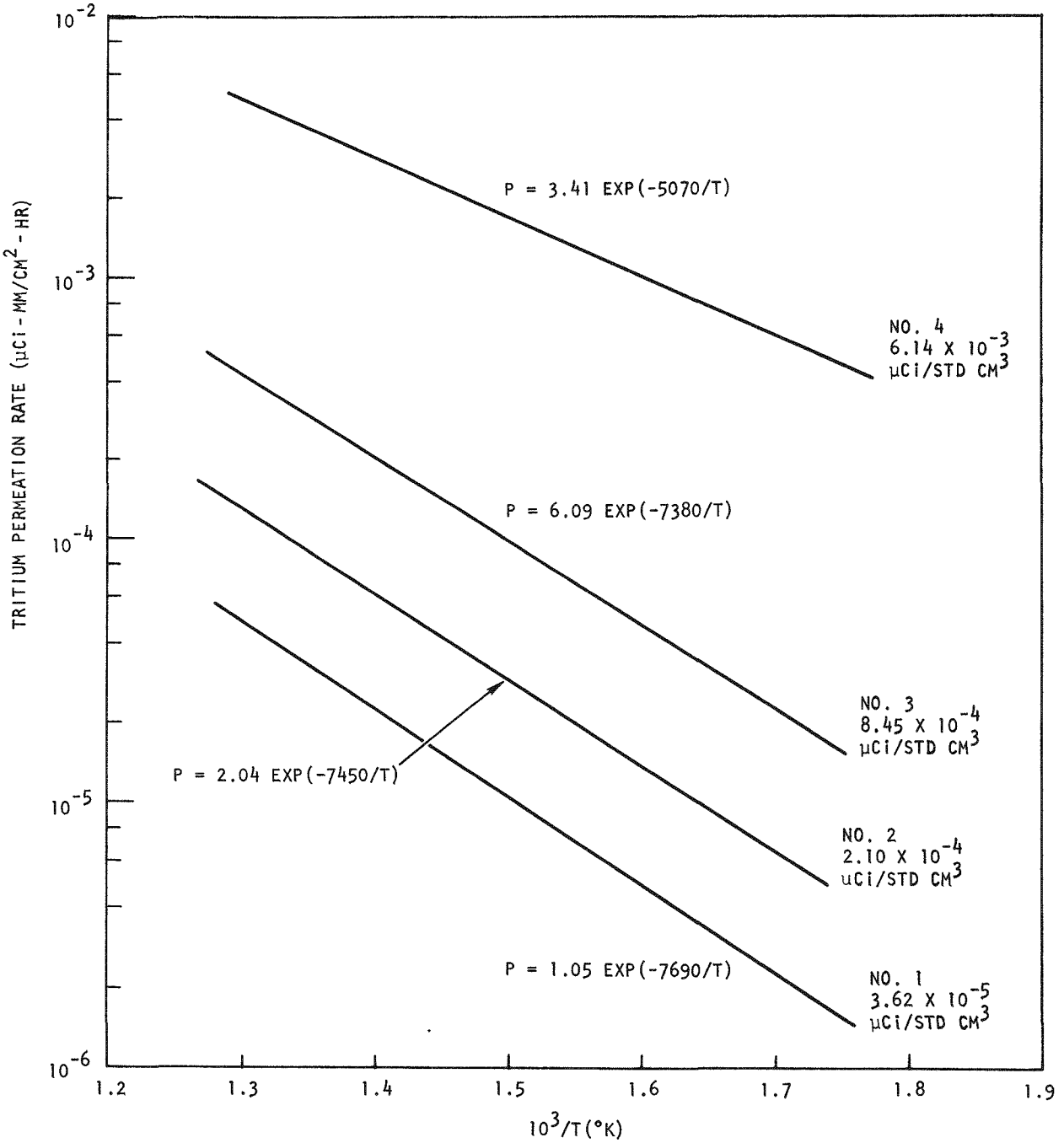

Fig. 4-1. Least-square plots of tritium permeation rates versus reciprocal temperature for the four tritium-helium sources studied

TABLE 4-6
COMPARISON OF RELATIVE VALUES OF $P_{HT}/\sqrt{P_{H_2}}$ WITH RELATIVE VALUES OF OBSERVED TRITIUM PERMEATION RATES

Tritium-Helium Mixture	Relative $P_{HT}/\sqrt{P_{H_2}}$	Relative Observed Tritium Permeation Rate	
		300°C	500°C
1	1	1	1
2	2.8	2.7	2.7
3	7	10	9
4	15	300	96

It appears from Table 4-6 that the tritium permeation rate is proportional to $P_{HT}/\sqrt{P_{H_2}}$ when the hydrogen concentration in the tritium-helium mixture is low (e.g., mixture 2, H_2 = 230 ppm). For higher hydrogen concentrations (e.g., mixture 4, H_2 = 6500 ppm), the observed tritium permeation rate is much higher than that predicted on the basis of the $P_{HT}/\sqrt{P_{H_2}}$ rule, and the deviation is higher at lower temperature.

Thus, the presence of hydrogen in the tritium-helium mixture appears to affect the tritium permeation rate in two ways: (1) by changing the tritium atom concentration on the metal sample surface, and (2) by changing the activation energy of diffusion in the metal sample. When the hydrogen concentration is low, the effect is mainly the reduction of tritium atom concentration (thus the tritium permeation rate) by promoting the recombination of H and T to form HT. The tritium permeation rate will vary with $P_{HT}/\sqrt{P_{H_2}}$, but the activation energy of diffusion stays essentially constant. At higher hydrogen concentration, the hydrogen atom concentration becomes high enough to fill all the trapping sites for hydrogen isotopes in the metal. The effect is mainly the lowering of the activation energy of diffusion in the metal and the tritium permeation rate becomes much higher than that predicted on the basis of the $P_{HT}/\sqrt{P_{H_2}}$ rule. This explanation is consistent with the data shown in Tables 4-5 and 4-6.

For further evaluation of the effect of hydrogen and tritium activity on the tritium permeation rate, a high specific activity and high purity tritium source was procured from ORNL. This source will be used for the preparation of tritium-helium mixtures of low hydrogen, oxygen, and moisture contents. A micrometering valve has been incorporated in the permeation apparatus, allowing the addition of controlled amounts of hydrogen into the tritium-helium stream so that the tritium permeation rates from tritium-helium mixtures of given tritium activities can be measured as a function of hydrogen concentration. The same metering valve can be used for injecting controlled amounts of CO and CH_4 into the tritium-helium stream for the study of the effect of these impurities on the tritium permeation rate through T-22.

EFFECT OF FUEL HYDROLYSIS ON FISSION GAS RELEASE

Experiments are under way to study the effect of hydrolysis of exposed carbide particles on the steady-state fission gas release, or R/B, of HTGR fuel. Previous work has been described and reported in Ref. 4-3. The tests involve exposure of laboratory-prepared fuel rods containing known quantities of failed fuel to water vapor at temperatures from 300° to 900°C. The R/B measurements are performed intermittently during the exposures, which have ranged up to 1315 hr. The fissionable material in the rods is either several laser-drilled TRISO coated UC_2 particles or bare uncoated UC_2 kernels. In the former case, the TRISO coatings were penetrated three times using a laser beam. The three holes were 10 to 20 μm in diameter and were drilled into each particle to a depth of approximately the kernel surface to assure that the UC_2 kernels would be exposed to the hydrolysis conditions.

The laser-drilled particles or bare kernels were positioned in the center of green fuel rods prepared from dummy (nonfissionable) PyC coated ZrO_2 particles and matrix material. The rods were carbonized at 1000°C and fired to 1800°C in the usual manner. The rods were then inserted into individual graphite crucibles and measured for Kr-85m R/B at 1100°C in the TRIGA King furnace facility. The rods were then gamma counted to determine the quantity of U-235 in each rod to allow accurate calculation of the birth rate of the noble gas isotopes (i.e., the "B" term in R/B). The test rods in their

graphite crucibles were placed inside quartz furnace tubes, which were continuously swept with helium containing 100 ppm water vapor at 1 atm total pressure (equivalent to 2 ppm H_2O at 50 atm He). The R/B measurements were performed intermittently throughout the exposures.

In another experiment the effect of prior irradiation has been examined. A small sample of irradiated fuel compact (D1305-29) material containing essentially 100% failed $(Th,U)C_2$ particles (burnup = 4% FIMA) from the Peach Bottom HTGR (Core 1) has been exposed to 100 ppm water vapor at 900°C for 2012 hr. In this test, because of the high radiation level of the previously irradiated sample, the hydrolysis exposure was conducted in the pool-side TRIGA King furnace. Thus, R/B measurements on this sample were performed in situ without having to remove the sample from the exposure furnace. Since the exact quantity of U-235 in this specimen was unknown, the Kr-85m R/B values have been normalized to a value of 1.0%, which is consistent with other measurements of Peach Bottom Core 1 fuel material including the end-of-life average R/B measured during the last several weeks of reactor operation.

The results of the R/B measurements of the unirradiated samples are listed in Table 4-7. Smoothed curves of these data are shown in Figs. 4-2a through 4-2d. The irradiated (Peach Bottom sample) data are given in Fig. 4-2e.

Results and Discussion

The results of the tests on fuel rods hydrolyzed at representative HTGR fuel temperatures (700° to 900°C) are shown in Figs. 4-2a and 4-2b for bare kernels and laser-drilled particles, respectively. In Fig. 4-2a hydrolysis of bare kernels causes a rapid increase in R/B to 40 to 60% within 50 to 100 hr of exposure. The R/B then slowly declines to a value of 10 to 16% after an exposure of ∿1200 hr. The rods prepared from laser-drilled particles (Fig. 4-2b) reached lower R/B maxima (25 to 40%) after 200 to 600 hr of exposure, indicating significantly slower overall hydrolysis rates due to the lower fraction of carbide kernel material exposed. It is of interest

TABLE 4-7

R/B[a] VERSUS HYDROLYSIS TIME FOR UC_2 PARTICLES IN RODS EXPOSED TO 100 PPM H_2O IN HELIUM

(%)

Time (hr)	300°C		400°C		500°C		700°C		800°C		900°C	
	Laser[b] Drilled	Bare[c] Kernel	Laser Drilled	Bare Kernel	Laser Drilled	Bare Kernel	Laser Drilled	Bare Kernel	Laser Drilled	Bare Kernel	Laser Drilled	Bare Kernel
0	0.8	1.5	1.5	1.7[d]	0.7	2.2	0.3	2.9	0.2	4.1	0.2	5.6
7											2.4	23
10							2.5	24	6.7	31		
15	1.5	3.2	6.6	16	1.5	14						
20											1.5	50
30							3.1	23	9.6	36		
50			6.6	21	2.4	39	2.4	24	8.7	43		
60	3.2	7.0									11	63
90								33				
100			6.2	25	3.6	29					11	12
110	2.7	16.0					2.1		11	42		
200							6.1	42	18	41	14	14
300	7.4	39.0	9.9	19	6.3	23	38	35	25	34	5.7	14
400							32	17	27	31	4.5	26
455												
560							25		27	32	8.3	11
630	21	23	12	17	10	22						
670								22				
780							16		30	32	9.1	21
1185								12				
1216			6.5[d]	8.6[d]	5.3[d]	9.4[d]						
1226	12.6[d]	7.2[d]										
1292							10					
1315									13	16	4.2	10

Average final R/B values (Kr-85m at 1100°C)
"Laser" rods hydrolyzed at 300, 400, and 500°C = 8.1%
Bare kernel rods hydrolyzed at 300, 400, and 500°C = 8.4%
"Laser" rods hydrolyzed at 700, 800, and 900°C = 9.1%
Bare kernel rods hydrolyzed at 700, 800, and 900°C = 12.7%

[a] Kr-85m R/B values at 1100°C, corrected for steady state (i.e., multiplied by 1.9).

[b] Fuel rods prepared from laser-drilled UC_2 TRISO particles.

[c] Fuel rods prepared from bare kernel UC_2 particle.

[d] Average of two successive measurements.

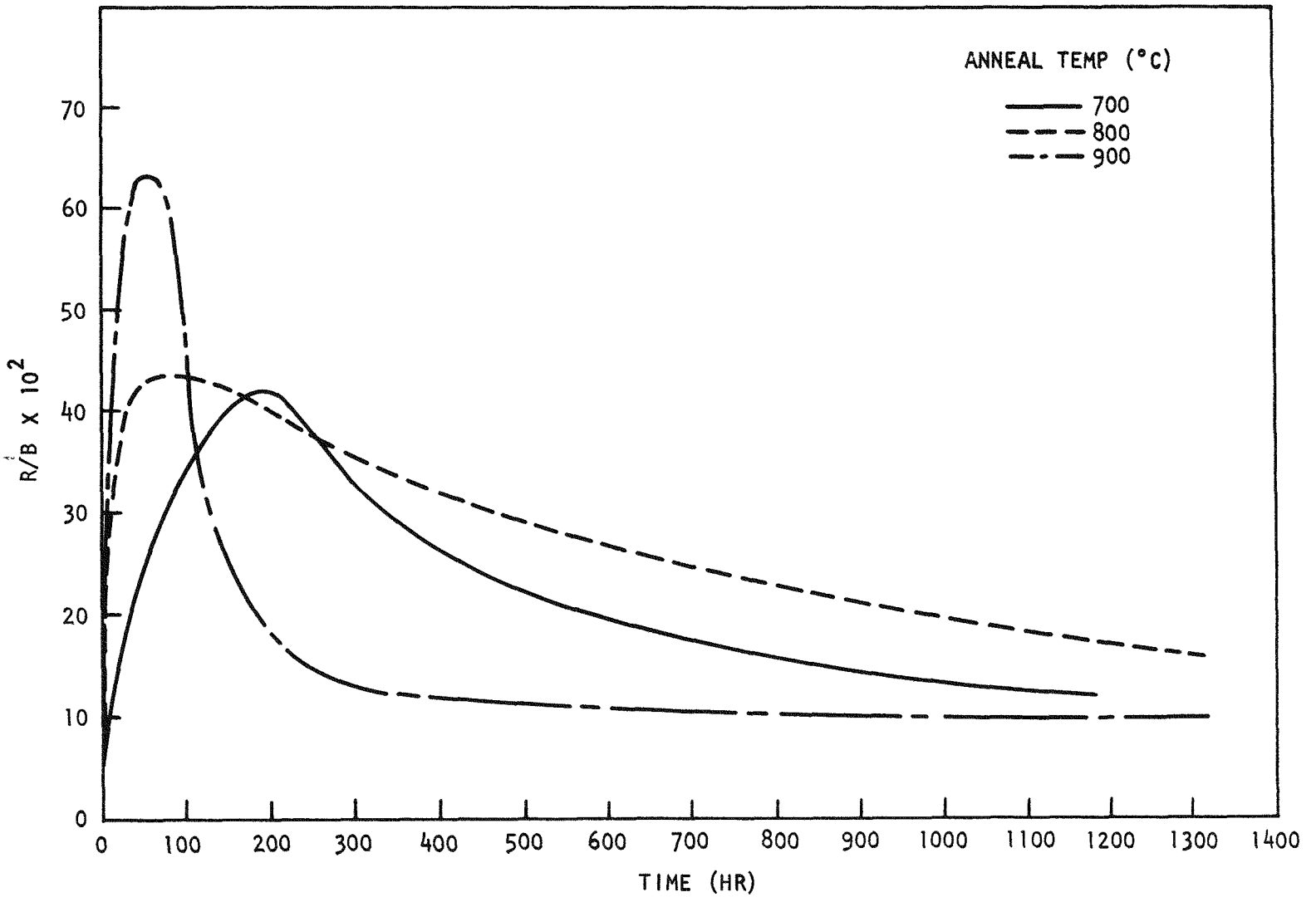

Fig. 4-2. R/B_f (Kr-85m at 1100°C) versus hydrolysis exposure. P_{H_2O} = 100 ppm (in He). (a) Nonirradiated fuel rods prepared with bare UC_2 kernels; 700°, 800°, 900°C.

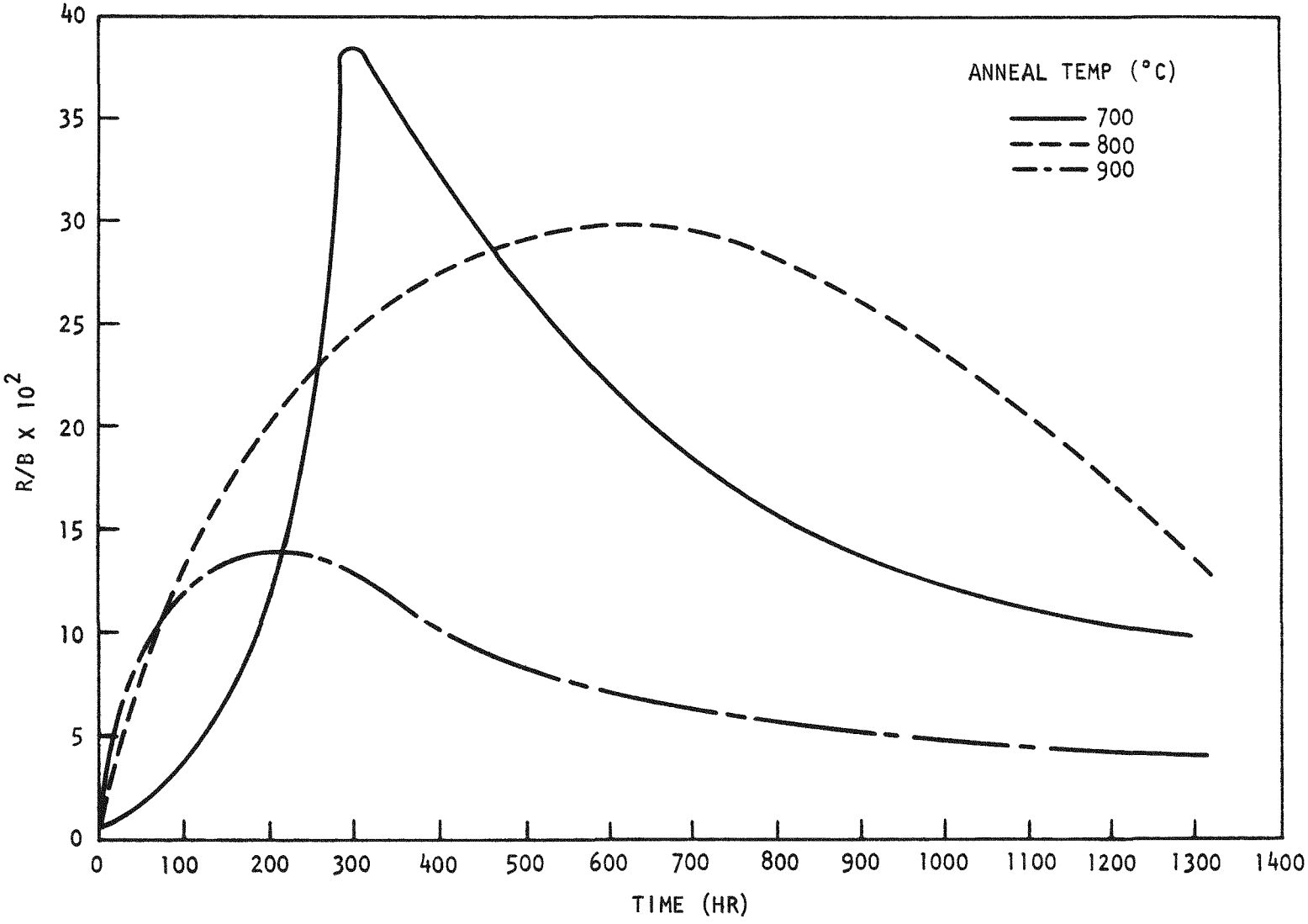

Fig. 4-2. R/B_f (Kr-85m at 1100°C) versus hydrolysis exposure. P_{H_2O} = 100 ppm (in He). (b) Nonirradiated fuel rods prepared with laser-drilled TRISO coated UC_2 particles; 700°, 800°, 900°C.

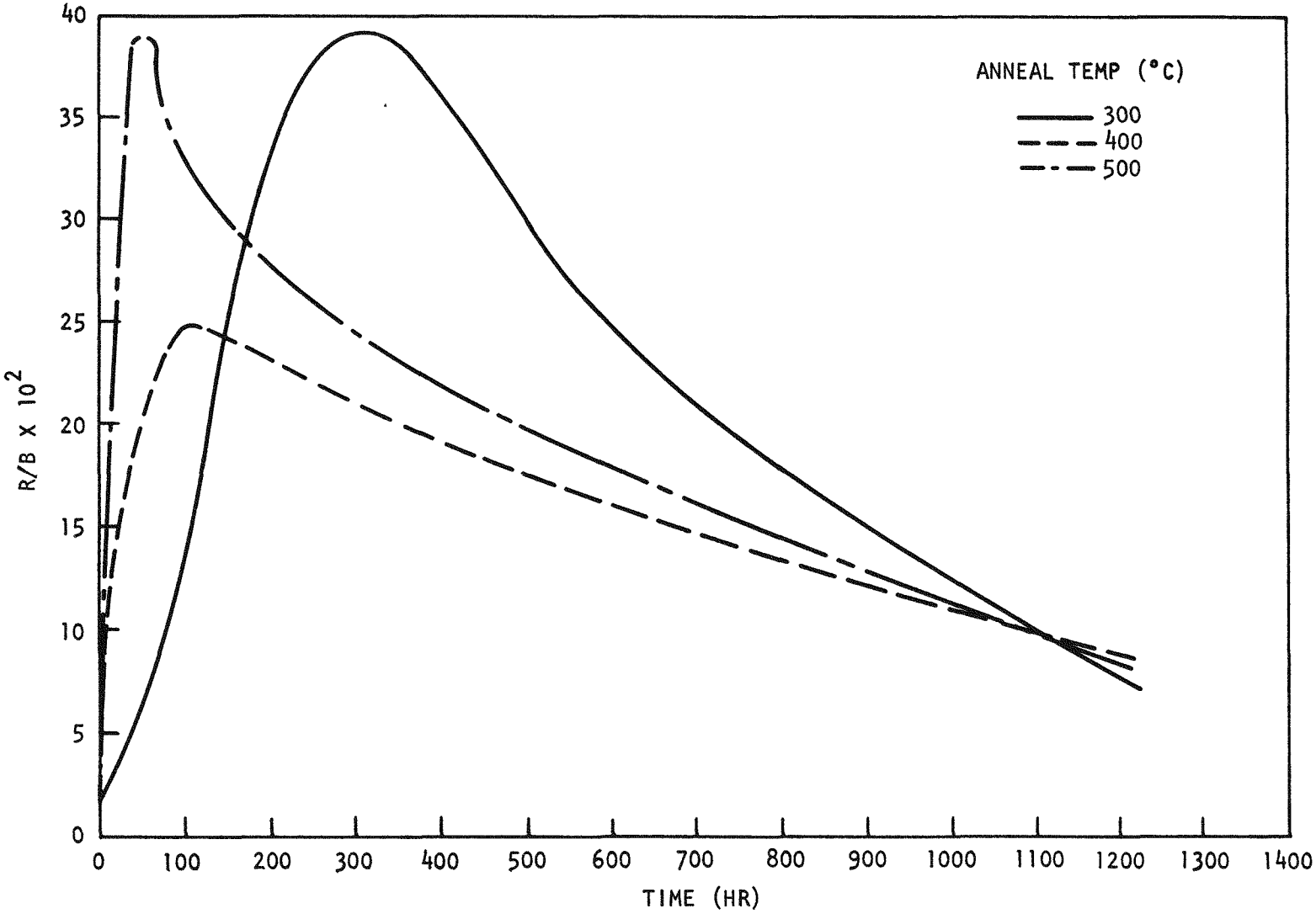

Fig. 4-2. R/B_f (Kr-85m at 1100°C) versus hydrolysis exposure. P_{H_2O} = 100 ppm (in He). (c) Nonirradiated fuel rods prepared with bare UC_2 kernels; 300°, 400°, 500°C.

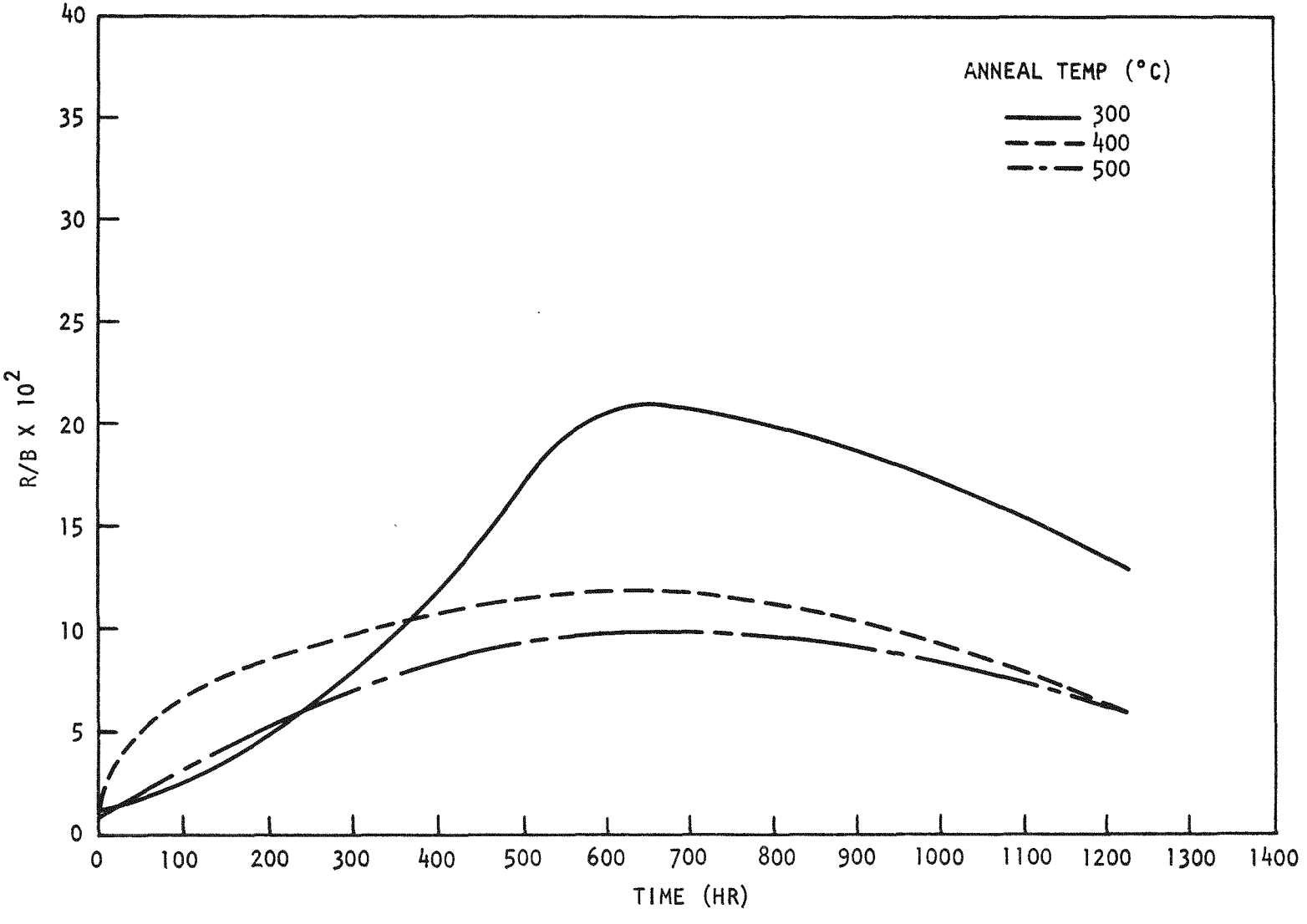

Fig. 4-2. R/B_f (Kr-85m at 1100°C) versus hydrolysis exposure. P_{H_2O} = 100 ppm (in He).
(d) Nonirradiated fuel rods prepared with laser-drilled TRISO UC_2 particles; 300°, 400°, 500°C.

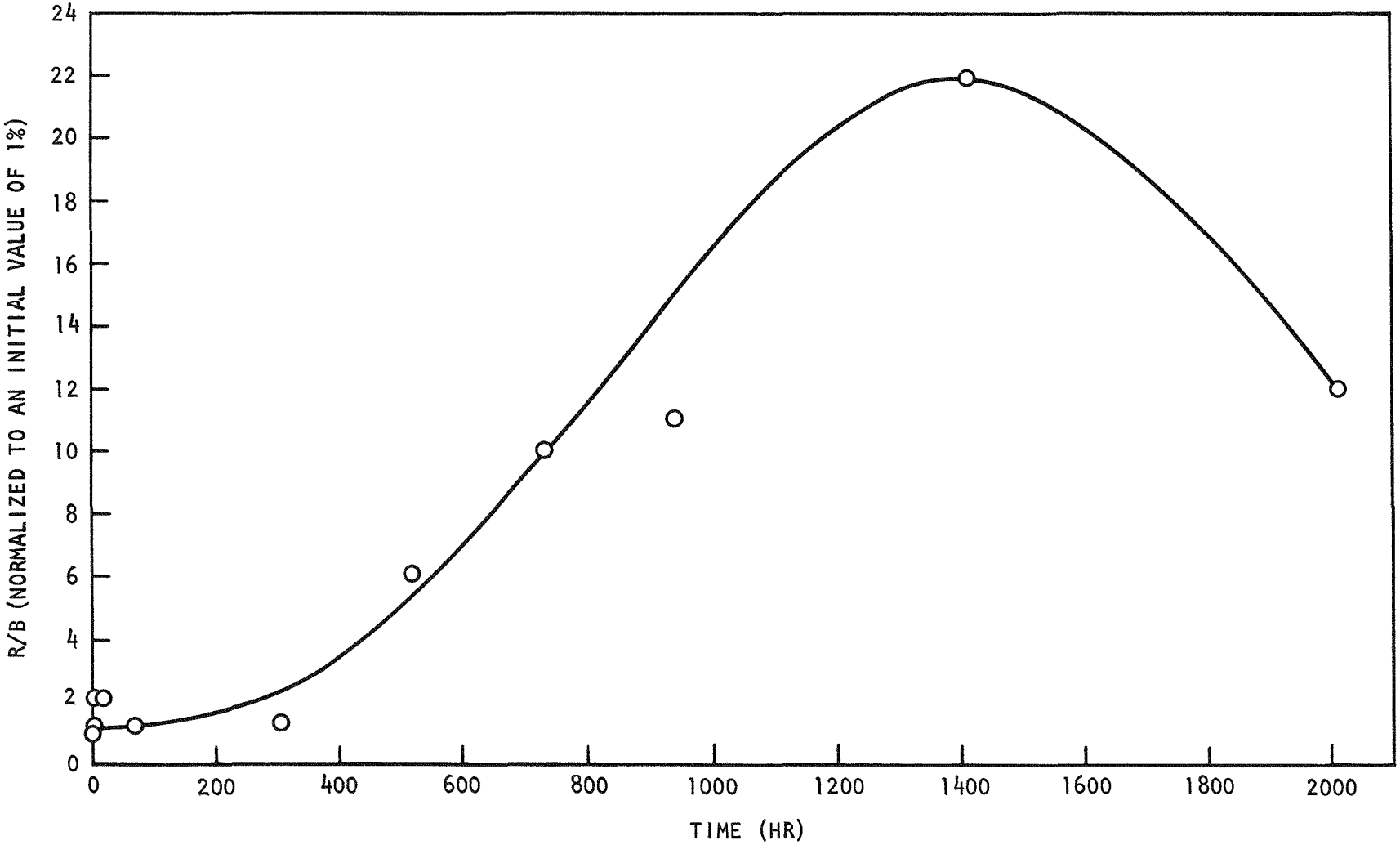

Fig. 4-2. R/B_f (Kr-85m at 1100°C) versus hydrolysis exposure. P_{H_2O} = 100 ppm (in He). (e) Irradiated $(Th,U)C_2$ compact material from Peach Bottom Core 1; exposure temperature = 900°C, burnup = ∿4% FIMA, failure fraction = ∿1.

that the final R/B values after long-term exposure are quite similar for the laser-drilled and bare kernel specimens. The average final R/B values were 9.1% and 12.7% for the rods with laser-drilled particles and bare kernels, respectively.

The increase in R/B followed by the slow decline is believed to be associated with formation of a loose finely divided oxide product, followed by a slow sintering process in which the hydrolyzed kernel material somewhat densifies. A process akin to this has been observed in thermogravimetric studies in which pure UC_2 when exposed to moisture at temperatures above 700°C gains weight rapidly and then loses weight upon continued exposure.

Hydrolysis of fuel at low temperatures representative of reactor shutdown conditions (300°, 400°, and 500°C) is shown in Figs. 4-2c and 4-2d. These results show that the initial rates of hydrolysis (as indicated by the time to reach the R/B maxima) are significantly slower than their higher temperature counterparts. The final R/B for the rods exposed at 300° to 500°C after long-term exposure were similar to the higher temperature exposures, averaging about 8.2%.

The long-term effect of hydrolysis on the R/B of the slightly irradiated carbide fuel (Fig. 4-2e) appears to be virtually identical to the effect on the unirradiated samples. This was an expected result since the burnup of this specimen was only 4% FIMA. It is of interest, however, that this small degree of burnup caused a significant passivation during the early stages of the exposure; that is, the effects of hydrolysis were insignificant until after 400 hr of exposure to water vapor. This result suggests that higher burnups could cause an even longer term passivation effect. Hydrolysis of high burnup fuel rods is planned for the near future.

Conclusions

These data indicate that the R/B_f (Kr-85m at 1100°C) of hydrolyzed exposed UC_2 particles in the HTGR will be on the order of 10%. This relatively low value is supported by the data given in Ref. 4-5, which indicated an R/B_f of approximately 2.5% for a $(Th,U)C_2$ fuel rod taken from a fuel test element (FTE-3) irradiated in Peach Bottom to about 3% FIMA burnup, and hydrolyzed at 900°C for 240 hr in 100 ppm water vapor and for an additional 18 hr in 30,000 ppm water vapor. These are encouraging results and will be verified by tests on more highly irradiated fuel rods.

EFFECT OF OXIDATION ON THE MECHANICAL PROPERTIES OF GRAPHITE

An experimental program to measure the effect of steam oxidation on the mechanical properties of H-451 graphite has been initiated. In this study cylindrical tensile specimens 1.25 in. long by 0.25 in. in diameter will be oxidized at 800° and 1000°C in He containing 3% water vapor and 1% H_2. Sample weight losses ranging from 1% to 4% will be studied.

A test-sample matrix for this study is shown in Table 4-8. A total of 320 samples will be involved in this study, which includes 20 specimens reserved for each parameter. Parameters to be studied are (1) sample position in the log, either center or edge; (2) orientation, either parallel or perpendicular to the extrusion axis; (3) burnoff, 0% (controls), ∿1%, ∿2%, and ∿4% weight loss; and (4) temperatures of 800° and 1000°C. After oxidation, the samples will be decreased in length from 1.25 in. to 0.9 in. by grinding both ends 0.175 in. The inordinate weakness due to surface oxidation at the extreme ends of the samples will thus be minimized. The specimens will then be tested in an Instron tensile machine, which will provide stress-strain curves for each sample. From these data the elastic modulus (which is normally measured as the chord modulus between two stress values, e.g., 100 and 1000 psi), ultimate tensile strength, and strain-to-failure will be determined.

TABLE 4-8

TEST MATRIX FOR GRAPHITE
STRENGTH/OXIDATION STUDY

Specimen Type[a,b]	Control Specimens, 0% Burnoff	Test Temp = 800°C			Test Temp = 1000°C			Total Number of Specimens by Type
		1%[c]	2%	4%	1%	2%	4%	
QLC (∥)	20	20	20	20	20	20	20	140
QLC (⊥)	20			20			20	60
QLE (∥)	20			20			20	60
QLE (⊥)	20			20			20	60
Total Specimens								320[d]

[a] 0.25 in. in diameter by 0.9 in. long.

[b] QLC = quarter-length center
QLE = quarter-length edge
∥ = parallel to extrusion axis
⊥ = perpendicular to extrusion axis

[c] Burnoff.

[d] All samples taken from slabs 5A and 5B of H-451 log No. 5651-34.

FISSION PRODUCT TRANSPORT CODE AND DATA VALIDATION

Validation of Strontium Diffusion Coefficient Data

The analysis of diffusion samples in fuel test element FTE-4 (irradiated for 449 effective full-power days in the Peach Bottom HTGR) is providing diffusion coefficient data for use in validating reference diffusion coefficient data for strontium in graphite.

The center spine of FTE-4 and several other test elements of the FTE series contained diffusion samples for use in:

1. Determining the diffusion behavior of selected metal fission products in graphite under HTGR conditions as a function of metal concentration and temperature.

2. Providing data on the effects of the presence of other fission product metals on the migration rate of individual metals.

3. Determining the distribution of metal fission products between matrix material and graphite.

FTE-4 contained 22 metallic diffusion samples, located in fuel element spine bodies 1, 2, and 3. The samples contained isotopes of barium, strontium, samarium, and cesium, or mixtures of these isotopes in varying concentrations.

The experimental procedure for determining diffusion coefficients of these metals is discussed in Ref. 4-6. Briefly, each diffusion sample consists of metal-impregnated matrix material contained in the annular section of a graphite crucible consisting of a center post and crucible wall. After irradiation and a suitable cooling period, the diffusion samples are removed from the fuel test element and sectioned (after the matrix material is removed) by turning the crucible walls and center posts on a lathe,

uniformly removing a layer of graphite for each section. The section samples are weighed and gamma-counted using a Ge(Li) crystal detector and a 4096-channel pulse height analyzer. The resulting concentration profiles are analyzed utilizing the computer program CPROFIT (concentration profile fit) developed at North Carolina State University.

Analyses of the FTE-4 diffusion samples are in progress using the computer program; in the meantime, three preliminary diffusion coefficients for strontium in graphite have been hand calculated using a method described by Crank (Ref. 4-7). In Table 4-9, the three values are compared with reference values calculated from the equation given in Table 3-1 of Ref. 4-4. The observed values are found to be smaller than the reference values, which is a satisfactory result.

TABLE 4-9
COMPARISON OF OBSERVED[a] AND REFERENCE DIFFUSION COEFFICIENT DATA FOR STRONTIUM IN H-327 GRAPHITE

Crucible Number	Calculated Irradiation Temperature (°C)	D_{Sr} (cm^2/sec)	
		Observed	Reference
10	891	8.7×10^{-11}	1.59×10^{-10}
18	1041	1.47×10^{-10}	3.8×10^{-9}
22	1129	2.5×10^{-9}	1.75×10^{-8}

[a] Hand calculated from concentration profiles.

Postirradiation Examination of Peach Bottom Driver Elements

Important information for use in validating design codes (including codes for calculating power and temperature histories, fission product release into the primary coolant, and tritium release into the primary coolant) will be provided by postirradiation examination of five Peach Bottom Core 2 driver elements. This work will be done at ORNL.

A preliminary test plan, which is summarized below, was written to present GA's recommendation for the PIE work. The test plan was discussed with ORNL representatives (A.P. Malinauskas and R.P. Wichner) at a meeting in San Diego (February 3-5, 1975).

The plan includes a step-by-step procedure for fuel element disassembly, metrology (dimensional measurements), determination of fission product distributions, and fuel compact examination. The recommended work will provide the following information:

1. Axial burnup and fission product distributions (from gamma-scans) for use in validating codes used in calculating power histories.

2. Metrology (dimensional) data to permit more accurate calculation of fuel element temperature histories.

3. Particle failure fractions for use in validating particle failure models.

4. Fission product distribution (including concentration profiles for fission products in fuel compacts, spine and sleeve, determined utilizing radiochemistry techniques) for use in validating design fission product transport codes.

5. Fission product concentrations in upper reflector and lower reflector for use in (1) estimating fission product metal concentrations in helium coolant at core exit, (b) estimating depletion of fission products per pass of coolant through the primary circuit, and (c) validating design fission product transport codes.

6. Tritium retention in fuel compacts and sleeve and spine graphite for use in validating models for predicting tritium release into the primary coolant.

7. C-14 in graphite for use in checking predicted levels.

The recommended PIE measurements and methods are listed in Table 4-10.

Since the PIE work is relatively expensive, the number of fuel elements on which these measurements will be performed is necessarily a small fraction of the total number of elements in the core. However, the 804 fuel elements comprising the Peach Bottom core can be grouped into a relatively small number of types, which can be characterized by a PIE of one or two of a given type. Accordingly, it is believed that the core can be adequately modeled by the PIE of five driver elements.

TABLE 4-10

RECOMMENDED PIE MEASUREMENTS AND METHODS

Measurement	Candidate Methods
Complete element	
Integrity and structure	Visual examination
Burnup distribution	Axial gamma-scan
Fission product distribution	Axial gamma-scan
Fuel stack length	Axial gamma-scan and metrology
Fuel compacts, spine and sleeve graphite	
Fuel compact/sleeve gap determination and compact/spine gap determination	Metrology
Fuel performance	Metallography for kernel migration, failure fraction, fission gas release measurements on selected samples from fuel compacts
Burnup	Wet chemistry, mass spectrometry
C-14 content of fissile particles and graphite	Mass spectrometry or radiochemistry
Fission product (including Cs, Sr, and I) distribution in selected fuel compact, spine, and sleeve samples	Gamma-counting and radiochemistry techniques
Heavy metal distribution	Wet chemical analysis
Fission product (including Cs and Sr nuclides) release fractions in selected fuel compact samples	Gamma-scan and radiochemistry techniques
Tritium retention in selected graphite and fuel compact samples	Combustion, wet chemistry, beta-counting
Dimensional changes, bowing of graphite sleeve and spine	Metrology
Other components	
Thermocouple performance (instrumented elements)	Resistance measurements, metallurgical examination
Fission product concentrations on selected samples from top and bottom reflectors and fission product trap	Gamma-counting and radiochemistry techniques

REFERENCES

4-1. Burnette, R.D., W.E. Bell, and N.L. Baldwin, "Fission Product Retention Characteristics of HTGR Fuel," paper presented at the International Conference on Nuclear Fuel Performance, British Nuclear Energy Society, London, October 15-19, 1973, Paper No. 16.

4-2. "HTGR Fuels and Core Development Program, Quarterly Progress Report for the Period Ending November 30, 1974," USAEC Report GA-A13253, General Atomic Company, January 31, 1975.

4.3. "HTGR Fuels and Core Development Program, Quarterly Progress Report for the Period Ending August 30, 1974," USAEC Report GA-A13126, General Atomic Company, September 30, 1974.

4-4. Myers, B.F., and W.E. Bell, "Strontium Transport Data for HTGR Systems," USAEC Report GA-A13168 (GA-LTR-16), General Atomic Company, December 6, 1974.

4-5. "HTGR Base Program Quarterly Progress Report for the Period Ending August 31, 1973," USAEC Report Gulf-GA-A12725, Gulf General Atomic, September 23, 1973, p. 178.

4-6. Wallroth, C.F., et al., "Postirradiation Examination of Peach Bottom Fuel Test Element FTE-3," USAEC Report GA-A13004, General Atomic Company, August 15, 1974.

4-7. Crank, J., Mathematics of Diffusion, Oxford Press, London, 1957, p. 12.

TASK 8 (189a 13118)
REACTOR PHYSICS

XENON STABILITY AND CONTROL STUDY

As the size of a nuclear reactor increases, the need for a detailed consideration of the possible impact of xenon redistribution upon the performance of the core becomes more pronounced at every stage of the physics design. This is true because the inherent stability of the flux distribution will decrease with increasing core size. As a consequence, the time-dependent behavior of the power distribution in a large core can become quite sensitive to time-dependent variations in localized nuclear properties such as, for example, the change in absorption cross section associated with an oscillation in xenon concentration induced by a control rod movement. In a very stable core, a localized perturbation such as this would have very little effect upon the power distribution. However, in an unstable core it would cause an oscillation which, if unchecked, could lead to serious fuel damage.

This is a well known problem which has been examined very thoroughly in the past, especially for pressurized water reactors. In some cases this has led to designs that deliberately accept the penalties of increased instrumentation requirements and sophisticated control rod programming schemes associated with a core unstable to xenon oscillations in return for other benefits. However, HTGRs have been confined to designs that are intrinsically stable to xenon oscillations. Past studies (Refs. 8-1, 8-2) have defined certain ground rules for these designs, and the stability of a specific core is then further confirmed by explicit numerical studies (Ref. 8-3). It is not clear that this approach is optimal for the design of the 4000-MW(t) HTGR.

The goal of this study is to provide a more general approach to the analysis of xenon instability in HTGRs. This will be achieved by:

1. Identifying techniques that can be used to accurately predict the stability of a specific design without recourse to detailed numerical simulations.

2. Using these techniques to quantify any uncertainties associated with their predictions.

3. Examining procedures that can be employed to inhibit the growth of any oscillations which might occur.

During this quarter a thorough review of the literature has been completed. As a result of this review, two methods for predicting stability were selected for further examination. Both methods are based on an analysis of the eigenvalues of the set of equations obtained by Laplace transforming the linearized form of the coupled neutron flux, xenon, and iodine equations. These methods are generally referred to as λ- and μ-mode approximations in the literature (Refs. 8-4, 8-5). As a first step, the derivations of these approximations were extended for use in the multigroup calculations frequently used in HTGR design. Next their predictions were compared to the results of an explicit numerical simulation of the behavior of the axial power profile during a xenon transient. The agreement was excellent for both a realistic design and a design arbitrarily selected so as to be unstable. The details of the derivations and the results of the simulation study will be formally documented during FY-76.

REFERENCES

8-1. Dahlberg, R. C., and D. Mangan, "Linear Analysis of Xenon Instability in High-Temperature Gas-Cooled Reactors," USAEC Informal Report GAMD-7213, General Dynamics, General Atomic Division, July 29, 1966.

8-2. Dahlberg, R. C., and D. Mangan, "Non-Linear Analysis of Xenon Stability in High-Temperature Gas-Cooled Reactors," USAEC Informal Report GAMD-6924, General Dynamics, General Atomic Division, January 26, 1966.

8-3. Baxter, A. M., "3000-MW(t) HTGR Reference 2 Physics Design Report," General Atomic Report GA-A12653, to be published.

8-4. Stacey, W. M., Jr., Space Time Nuclear Reactor Kinetics, Academic Press, New York, 1969.

8-5. Radkowsky, A. (Ed.), Naval Reactor Physics Handbook, Volume I, Selected Basic Techniques, U. S. Atomic Energy Commission, 1964.

TASK 9 (189a 13119)
FUEL DEVELOPMENT AND ENGINEERING

CAPSULE P13Q

Capsule P13Q is designed to demonstrate the performance of fuel rods fabricated using candidate large HTGR processes and materials. Experiment P13Q is the GA portion of GA-ORNL cooperative experiment OF-1. The P13Q experiment began its irradiation in the E-3 position of the ORR on August 29, 1973. The estimated peak fast fluence in capsule P13Q as of February 6, 1975 was 10.3×10^{21} n/cm^2 $(E > 0.18 \text{ MeV})_{ORR}$. The last fission gas release measurement based on Kr-85m R/B was 6.8×10^{-7}, which is consistent with the very low release measured throughout the irradiation and indicates a low fuel failure fraction (<<1%). Capsule P13Q is tentatively scheduled to be removed from the ORR on February 26, 1975 with an estimated EOL exposure of 10.7×10^{21} n/cm^2 $(E > 0.18 \text{ MeV})_{ORR}$. The capsule is expected to arrive at the GA hot cell facility during late March 1975.

CAPSULES P13R and P13S

Capsules P13R and P13S are the seventh and eighth in a series of irradiation tests conducted under the AEC-sponsored HTGR Fuels and Core Development Program. The purpose of these tests is to demonstrate the integrity of reference and alternate large HTGR fuels over a wide range of irradiation conditions. Capsules P13R and P13S began irradiation in December 1973 in the E7 position of the GETR. The capsules were discharged from the GETR on October 31, 1974 and disassembly commenced at the GA hot cell facility on December 5, 1974. Removal of all fuel specimens was completed on January 28, 1975.

The objectives of the postirradiation examination and analyses are the characterization of fuel irradiation performance and the identification of potential problems and fuel particle failure modes. The major objectives of the capsule P13R and P13S irradiation tests and subsequent postirradiation examinations are summarized as follows:

1. To obtain irradiation data over a wide range of test conditions on reference and alternate large HTGR fuels.

2. To evaluate fuel rod dimensional change as a function of irradiation conditions, shim content, particle coating density, matrix type, firing temperature, and firing mode (e.g., packed bed versus cure-in-place).

3. To evaluate the effect of thermal cycling on fuel particle irradiation performance. Cell 1 of capsules P13R and P13S contains identical fuel rod specimens. Cell 1 of capsule P13S was thermal cycled 21 times from its nominal operation temperature of 1075°C to 1500°C, while cell 1 of capsule P13R was operated at a nominal temperature of 1075°C throughout its irradiation history. This test is the first attempt to simulate temperature cycling that results from load following and/or control rod pattern changes in the large HTGR. All fuel rods from these two cells will be submitted for postirradiation fission gas release measurements, and selected fuel rods will be examined metallographically to ascertain the effects of thermal cycling on fuel irradiation performance.

4. To investigate the effects of complete oxidation of bonded fuel rods on TRISO coated fissile particle integrity. The HTGR Fuels and Core Development Program has established a criterion that fissile particle failure shall be $\leq$10% after irradiation to full burnup and fluence at 1250°C followed by complete oxidation in air of bonded fuel rods at temperatures of $\leq$1000°C. To provide initial data for support of this criterion, selected rods from cell 1,

position b or c, in capsules P13R and P13S will be burned in air at $\leq$1000°C. These rods were selected because they contain no TRISO inert particles and therefore fissile particle failure fractions can be ascertained by visual examination.

5. To investigate the effect of coating variables, such as coating deposition rate and coating gas, on fuel particle irradiation performance.

6. To investigate the effects of particle attributes, e.g., faceted coatings and nonspherical fuel kernels, on fuel particle irradiation performance.

7. To investigate the irradiation performance of TRISO coated $(Th,U)O_2$ fissile particles with different Th/U ratios and coating designs.

Postirradiation examination of capsules P13R and P13S is in progress. All dosimeter vials were recovered from the capsules, with the exception of two secondary vials from capsule P13S, and submitted for chemical analysis. Dimensional measurements made on the thermal bond spacers and primary and secondary containments revealed that these components exhibited no measureable change during irradiation.

Fuel rod dimensional measurements and visual examination with an in-cell stereomicroscope of all fuel specimens have been completed. All fuel rods were removed from the capsules intact. The radiation damage incurred by the fuel rods was considered to be minimal.

Fission gas release measurements (TRIGA activation), metallography, radiography, and density gradient column separations in addition to the examinations mentioned above will be used to evaluate the postirradiation condition of fuel specimens tested in capsules P13R and P13S. The results of these examinations will be reported in future Quarterly Progress Reports.

CAPSULE P13T

The start of irradiation of capsule P13T has been delayed to April 20, 1975 because of problems encountered during the firing of the fuel bodies. During the fabrication of fuel for capsule P13T by the cure-in-place method, a strong bond between fuel rod and graphite was evidenced by the fact that fuel rods could not be removed by axial pushing with forces of 100 kg. In addition, splitting the graphite fuel holes in a manner that normally exposes the fuel rods for easy removal resulted in axial fracture of the rod. The halves of the rods could not be removed from the portion of the fuel hole without complete destruction. The cause of the bonding has been attributed to the smooth surface finish of the fuel holes in the P13T bodies.

During fabrication of fuel elements for capsule P13T the fuel holes in graphite bodies were machined to the proper size by use of a reaming device, which produced an extremely smooth and reflective wall texture. This technique was selected rather than the normal gun-drilling operation because of schedule delays and higher costs anticipated in the shop with gun-drilling capability. It is postulated that the pitch concentration at the fuel rod - graphite interface was greater than previous experience with gun-drilled holes where the fuel hole wall was not impacted with dust and highly polished. The high pitch concentration at the fuel rod - graphite interface appears to have resulted in the unacceptably strong fuel rod - graphite bond. Although the fuel rod coking yield was nominal ($\sim$25%) in the fuel rods and no obvious microstructural abnormalities were noted, the strongest reason for suspecting the surface effect is that this difficulty has not been experienced when fuel holes have been gun drilled to produce a nonreflective surface.

Four sets of fuel bodies have subsequently been manufactured in which the fuel holes were machined using a gun drill. No difficulties were encountered in removing fuel rods from the first set of bodies. These rods were used to perform quality control measurements on each of the 36 rod

types to be tested in capsule P13T. Rods fired in the second set of bodies are to be used for radial gap measurements. The third set of fuel elements also has been fired and will be irradiated in the capsule. Preirradiation fission gas release measurements were made on these bodies prior to acceptance and all were found to be within specification (i.e., Kr-85m R/B < 3 x 10^{-5} at 1100°C).

A summary description of the fuel particles used in the P13T rods is given in Table 9-1. Table 9-2 summarizes the fuel particle loadings in the fuel rods, and Table 9-3 summarizes the preliminary quality control measurements obtained from the above mentioned fuel element firings.

CAPSULES P13U and P13V

The preliminary Irradiation Test Plan for capsules P13U and P13V was submitted on February 14, 1975 to RRD to request approval-in-principle for these irradiation experiments.

FUEL TEST ELEMENT FTE-4

The test objectives for FTE-4 are incorporated in the overall Peach Bottom Phase II fuel test element program for FTE-3, FTE-4, and FTE-6 (Ref. 9-1). These three elements contained nearly identical fuel in both the fuel rods and spine samples and were irradiated for 133, 449, and 645 effective full power days, respectively. This series of FTEs offers the largest test of fuels relevant to reference and alternate HTGR fuel types that were irradiated in a He-cooled HTGR-type environment to a wide range of irradiation exposures and temperatures. Evaluation of these fuels will aid in the characterization of irradiation effects on fuel rod and fuel particle production variables and the thermal stability of a wide variety of fuel types. The examination of FTE-3 has been completed and the results have been reported in Ref. 9-2.

FTE-4 was the second in the series and was irradiated in Peach Bottom core position A14-08 at a maximum temperature of ∿1135°C and a maximum fluence of ∿1.9 x 10^{21} n/cm^2 (E ≥ 0.18 MeV). A preliminary irradiation history is presented in Ref. 9-3 and the postirradiation plan of the fuel is outlined in Ref. 9-4.

Fuel Rod Irradiation Performance

Sample Description

FTE-4 had four fuel rod types that were loaded into three H-327 graphite bodies of eight-hole telephone dial design. Fuel loadings in all three bodies were the same (see Table 9-4).

All fuel rods were fabricated by the reference Fort St. Vrain hot-injection process using natural-flake graphite filler and pitch binder followed by a 1800°C heat treatment in an alumina packed bed. The nominal dimensions of the rods were 0.490 in. in diameter and 1.94 in. long. The fuel rods in this test element that were examined and the extent of the examination are presented in Table 9-5. Most of the examination was done in body 2, which showed the highest EOL fluence [∿1.9 x 10^{21} n/cm^2 (E ≥ 0.18 MeV)] and temperature (1135°C).

Fuel Rod Postirradiation Examination

The purpose of the postirradiation examination is to determine fuel rod and fuel particle integrity and to characterize any irradiation effects. Visual examination with a stereomicroscope is used to determine fuel rod integrity. Fission gas release measurements give an estimate of the extent of fuel failure, while metallography and autoradiography characterize the fuel failure modes and thermal effects in the fuel.

TABLE 9-1

GENERAL DESCRIPTION OF COATED PARTICLES BEING TESTED IN CAPSULE P13T

Particle Batch Data Retrieval Number	Kernel		Coatings															Total Coated Particle						
				Buffer			Inner Isotropic PyC			SiC		Outer Isotropic PyC					Total Coating Thickness (μm)			Metal Loading			Heavy Metal Contamination[f]	
	Type[a]	Diameter (μm)	Type[b]	Thickness (μm)	Density (g/cm³)	Seal Coat	Thickness (μm)	Density (g/cm³)	OPTAF[c]	Thickness (μm)	Density (g/cm³)	Thickness (μm)	Coating Gas	Density (g/cm³)	Coating Rate (μm/min)	OPTAF[c]		Diameter (μm)	Density[d] (g/cm³)	Uranium (wt %)	Thorium (wt %)	Fission[e] Gas Release	Uranium[g]	Thorium[h]
Fissile Particles																								
6151-00-035	UC_2	201	TRISO	87	1.07	None	33	1.92	1.22	27	3.20	37	C_3H_6	1.85	3.85	1.17	191	577	2.29	18.86	(i)	3×10^{-7}	4×10^{-7}	$<1 \times 10^{-7}$
6151-10-015	UC_2	205	TRISO	89	1.05	None	32	1.90	1.14	30	3.22	42	C_2H_2/C_3H_6	1.85	4.12	1.11	193	596	2.22	18.88	0.31	2×10^{-6}	6×10^{-5}	$<1 \times 10^{-7}$
6151-12-015	UC_2	191	TRISO	100	1.11	Yes	23	1.93	1.15	28	3.21	43	C_2H_2/C_3H_6	1.78	4.78	1.13	193	578	2.22	16.57	0.46	4×10^{-7}	1×10^{-6}	1×10^{-5}
6151-17-015	UC_2	204	TRISO	94	1.08	None	36	1.87	1.15	37	3.21	38	C_2H_2/C_3H_6	1.81	4.11	1.11	205	613	2.38	17.67	(i)	3×10^{-6}	5×10^{-6}	$<1 \times 10^{-7}$
6151-17-025	UC_2	204	TRISO	100	1.23	None	35	1.87	1.14	30	3.20	33	C_2H_2/C_3H_6	1.84	3.57	1.14	198	602	2.29	16.50	0.35	1×10^{-6}	2×10^{-6}	$<1 \times 10^{-7}$
6151-18-015	UC_2	209	TRISO	107	1.05	None	27	1.90	1.14	39	3.20	41	C_2H_2/C_3H_6	1.81	4.44	1.14	191	594	2.36	19.29	0.36	2×10^{-6}	3×10^{-6}	$<1 \times 10^{-7}$
6151-19-015	UC_2	201	TRISO	102	1.06	None	32	1.89	1.13	33	3.21	37	C_2H_2/C_3H_6	1.82	3.90	1.15	191	589	2.34	17.88	0.42	4×10^{-6}	8×10^{-7}	1×10^{-5}
6157-02-015	$U(C,O)_2$[j]	297	TRISO	38	1.09	None	32	1.96	1.15	34	3.22	30	C_2H_2/C_3H_6	1.89	3.57	1.17	132	572	2.39	16.26	0.07	5×10^{-6}	7×10^{-6}	$<1 \times 10^{-7}$
Fertile Particles																								
6542-02-025	ThO_2	484	BISO	73	1.08	Yes	(i)	(i)	(i)	(i)	(i)	80	C_3H_6	1.91	8.50	1.06	159	784	3.59	(i)	56.18	(i)	(i)	(i)
6542-27-015	ThO_2	512	BISO	84	1.09	None	(i)	(i)	(i)	(i)	(i)	81	C_2H_2/C_3H_6	1.86	4.59	1.09	164	836	3.47	(i)	56.70	(i)	$<1 \times 10^{-7}$	4×10^{-6}
6542-29-015	ThO_2	499	BISO	81	1.18	None	(i)	(i)	(i)	(i)	(i)	76	C_2H_2/C_3H_6	1.96	4.31	1.18	157	797	3.60	(i)	59.65	(i)	$<1 \times 10^{-7}$	4×10^{-6}
6542-32-015	ThO_2	515	BISO	82	1.12	Yes	(i)	(i)	(i)	(i)	(i)	82	C_2H_2/C_3H_6	1.84	4.65	1.10	163	840	3.45	(i)	57.32	(i)	5×10^{-7}	2×10^{-5}
6542-33-025	ThO_2	505	BISO	81	1.08	None	(i)	(i)	(i)	(i)	(i)	66	C_2H_2/C_3H_6	1.86	4.31	1.13	147	802	3.66	(i)	61.29	(i)	1×10^{-5}	7×10^{-6}
6542-34-015	ThO_2	505	BISO	84	1.09	None	(i)	(i)	(i)	(i)	(i)	80	C_2H_2/C_3H_6	1.86	6.40	1.12	164	839	3.48	(i)	57.80	(i)	2×10^{-7}	3×10^{-6}
6542-35-015	ThO_2	505	BISO	86	1.09	None	(i)	(i)	(i)	(i)	(i)	70	C_2H_2/C_3H_6	1.94	5.60	1.13	156	824	3.57	(i)	58.71	(i)	2×10^{-7}	1×10^{-6}
6542-36-015	ThO_2	509	BISO	82	1.11	None	(i)	(i)	(i)	(i)	(i)	76	C_2H_2/C_3H_6	1.87	5.22	1.15	158	824	3.54	(i)	57.56	(i)	5×10^{-7}	5×10^{-6}
Inert Particles																								
6351-01-020	C	(i)	TRISO	(i)	(i)	None	29	1.76	1.09	29	3.22	36	C_3H_6	1.75	1.06	1.12	(i)	573	1.83	(i)	(i)	(i)	(i)	(i)

[a] Kernels are VSM UC_2 and sol-gel ThO_2 except where noted.

[b] TRISO denotes a coating design with a SiC layer and BISO denotes a particle with no SiC layer.

[c] Optical anisotropy factor, relative units.

[d] Determined using air pycnometer.

[e] Release rate/birth rate for Kr-85m at 1100°C.

[f] Determined by leach test.

[g] Units are gU/gU for fissile particles and gU/gTh for fertile particles.

[h] Units are gTh/gU for fissile particles and gTh/gTh for fertile particles.

[i] Not applicable.

[j] Weak-acid-resin kernel.

TABLE 9-2

PARTICLE LOADINGS FOR CAPSULE P13T

Rod Type	Fissile				Fertile				Inert[a]			Shim			Total Particle Weight (g)	Total Particle Volume Fraction[b]
	Data Retrieval Number	Weight (g)	Volume Fraction[b]	Number of Particles	Data Retrieval Number (6542-)	Weight (g)	Volume Fraction[b]	Number of Particles	Weight (g)	Volume Fraction[b]	Number of Particles	Batch Number	Weight (g)	Volume Fraction[b]		
1-1A1	6151-17-015	0.808	0.062	2800	36-015	4.637	0.237	4500	0.769	0.076	2900	F0215	2.175	0.575	8.389	0.575
1-1A2	6151-17-015	0.753	0.054	2600	36-015	3.428	0.164	3300	1.074	0.102	4200	F0215	2.908	0.250	6.719	0.570
1-1A3	6151-17-015	1.349	0.048	4700	36-015	5.681	0.136	5500	1.883	0.087	7200	F0215	6.979	0.300	15.892	0.571
1-1A4	6151-17-015	1.154	0.041	4000	36-015	5.217	0.125	5000	1.019	0.047	3900	F0215	8.142	0.350	15.532	0.563
1-1B1	6151-12-015	0.862	0.070	3800	32-015	4.656	0.245	4300	0.655	0.065	2500	F0218	2.175	0.200	8.348	0.580
1-1B2	6151-12-015	0.804	0.061	3600	32-015	3.442	0.169	3200	1.034	0.096	3900	F0218	2.908	0.250	8.188	0.576
1-1B3	6151-12-015	1.439	0.055	6400	32-015	5.705	0.140	5300	1.709	0.079	6500	F0215	6.979	0.300	15.832	0.574
1-1B4	6151-12-015	1.231	0.047	5500	32-015	5.239	0.129	4900	0.917	0.042	3500	F0215	8.142	0.350	15.530	0.568
1-1C1	6151-17-025	0.866	0.068	3300	27-015	4.707	0.246	4400	0.627	0.062	2400	F0176	2.153	0.200	8.352	0.576
1-1C2	6151-17-025	0.807	0.060	3100	27-015	3.480	0.170	3300	1.226	0.113	4700	F0199	2.672	0.250	8.185	0.593
1-1C3	6151-17-025	1.444	0.053	5500	27-015	5.767	0.141	5400	1.793	0.083	6800	F0176	6.908	0.300	15.913	0.577
1-1C4	6151-17-025	1.237	0.046	4700	27-015	5.296	0.129	5000	1.621	0.075	6200	F0199	7.481	0.350	15.635	0.600
2-2A1	6151-17-025	0.950	0.043	3600	27-015	3.076	0.092	2900	1.516	0.083	5600	F0218	6.674	0.350	12.163	0.567
2-2A2	6151-00-035	0.894	0.043	3900	02-025	3.457	0.106	3600	1.083	0.065	4100	F0218	6.239	0.350	11.673	0.565
2-2B1	6151-18-015	0.813	0.036	3100	35-015	2.971	0.086	2800	1.638	0.092	6200	F0176	6.606	0.350	12.028	0.564
2-2B2	6151-10-015	0.893	0.044	3600	34-015	3.360	0.107	3100	1.604	0.097	6100	F0199	5.732	0.350	11.588	0.598
2-2C1	6157-02-015	0.965	0.042	4100	27-015	3.076	0.092	2900	1.554	0.084	5600	F0218	6.674	0.350	12.197	0.567
2-2C2	6157-02-015	0.915	0.046	4100	33-025	3.169	0.096	3200	1.126	0.075	4700	F0221	6.239	0.350	11.559	0.567
2-3A1	6151-17-015	1.136	0.049	4000	29-015	3.621	0,104	3800	2.033	0.115	7700	F0215	5.721	0.300	12.511	0.568
2-3A2	6151-10-015	1.291	0.060	5200	33-025	4.399	0.124	4500	1.520	0.086	5800	F0215	5.721	0.300	12.930	0.570
2-3B1	6151-18-015	1.041	0.046	4000	31-015	3.768	0.108	3700	2.044	0.115	7800	F0176	5.663	0.300	12.516	0.569
2-3B2	6151-19-015	1.363	0.060	7400	36-015	4.684	0.137	7400	1.738	0.098	6600	F0199	5.256	0.300	13.041	0.595
2-3C1	6157-02-015	1.235	0.053	5300	34-015	3.737	0.111	3500	1.840	0.104	7000	F0221	5.721	0.300	12.533	0.568
2-3C2	6157-02-015	1.500	0.065	6400	34-015	4.664	0.138	4300	1.022	0.058	3900	F0221	4.721	0.300	12.907	0.561
2-4A1	6151-12-015	1.089	0.083	4900	35-015	3.853	0.183	3700	0.564	0.052	2142	F0215	2.908	0.250	8.413	0.568
2-4A2	6151-18-015	1.075	0.077	3500	34-015	3.495	0.170	3200	0.787	0.073	3000	F0218	2.908	0.250	8.264	0.570
2-4A3	6151-19-015	1.345	0.097	5600	36-015	4.451	0.213	7000	0.699	0.065	2700	F0221	2.326	0.200	8.822	0.575
2-4A4	6151-00-035	1.509	0.119	6600	02-025	6.604	0.333	7000	-	-	-	F0218	1.312	0.121	9.426	0.573
2-4B1	6151-17-025	1.093	0.081	4200	33-025	3.691	0.171	3700	0.685	0.063	2600	F0176	2.879	0.250	8.347	0.565
2-4B2	6151-10-015	1.097	0.084	4500	29-015	3.386	0.159	3500	1.094	0.097	4000	F0199	2.672	0.250	8.203	0.590
2-4B3	6151-17-015	1.361	0.097	4700	31-015	4.470	0.210	4400	0.654	0.060	2500	F0176	2.303	0.200	8.787	0.567
2-4B4	6151-18-015	1.475	0.113	4800	27-015	6.543	0.342	6200	-	-	-	F0199	1.426	0.135	9.368	0.590
2-4C1	6157-02-015	1.109	0.079	4700	31-015	3.946	0.185	3900	0.609	0.056	2300	F0221	2.908	0.250	8.571	0.570
2-4C2	6157-02-015	1.274	0.090	5400	27-015	3.563	0.174	3400	0.604	0.056	2300	F0221	2.908	0.250	8.348	0.570
2-4C3	6157-02-015	1.478	0.105	6300	35-015	4.364	0.207	4200	0.683	0.063	2600	F0221	2.326	0.200	8.852	0.575
2-4C4	6157-02-015	1.749	0.133	7500	29-015	6.220	0.313	6500	-	-	-	F0221	1.462	0.134	9.430	0.580

[a] The inert particle batch 6542-01-020 was used in all fuel rod types.

[b] Based on nominal fuel rod dimensions.

TABLE 9-3

DESCRIPTION OF FUEL RODS BEING TESTED IN CAPSULE P13T

Capsule Identification	Fuel Rod Data Retrieval Number (7161-008-)	Coated Particles[a]				Shim Particle Type	Green Rod Dimensions (cm)		Green Rod Packing Fraction[d]	Matrix					Fuel Loading Uniformity[j]		Heavy Metal Contamination[k] (g heavy metal/g heavy metal)		Fission Gas Release[l]		Push-out Force on Fuel Rod Stack[n] (kg)
		Fissile		Fertile						Filler[e] (wt %)	Apparent Fired Density[d,f] (g/cm³)	Macro-porosity[g,h] (%)	Coke Yield[i]								
		Type[b]	Data Retrieval Number	Type[c]	Data Retrieval Number (6542-)		Length	Diameter					Rods from Tubes[g]	Rods from Bodies[f]	U-235	Th-232	Rods from Tubes[g]	Rods from Bodies[f]	Rods from Tubes[g]	Fuel Body[m]	
1-1A1	01-9	UC_2	6151-17-015	ThO_2	36-015	1099[o]	3.012	1.573[p]	0.542	31.1	0.65	36.1	30.6	33.6	1.03	1.02	1.2×10^{-4}	$<9.0 \times 10^{-7}$	2.0×10^{-6}	2.3×10^{-7} (83-001-01-3)	113
1-1A2	04-3	UC_2	6151-17-015	ThO_2	36-015	1099[o]	3.067	1.573	0.562	31.1	0.66	40.3	32.2	30.6	1.01	1.06	$<2.5 \times 10^{-6}$		1.7×10^{-6}		
1-1A3	07-9	UC_2	6151-17-015	ThO_2	36-015	1099[o]	6.057	1.575	0.571	31.1	0.67	37.3	29.8	30.9	1.03	1.03	$<1.5 \times 10^{-6}$		5.3×10^{-7}		
1-1A4	10-6	UC_2	6151-17-015	ThO_2	36-015	1099[o]	6.098	1.574	0.560	31.1	0.64	37.3		28.5	1.02	1.03	$<1.6 \times 10^{-6}$		9.8×10^{-7}		
1-1B1	02-10	UC_2	6151-12-015	ThO_2	32-015	1099[o]	3.050	1.572[p]	0.541	39.4	0.68	34.6	24.0	22.1	1.01	1.00	$<2.0 \times 10^{-6}$		$<1.0 \times 10^{-7}$		99
1-1B2	05-20	UC_2	6151-12-015	ThO_2	32-015	1099[o]	3.040	1.572	0.576	39.4	0.70	37.0	24.2	24.3	1.02	1.02	1.3×10^{-5}		3.8×10^{-6}		
1-1B3	08-11	UC_2	6151-12-015	ThO_2	32-015	1099[o]	6.115	1.573	0.570	39.2	0.67	43.4	23.5	21.8	1.00	1.03	$<1.5 \times 10^{-6}$		1.4×10^{-6}		
1-1B4	11-7	UC_2	6151-12-015	ThO_2	32-015	1099[o]	6.124	1.573	0.564	39.4	0.68	38.5	23.6	21.6	1.02	1.00	$<1.6 \times 10^{-6}$		3.6×10^{-7}		
1-1C1	03-12	UC_2	6151-17-025	ThO_2	27-015	TS-1240X	3.038	1.572[p]	0.539	40.1	0.76	25.8	29.4	28.3	1.01	1.00	$<1.9 \times 10^{-6}$		1.8×10^{-7}		32
1-1C2	06-2	UC_2	6151-17-025	ThO_2	27-015	X4029A	3.031	1.572	0.594	40.1	0.78	29.0	31.0	30.8	1.03	1.02	9.0×10^{-5}		1.4×10^{-6}		
1-1C3	09-12	UC_2	6151-17-025	ThO_2	27-015	TS-1240X	6.079	1.573	0.577	40.1	0.79	26.7	31.0	32.0	1.02	1.00	$<1.5 \times 10^{-6}$		1.3×10^{-6}		
1-1C4	12-1	UC_2	6151-17-025	ThO_2	27-015	X4029A	6.053	1.574	0.601	40.1	0.80	33.3	31.2	32.8	1.03	1.01	$<1.7 \times 10^{-6}$		2.7×10^{-7}		
2-2A1	13-2	UC_2	6151-17-025	ThO_2	27-015	1099[o]	4.985	1.574	0.569	31.1	0.66	40.5	25.2	30.3	1.01	1.04	$<2.8 \times 10^{-6}$	$<6.6 \times 10^{-7}$	4.1×10^{-6}	1.7×10^{-5} (83-001-02-3)	45
2-2A2	16-12	UC_2	6151-00-035	ThO_2	02-025	1099[o]	5.007	1.573[p]	0.525	31.1	0.63	41.9	26.8	27.3	1.01	1.03	$<2.5 \times 10^{-6}$		7.6×10^{-7}		
2-2B1	14-5	UC_2	6151-18-015	ThO_2	35-015	TS-1240X	4.976	1.573	0.565	31.1	0.70	38.3	32.4	32.2	1.00	1.05	$<2.8 \times 10^{-6}$		4.8×10^{-7}		23
2-2B2	17-14	UC_2	6151-10-015	ThO_2	34-015	X4029A	5.023	1.573[p]	0.554	31.1	0.68	43.2	29.2	29.8	1.04	1.05	1.9×10^{-4}		5.0×10^{-7}		
2-2C1	15-3	$U(C,O)_2$	6157-02-015	ThO_2	27-015	1099[o]	4.977	1.573	0.571	31.1	0.63	43.1	27.8	28.6	1.04	1.04	$<2.8 \times 10^{-6}$		2.7×10^{-5}		41
2-2C2	18-4	$U(C,O)_2$	6157-02-015	ThO_2	23-025	1099[o]	5.030	1.573[p]	0.515	31.1	0.64	33.8	24.7	27.6	1.06	1.07	$<2.5 \times 10^{-6}$		1.9×10^{-6}		
2-3A1	19-6	UC_2	6151-17-015	ThO_2	29-015	1099[o]	5.018	1.573	0.564	39.4	0.68	33.0	24.4	21.5	1.02	1.06	$<2.1 \times 10^{-6}$	6.9×10^{-5}[q]	9.1×10^{-7}	2.8×10^{-6} (83-001-03-3)	91
2-3A2	22-6	UC_2	6151-10-015	ThO_2	33-025	1099[o]	5.035	1.572	0.565	39.4	0.65	32.1	24.6	17.9	1.04	1.04	2.8×10^{-5}	6.1×10^{-5}[r]	3.9×10^{-7}		
2-3B1	20-8	UC_2	6151-18-015	ThO_2	31-015	TS-1240X	5.027	1.572	0.564	39.4	0.70	25.1	26.0	25.0	1.03	1.03	$<2.5 \times 10^{-6}$		2.8×10^{-7}		45
2-3B2	23-4	UC_2	6151-19-015	ThO_2	36-015	X4029A	5.020	1.572	0.591	39.2	0.70	29.6	25.4	24.7	1.02	1.06	$<1.8 \times 10^{-6}$		2.3×10^{-7}		
2-3C1	21-5	$U(C,O)_2$	6157-02-015	ThO_2	34-015	1099[o]	4.969	1.572	0.570	39.2	0.69	34.8	25.2	23.9	1.04	1.04	4.6×10^{-5}		2.0×10^{-6}		84
2-3C2	24-10	$U(C,O)_2$	6157-02-015	ThO_2	34-015	1099[o]	4.975	1.572	0.562	39.4	0.64	36.3	22.7	21.6	1.05	1.03	$<1.8 \times 10^{-6}$		1.5×10^{-6}		
2-4A1	25-6	UC_2	6151-12-015	ThO_2	35-015	1099[o]	3.063	1.574	0.563	40.1	0.77	28.7	27.6	30.8	1.01	1.02	$<1.9 \times 10^{-6}$	5.5×10^{-4}	2.7×10^{-7}	3.5×10^{-7} (83-001-04-3)	18
2-4A2	28-6	UC_2	6151-18-015	ThO_2	34-015	1099[o]	3.057	1.574	0.566	40.1	0.77	31.3	30.7	31.9	1.01	1.03	$<2.4 \times 10^{-6}$		3.1×10^{-7}		
2-4A3	31-7	UC_2	6151-19-015	ThO_2	36-015	1099[o]	3.061	1.574	0.570	40.1	0.77	30.0	28.8	30.0	1.00	1.04	$<1.9 \times 10^{-6}$		2.7×10^{-7}		
2-4A4	34-7	UC_2	6151-00-035	ThO_2	02-025	1099[o]	3.025	1.573[p]	0.538	40.1	0.64	33.1	27.6	33.7	1.07	1.03	$<1.4 \times 10^{-6}$		4.5×10^{-7}		
2-4B1	26-12	UC_2	6151-17-025	ThO_2	33-025	TS-1240X	3.006	1.573	0.571	40.1	0.79	28.1	29.1	34.0	1.00	1.02	$<2.2 \times 10^{-6}$		3.9×10^{-7}		18
2-4B2	29-2	UC_2	6151-10-015	ThO_2	29-015	X4029A	3.024	1.574	0.596	40.1	0.79	29.6	31.9	32.2	1.03	1.02	1.5×10^{-4}		2.5×10^{-7}		
2-4B3	32-15	UC_2	6151-17-015	ThO_2	31-015	TS-1240X	3.068	1.573	0.562	40.1	0.78	34.5	34.5	33.1	1.02	1.00	$<1.6 \times 10^{-6}$		1.1×10^{-6}		
2-2B4	35-3	UC_2	6151-18-015	ThO_2	27-015	X4029A	3.021	1.573[p]	0.562	40.1	0.60	25.9	29.3	31.9	1.08	1.04	$<1.4 \times 10^{-6}$		1.3×10^{-7}		
2-4C1	27-4	$U(C,O)_2$	6157-02-015	ThO_2	31-015	1099[o]	3.070	1.573	0.564	40.1	0.75	31.8	28.2	30.9	1.04	1.03	$<2.2 \times 10^{-6}$		1.4×10^{-6}		18
2-4C2	30-1	$U(C,O)_2$	6157-02-015	ThO_2	27-015	1099[o]	3.043	1.573	0.569	40.1	0.75	32.7	28.5	28.9	1.04	1.04	$<2.4 \times 10^{-6}$		2.2×10^{-6}		
2-4C3	33-9	$U(C,O)_2$	6157-02-015	ThO_2	35-015	1099[o]	3.046	1.573	0.574	40.1	0.76	38.0	28.0	29.1	1.02	1.04	$<2.1 \times 10^{-6}$		2.2×10^{-6}		
2-4C4	36-8	$U(C,O)_2$	6157-02-015	ThO_2	29-015	1099[o]	3.046	1.573[p]	0.541	40.1	0.60	34.9	26.6	30.0	1.01	1.01	$<1.3 \times 10^{-6}$		2.3×10^{-6}		

[a] All fuel rod types except 2-4B1, 2-4B4, and 2-4C4 contain TRISO inert batch 6542-01-025.

[b] All fissile particles are TRISO coated.

[c] All fertile particles are BISO coated

[d] Calculated from rod and mean particle data.

[e] Measurement made on companion greed rods.

[f] Measurement made on companion rods fired in QC graphite bodies.

[g] Measurements made on companion rods fired in graphite tubes.

[h] Determined from metallographic cross section.

[i] Grams coke divided by initial grams of coke plus additives.

[j] Determined by gamma counting both ends of rod and calculating ratio of maximum and mean values.

[k] Determined by hydrolysis test; "<" denotes the amount is below the limits of detection of the apparatus. If detectable quantity, the value was corrected for total conversion of thorium oxide to thorium carbide.

[l] Release rate/birth rate for Kr-85m at 1100°C.

[m] Measurement made on cured-in-place fuel body containing all rods for that body.

[n] Each value is the total force required to push out all fuel rods in each hole.

[o] Impregnated with a 95% furfuryl alcohol based material.

[p] Thermocouple rod; central hole [approximately 0.34 cm (0.13 in.) in diameter through entire length of rod).

[q] First measurement.

[r] Second measurement.

TABLE 9-4
FTE-4 COMPOSITION AND LOCATION OF BONDED FUEL RODS[a]

Body	Hole	FOD No.	FMB. No.	Kernel		Coating Type	As Manufactured Coating Parameters							
				Type	Nominal Diam (μm)		Nominal Thickness (μm)					OPyC Density (g/cm^3)	OPyC OPTAF	SiC Density (g/cm^3)
							Buffer	IPyC	SiC	OPyC	Total			
Fissile Particle														
1,2,3	1,2	ED1258BIL(A)SL	4000-355	UO_2	201	TRISO	53	27	23	37	140	1.80	1.07	3.20
	3,4	ET1272BIL(A)SL	4000-357	$(Th,U)C_2$[b]	211	TRISO	56	28	27	44	147	1.80	1.06	3.19
	5,6	ET1272BIL(A)SL	4000-357	$(Th,U)C_2$	211	TRISO	56	28	27	44	147	1.80	1.06	3.19
	7,8	E1274BIL(A)SL	4000-358	UC_2	99	TRISO	57	27	27	33	137	1.79	1.11	3.20
Fertile Particle														
1,2,3	1,2	TO1236BL	4000-339	ThO_2	410	BISO	62	--	--	81	142	1.78	1.09	--
	3,4	T1254BL	4000-345	ThC_2	351	BISO	63	--	--	69	135	1.81	1.15	--
	5,6	CT6A56L	4000-335	ThC_2	360	TRISO	56	26	28	41	145	1.79	1.13	3.20
	7,8	T1254BL	4000-345	ThC_2	351	BISO	63	--	--	69	135	1.81	1.15	--

[a] All values are from data retrieval (FMB).

[b] Th/U ratio = 2.75.

Visual Examination. Representative fuel rods were examined and photographed immediately after unloading using the Kollmorgan periscope. Rods selected for further examination were examined with the Bausch and Lomb stereomicroscope. In all cases irradiation-induced damage of the rods was low except for slight debonding of particles at the end caps and spalling at the edges. In all cases the rods showed unloading damage. This damage was characterized by striations on the sides of the rods that, in many cases, caused extensive debonding and breaking of particles on the surface. Stereophotographs of four rods that represent the four fuel types from body 2 (Figs. 9-1 through 9-4)* give a clear idea of the extent of this damage. Particles that were clearly broken on the surface were counted for each rod and are tabulated in Table 9-5.

Fission Gas Release. Kr-85m R/B values were determined from fission gas release measurements performed at Triga II at 1100°C. The values are given in Table 9-5. If it is assumed the fission gas release percentage for a failed fissile particle is 1% and the failed fertile particles contribute negligible gas release at their low burnup (~0.4% FIMA), the fissile failure fraction is low (<1%) in all the fuel blends tested.

Several rods (2-1-7, 2-2-7, and 2-7-7) that had extensive surface damage caused by unloading showed higher fission gas release measurements than companion rods (2-1-8 and 2-8-7), which indicates that the unloading damage was a significant contribution to the R/B measurements.

Metallography. Metallography was done on at least one fuel rod from each fuel blend; the results are given on Table 9-5. All of these rods were located in the center of body 2, which had the highest fast fluence [$\sim 1.9 \times 10^{21}$ n/cm^2 (E $\geq$ 0.18 MeV)] and temperature (1135°C). Radial cross sections of each of these rods and high magnification microphotographs of the matrix are shown in Figs. 9-5 through 9-9. In general, the fuel had little coating failure, and there was no matrix cracking or interaction.

*Figures are at end of Section 9.

TABLE 9-5
SUMMARY OF POSTIRRADIATION EXAMINATION OF FTE-4 FUEL RODS

Fuel Rod I.D. No.[a]	Fissile Particle[b]	Fertile Particle	Peak EOL Fuel Temp[c] (°C)	Fast Fluence ($\times 10^{21}$ n/cm^2) (E > 0.18 MeV)	FIMA Fissile[d] (%)	Fission Gas Release (R/B)[e]	Visual Appearance	Broken Particles on Surface	Dimensional Change[f] (%)		Fissile Particle				Fertile Particle			
									Diameter	Length	OPyC Failure (%)	95% Confidence Limits P (%)	SiC Failure (%)	95% Confidence Limits P (%)	OPyC Failure (%)	95% Confidence Limits P (%)	• SiC Failure (%)	95% Confidence Limits P (%)
2-1-7[g]	201-μm UO_2 TRISO	410-μm ThO_2 BISO	1135	1.87		1×10^{-3}	Good	43			0	$0.0 \leq P \leq 8.3$	4.5	$0.3 \leq P \leq 15.7$	0	$0.06 \leq P \leq 9.2$	—	—
2-1-8	201-μm UO_2 TRISO	410-μm ThO_2 BISO	1135	1.87		2.9×10^{-4}	Excellent	19			—	—	—	—	—	—	—	—
2-2-7	201-μm UO_2 TRISO	410-μm ThO_2 BISO	1135	1.87		1.5×10^{-3}	Good	57			0.6	$0.1 \leq P \leq 4.1$	12.9	$9.8 \leq P < 21.7$	0	$0.0 \leq P < 2.0$	—	—
2-3-7	211-μm $(Th,U)C_2$ TRISO	351-μm ThC_2 BISO	1135	1.87		3.6×10^{-5}	Broken in two	—			—	—	—	—	—	—	—	—
2-3-8	211-μm $(Th,U)C_2$ TRISO	351-μm ThC_2 BISO	1135	1.87		1.5×10^{-5}	Excellent	0			0.1	$0.0 \leq P \leq 0.9$	0.1	$0.0 \leq P \leq 0.9$	0	$0.0 \leq P < 2.2$	—	—
2-4-7	211-μm $(Th,U)C_2$ TRISO	351-μm ThC_2 BISO	1135	1.87		3.6×10^{-6}	Excellent	1			—	—	—	—	—	—	—	—
2-4-8	211-μm $(Th,U)C_2$ TRISO	351-μm ThC_2 BISO	1135	1.87		2.7×10^{-6}	—	—			—	—	—	—	—	—	—	—
2-4-9	211-μm $(Th,U)C_2$ TRISO	351-μm ThC_2 BISO	1135	1.85		3.5×10^{-6}	—	—			—	—	—	—	—	—	—	—
2-4-10	211-μm $(Th,U)C_2$ TRISO	351-μm ThC_2 BISO	1132	1.82		4.2×10^{-6}	—	—			—	—	—	—	—	—	—	—
2-5-7	211-μm $(Th,U)C_2$ TRISO	360-μm ThC_2 TRISO	1135	1.87		1.6×10^{-5}	Excellent	3			5.0	$2.4 \leq P \leq 10.0$	1.4	$0.4 \leq P \leq 5.1$	4.0	$2.0 \leq P \leq 8.0$	0	$0.05 \leq P < 2.1$
2-6-7	211-μm $(Th,U)C_2$ TRISO	360-μm ThC_2 TRISO	1135	1.87		5.1×10^{-6}	Good	6			—	—	—	—	—	—	—	—
2-7-7	99-μm UC_2 TRISO	351-μm ThC_2 BISO	1135	1.87		1.3×10^{-4}	Good Cracked	10			—	—	—	—	—	—	—	—
2-8-7	99-μm UC_2 TRISO	351-μm ThC_2 BISO	1135	1.87		7.1×10^{-5}	Excellent	0			0.7	$0.1 \leq P \leq 1.6$	0.5	$0.2 \leq P \leq 2.0$	1.2	$0.4 \leq P \leq 3.5$	—	—

[a] Body no. - hole no. - position no.
[b] Th/U ratio = 2.75. Refer to Table 9-4.
[c] Calculated.
[d] Under preparation.
[e] Corrected for steady state.
[f] Under evaluation.
[g] Radial section; all other rods were longitudinal sections.

Fuel rods 2-3-8 [(Th,U)C_2 TRISO/ThC_2 BISO], 2-5-7 [(Th,U)C_2 TRISO/ThC_2 TRISO] and 2-8-7 (UC_2 TRISO/ThC_2 BISO) all showed excellent performance. Failure fractions were low and were attributed mostly to polishing damage. The TRISO particles all showed buffer densification and debonding. No fuel kernel migration or metallic fission product attack was observed. Representative photomicrographs of particles are shown in Figs. 9-10 through 9-12.

Several of the rods (2-8-7, 2-1-7, and 2-2-7) showed a nonhomogeneity in particle loading. Rods 2-1-7 and 2-2-7, which contained a UO_2 TRISO/ThO_2 BISO blend, showed significant performance defects. In both of these cases a high concentration of fissile particles in one area caused a high-temperature spot ("hot-spot"). This in turn caused the UO_2 kernels to deform plastically, migrate in random directions, and at times extrude through the buffer (see Fig. 9-13). Fissile particles outside of this "hot spot" area behaved normally, as shown in Fig. 9-14.

A simple analysis of a radial cross section of fuel rod 2-1-7 was done to better understand the extent of this nonhomogeneity. A count of the number of UO_2 fissile and ThO_2 fertile particles was made for four equal pie-shaped regions. A summary of these results is given in Table 9-6.

TABLE 9-6
ANALYSIS OF NONHOMOGENEITY OF FUEL ROD 2-1-7

	Fissile Particles	Fertile Particles
Section 1, %	40	60
Section 2, %	12	88
Section 3, %	7	93
Section 4, %	66	62
Total loading, %	39	62
Total particles	98	155
Theoretical loading, %	47	53

From the analysis it can be seen that there is a slight discrepancy in the total real loading to the theoretical loading at this plane. However, of greater importance is the considerable nonhomogeneity in loading in the various sections. Almost all the fissile particles were located in sections 1 and 4 and near the outer edge of the rod. In these regions the behavior of the UO_2 kernels was similar to that of the particles in Fig. 9-13.

Another rod (2-2-7) that contained the same UO_2 TRISO/ThO_2BISO blend was also analyzed for nonhomogeneity in an axial cross section and divided into 12 sections is shown in Table 9-7.

TABLE 9-7
ANALYSIS OF NONHOMOGENEITY OF FUEL ROD 2-2-7

Section	Number of Particles	
	Fissile	Fertile
1	80	21
2	21	62
3	28	53
4	16	42
5	54	69
6	15	95
7	10	120
8	24	90
9	12	35
10	6	50
11	6	50
12	8	51
Total	280	738
Total loading, %	27.5	72.5
Theoretical loading, %	47	53

1	2	3	4
5	6	7	8
9	10	11	12

Examination of these data shows that almost 50% of the fissile particles are located in sections 1 and 5, which is a gross nonhomogeneity. Metallographic examination showed behavior of the UO_2 kernels similar to those in the "hot spot" in rod 2-1-7.

No SiC failures were attributed to either of these "hot spots." At higher temperatures and burnups where fission product attack is more pronounced, this could be a problem.

Autoradiography. Beta-gamma autoradiography was used to show fission product migration into the graphite fuel bodies. Cross-sectional slices were cut from the fuel bodies and then ground parallel with abrasive paper to ∿1/8 in. Slices were then placed on top of Kodak Industrial M type film and exposed for 70 min.

Figures 9-15 through 9-17 show the autoradiography of the three fuel body slices. In bodies 2 and 3, which had relatively high temperatures, the greatest release was from holes 1 and 2 that contained the UO_2 TRISO/ThO_2 BISO fuel. The TRISO (2.75 Th,U)C_2/TRISO ThC_2 in holes 5 and 6 had the lowest release, as would be expected. Body 1, which had relatively lower temperatures than bodies 2 and 3, showed relatively little fission product release. All these results are consistent with FTE-3 results.

Thermal Stability Samples

Test Configuration

Thermal stability samples were contained in both type 1 and type 2 crucibles (Figs. 9-18 through 9-20). These crucibles were loaded into a 1.1-in.-diameter hole in the center of the fuel bodies (see Table 9-8). The types of fuels examined in these crucibles are also listed in Table 9-8.

TABLE 9-8

FTE-4 THERMAL STABILITY SPINE SAMPLES

Position[a]	Batch Number	Particle Type
1-G-1	4000-300	UC_2 BISO
1-G-7	4503-63	UC_2 TRISO
1-G-13	4423-3	UC_2 TRISO
1-G-19	4000-229	$(Th,U)C_2$ BISO
1-G-25	4503-27	$(Th,U)C_2$ TRISO
1-G-31	4423-35	$(Th,U)C_2$ BISO
1-G-37	4423-53	$(Th,U)C_2$ TRISO
1-H-49	4000-238	ThC_2 BISO
1-H-55	4503-25	ThC_2 TRISO
1-H-61	4413-149	ThC_2 BISO
1-H-67	4903-5	UC_2 BISO
1-H-73	4632-137	$(Th,U)C_2$ BISO
1-H-79	4493-149	ThO_2 BISO
1-H-85	4000-195	ThC_2 TRISO
1-H-4	4000-300	UC_2 BISO
2-16-1	4000-238	ThC_2 BISO
2-16-2	4000-225	ThC_2 BISO
2-16-3	4000-242	ThC_2 TRISO
2-16-4	4000-195	ThC_2 TRISO
2-16-5	4503-25	ThC_2 TRISO
2-16-6	4493-149	ThO_2 BISO
2-22-1	4423-33	$(Th,U)C_2$ BISO
2-22-2	4423-35	$(Th,U)C_2$ BISO
2-22-3	4423-41	$(Th,U)C_2$ TRISO
2-22-4	4423-53	$(Th,U)C_2$ TRISO
2-22-5	4000-211	$(Th,U)C_2$ TRISO

TABLE 9- (Continued)

Position[a]	Batch Number	Particle Type
2-22-6	4000-200	$(Th,U)C_2$ TRISO
2-28-1	4413-149	ThC_2 BISO
2-28-2	4413-127	ThC_2 BISO
2-28-3	3592-35	$(Th,U)C_2$ TRISO
2-28-4	4423-3	UC_2 TRISO
2-28-5	4413-137	UC_2 TRISO
2-28-6	4413-67	UO_2 TRISO
2-4-1	4000-246	UC_2 BISO
2-4-2	4000-300	UC_2 BISO
2-4-3	4902-5	UC_2 BISO
2-4-4	4503-63	UC_2 TRISO
2-4-5[b]	4000-302	UC_2 TRISO[c]
2-4-6	4503-59	UO_2 BISO
2-10-1	4000-229	$(Th,U)C_2$ BISO
2-10-2	4000-227	$(Th,U)C_2$ BISO
2-10-3	4000-232	$(Th,U)C_2$ BISO
2-10-4	4632-137	$(Th,U)C_2$ BISO
2-10-5	4503-27	$(Th,U)C_2$ TRISO
2-10-6	4503-53	$(Th,U)O_2$ BISO

[a] Crucible type - crucible number - hole number; all crucibles were located in body 3.

[b] Selected for initial examination. All other samples will be saved as historical samples until end of the the PIE examination.

[c] 100 μm (VSM)

The two types of crucibles were used to give both an isothermal experiment (i.e., type 2) and an experiment that had similar irradiation conditions but a constant high thermal gradient (i.e., type 1). This thermal gradient was achieved in the type 1 crucibles by placing one particle in each hole of the small inner crucibles (Fig. 9-19) and then packing TRISO fuel in the void space of the outer crucible. Samples in the type 2 crucible were simply loaded into the six small holes, which guaranteed a relatively isothermal condition for all the particles in a particular hole. Only one sample from a type 2 crucible has been examined to date (i.e., TS4-5).

Spine Sample Postirradiation Examination

Postirradiation examination of the spine samples included visual examination, radiography, and metallography.

Visual Examination. Thermal stability sample TS4-5 containing the 100-μm (VSM) UC_2 TRISO particles (Batch 4000-302) looked excellent under examination with the Bausch and Lomb stereomicroscope. There were no observed coating failures. Figure 9-21 is a photograph of representative particles.

Radiography. Radiographs of two sets of particles, each set containing 20 particles, were taken of spine sample TS4-5. No failures were observed in either case. Figure 9-22 is a photograph of one of these radiographs.

Metallography. Metallography of spine sample TS4-5 is represented in Fig. 9-23. The particles looked excellent in all cases. No SiC failures were observed and the 2.7% OPyC failures were attributed to polishing. Buffer densification and debonding were evident in all cases.

Discussion and Conclusions

FTE-4 fuel performance was consistent with current HTGR design data (Ref. 9-5) and the results from the previous companion test element FTE-3

(Ref. 9-2). Irradiation-induced fuel failure was low and there was no matrix-particle interaction. Except for the UO_2 kernel movement caused by the gross nonhomogeneity of several fuel rods, there were no thermochemical cases of either SiC attack by metallic fission products or kernel migration. This is as predicted for these low burnups (30% FIMA fissile and 0.4% FIMA fertile) and low temperatures ($\sim$1135°C).

In summary, the following conclusions and observations can be made from the postirradiation examination of the fuel in FTE-4:

1. Physical integrity and appearance of all the fuel rods examined were good except for unloading damage.

2. Irradiation-induced failure of the fuel from fission gas release measurement and metallography was low (<1%) at peak fluence and temperature conditions of 1.9×10^{21} n/cm^2 ($E \geq 0.18$ MeV) and 1190°C, respectively.

3. No metallic fission product attack of the SiC or kernel migration occurred at the peak temperature and fluence conditions of 1135°C, and 1.9×10^{21} n/cm^2 ($E \geq 0.18$ MeV) in any of the fuels tested except those noted in item (4).

4. Nonhomogeneity in the fuel rods containing UO_2 TRISO/ThO_2 BISO particles showed that concentrations of fissile particles in an area of the rods can cause high-temperature areas ("hot spots") that can be detrimental to fuel performance.

5. Unloading damage to the surface of the fuel rods can definitely affect fission gas R/B measurements.

6. Behavior of 100-μm (VSM) UC_2 particles in spine samples was excellent at a 918°C and 1.1×10^{21} n/cm^2 ($E \geq 0.18$ MeV) irradiation exposure.

FUEL TEST ELEMENT FTE-14

Autoradiography

Beta-gamma autoradiography was used to show fission product migration into the graphite fuel bodies. Cross-sectional slices were cut from the fuel bodies and then ground parallel with abrasive paper to ∿1/8-in. Slices were then placed on top of Kodak Industrial M type film and exposed for 70 min.

Figures 9-24 and 9-25 show the autoradiography photographs from fuel bodies 2 and 3. The slice from fuel body 1 was broken and could not be examined. Fuel body 2 (Fig. 9-24) showed the highest release from the fuel in holes 1 and 5, which contained UC_2 TRISO/ThC_2 BISO and UO_2 TRISO/ThC_2 BISO blends. The lowest release was from hole 2 with the UC_2 TRISO/ThC_2 TRISO blend. The two distinct black spots on the photograph near hole 2 may have been caused by nonhomogeneity in the fuel rods at this position in body 2. This is supported by the evidence of nonhomogeneity in fuel rod 2-2-6, which had an obvious nonhomogeneous fuel loading. Body 3 (Fig. 9-25) had fairly even release from the different fuel types. Hole 1 with the UC_2 TRISO/ThC_2 BISO had the highest release, with hole 4 which contained a $(ThU)O_2$ TRISO/ThC_2 BISO blend having the lowest release.

REFERENCES

9-1. Steward, K. P., Objectives and Plans for Fuel Testing in the Peach Bottom HTGR, USAEC Report GA-10065, General Atomic Company, April 23, 1970.

9-2. Wallroth, C. F., et al., "Postirradiation Examination of Peach Bottom Fuel Test Element FTE-3," USAEC Report GA-A13004, General Atomic Company, August 15, 1974.

9-3. Miller, C. M., General Atomic Company private communication, July 18, 1974.

9-4. Holzgraf, J. F., General Atomic Company unpublished data, September 10, 1974.

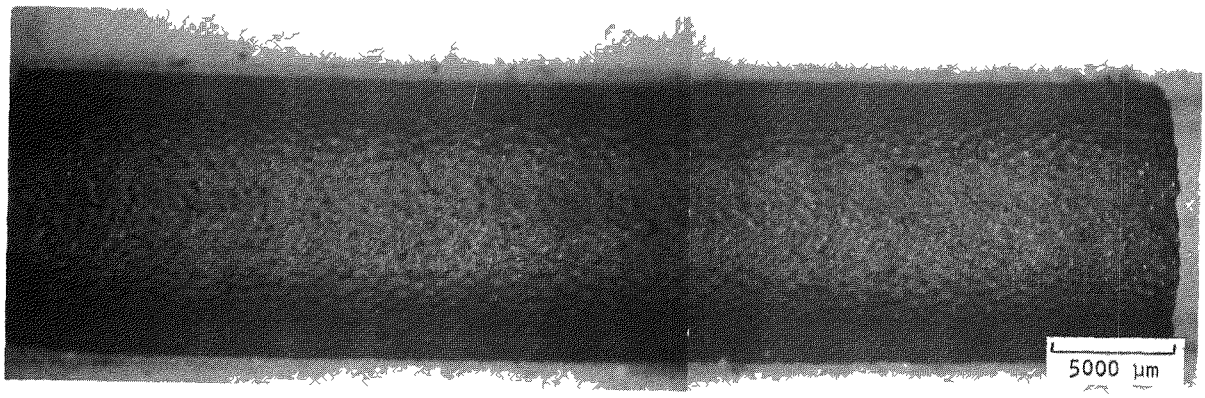

S7410 (61-62)

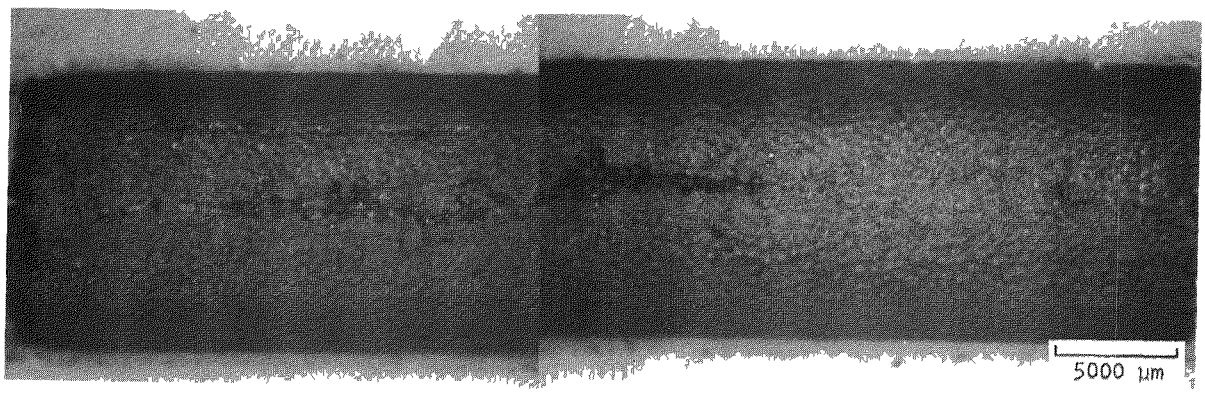

S7410 (63-64)

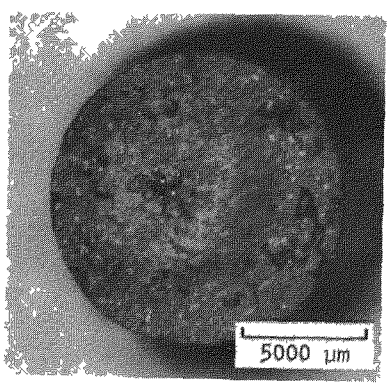

S7410-59

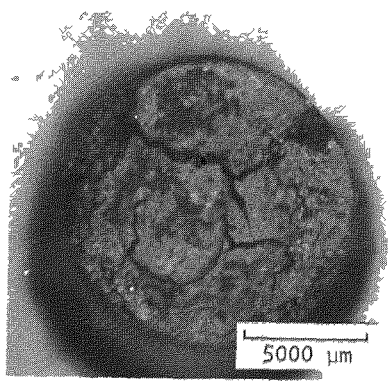

S7410-60

Fig. 9-1. Visual examination of FTE-4 fuel rod 2-2-7 (UO_2 TRISO/ThO_2 BISO blend); irradiated to 1.87 x 10^{21} n/cm^2 (E > 0.18 MeV) at 1135°C

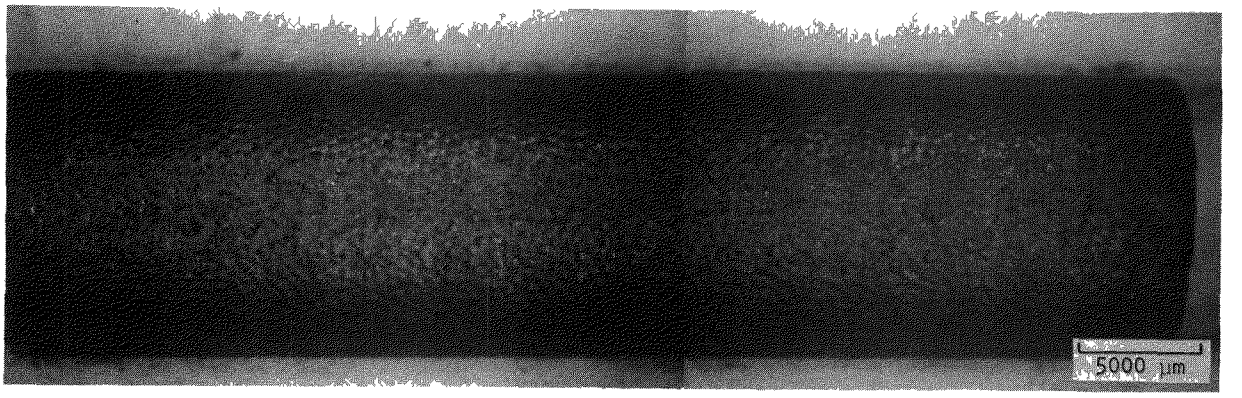

S7410 (48-49)

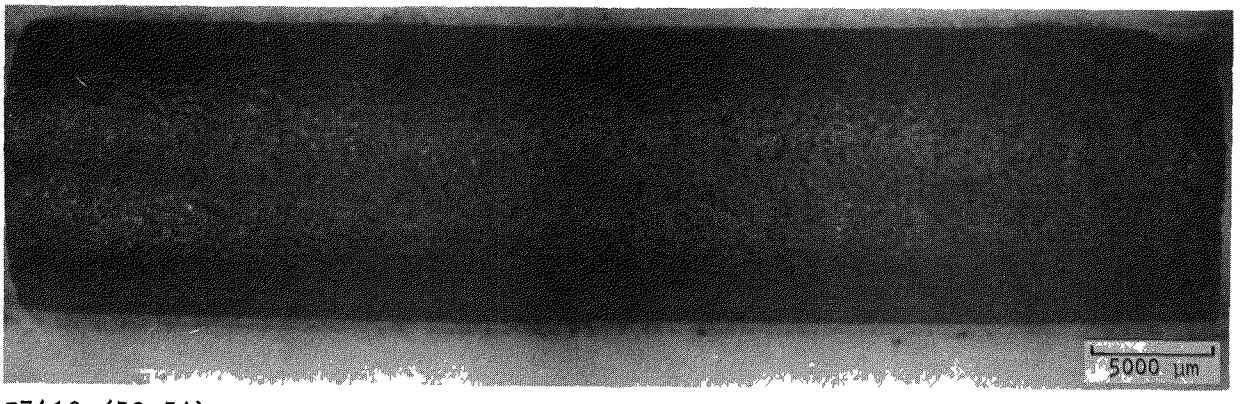

S7410 (50-51)

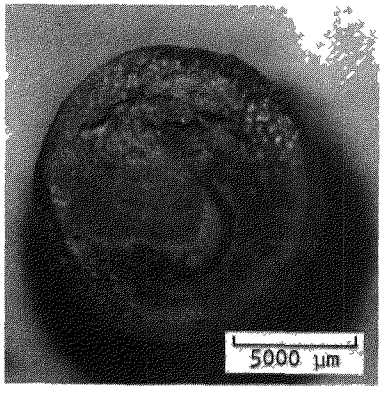

S7410-46

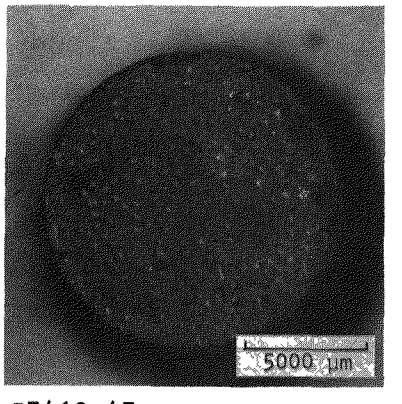

S7410-47

Fig. 9-2. Visual examination of FTE-4 fuel rod 2-3-8 [$(Th,U)C_2$ TRISO/ ThC_2 BISO blend]; irradiated to 1.87 x 10^{21} n/cm^2 ($E > 0.18$ MeV) at 1135°C

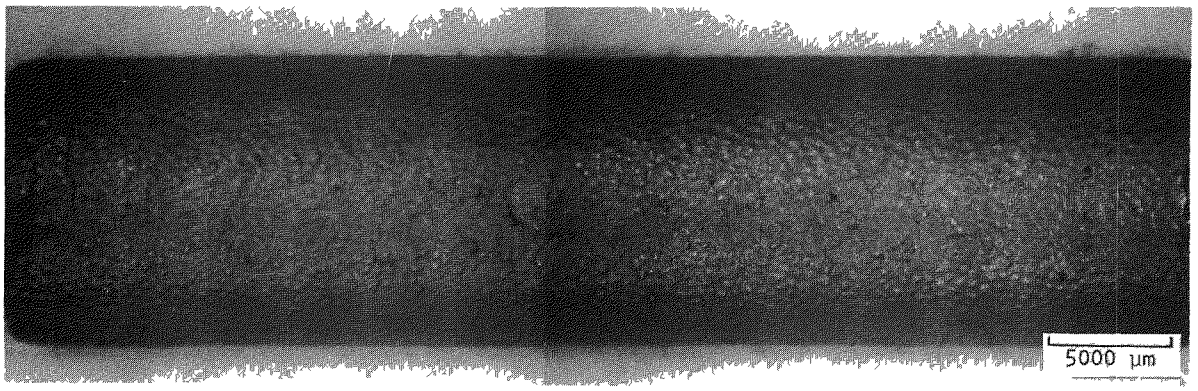

S7410 (24-25)

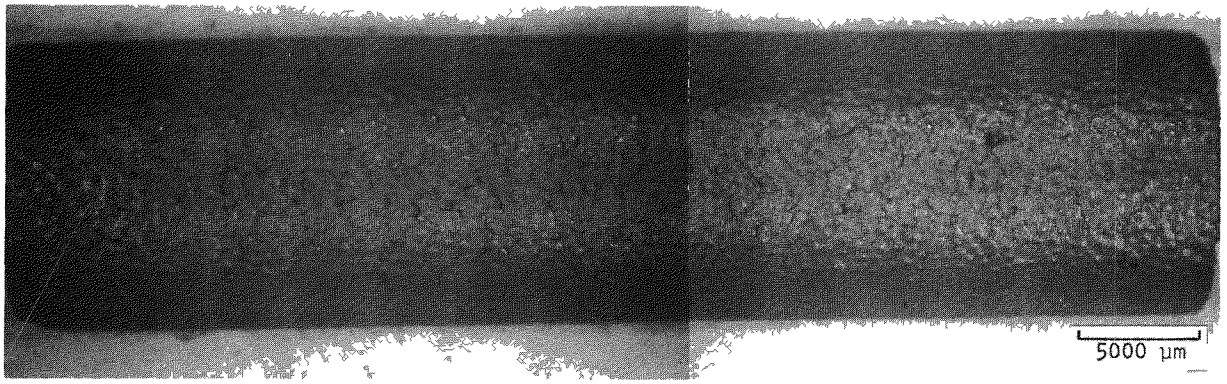

S7410 (26-27)

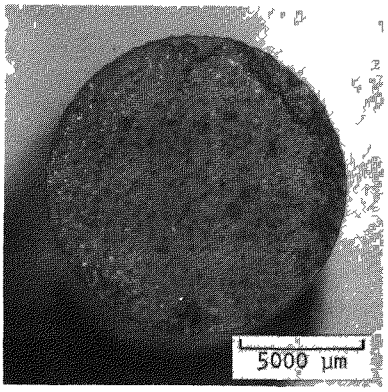

S7410-29

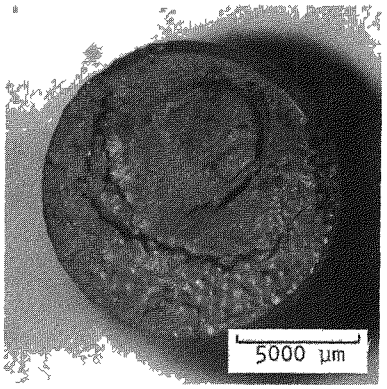

S7410-30

Fig. 9-3. Visual examination of FTE-4 fuel rod 2-5-7 [$(Th,U)C_2$ TRISO/ ThC_2 TRISO blend]; irradiated to 1.87 x 10^{21} n/cm^2 (E > 0.18 MeV) at 1135°C

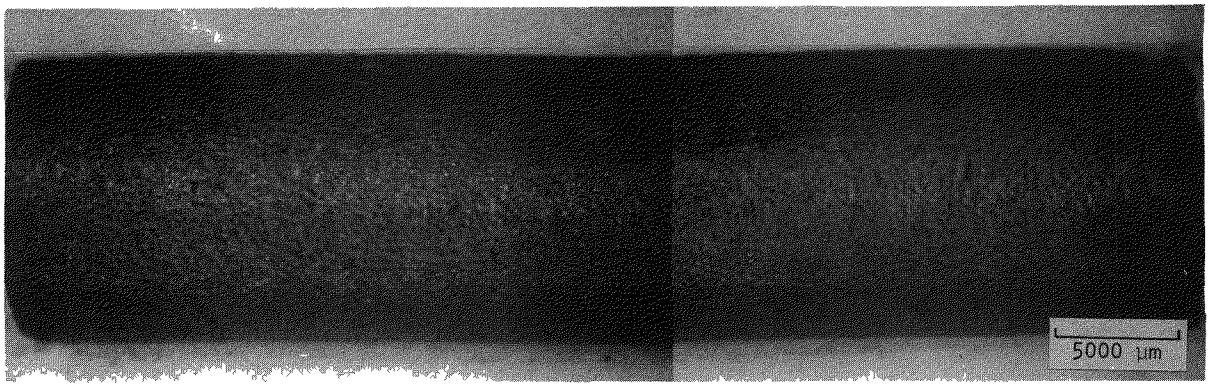

S7410 (11-12)

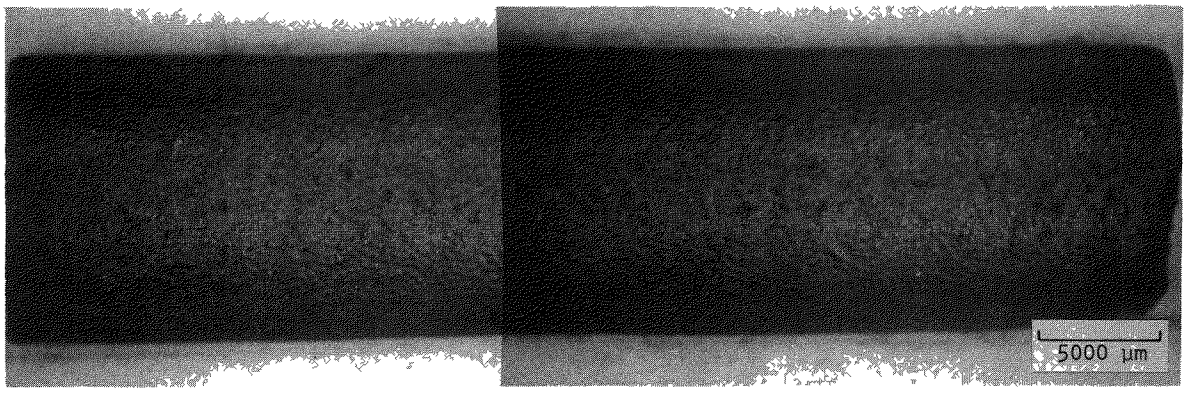

S7410 (9-10)

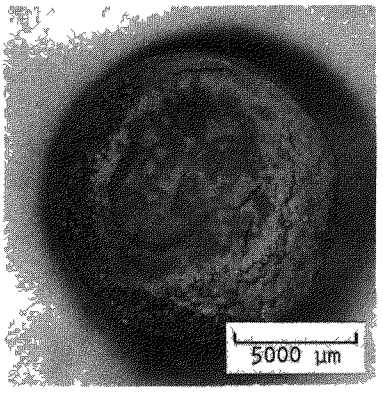

S7410-13

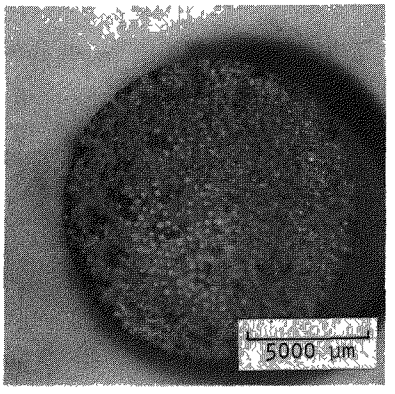

S7410-14

Fig. 9-4. Visual examination of FTE-4 fuel rod 2-8-7 (UC_2 TRISO/ThC_2 BISO blend); irradiated to 1.75 x 10^{21} n/cm^2 (E > 0.18 MeV) at 1140°C

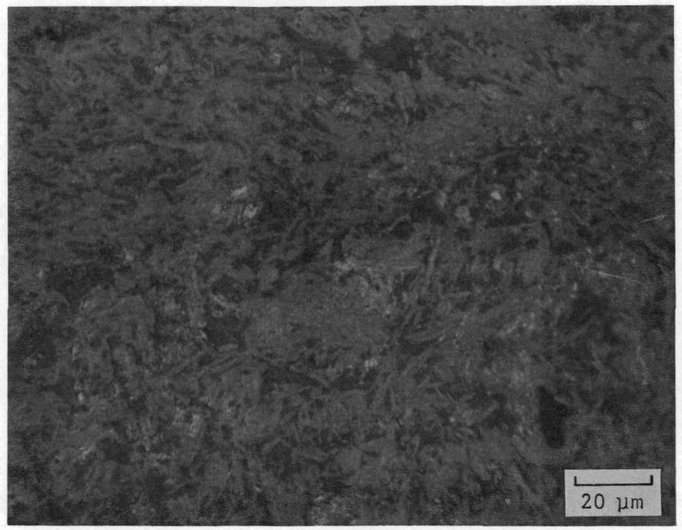

L7410-195 (a)

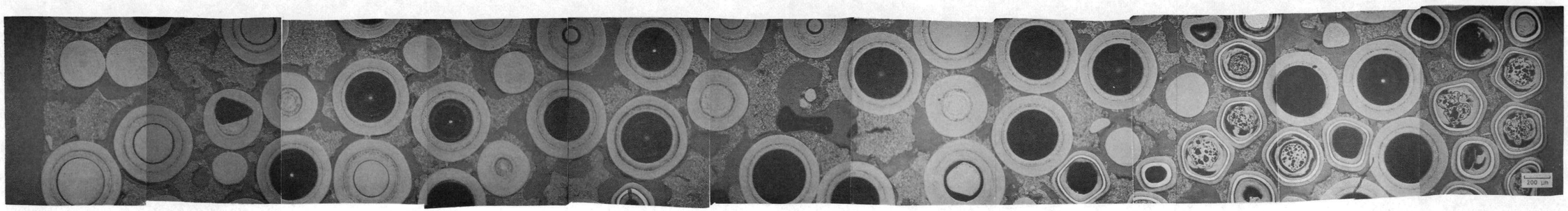

L7410 (183-193) (b)

Fig. 9-5. Photomicrographs of fuel rod 2-1-7 from FTE-4; irradiated to 1.87 x 10^{21} n/cm^2 (E > 0.18 MeV) at 1135°C: (a) typical graphite matrix and (b) composite radial cross section

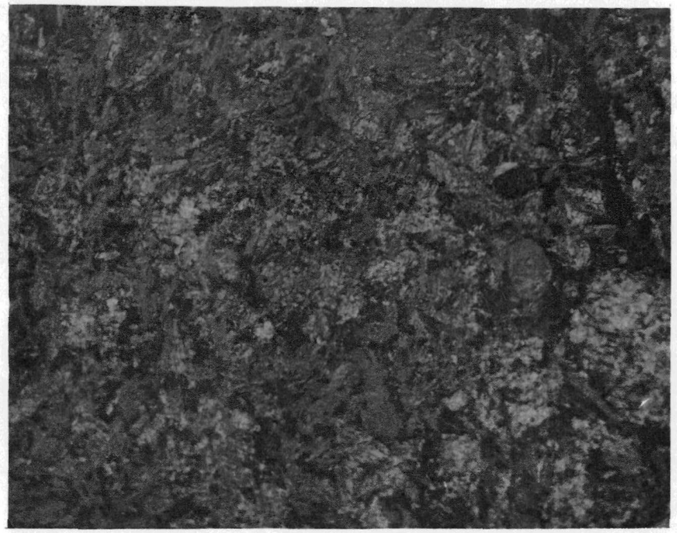

L7410-121 (a)

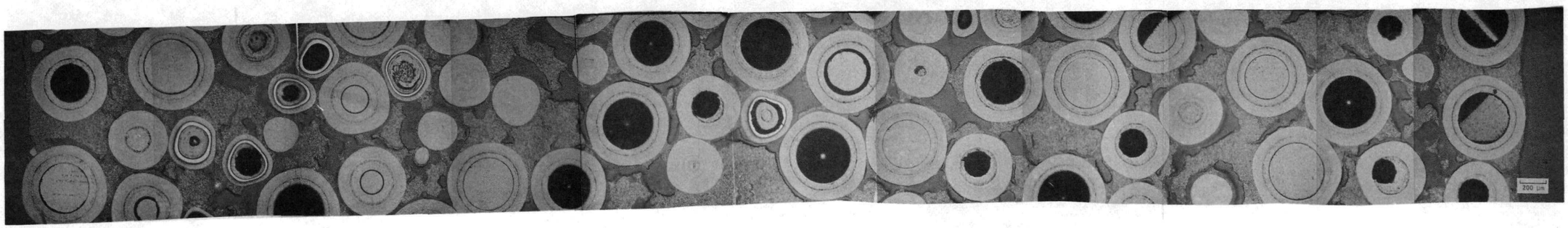

L7410 (122-132) (b)

Fig. 9-6. Photomicrographs of fuel rod 2-2-7 from FTE-4; irradiated to 1.87 x 10^{21} n/cm^2 (E > 0.18 MeV) at 1135°C: (a) typical graphite matrix and (b) composite radial cross section

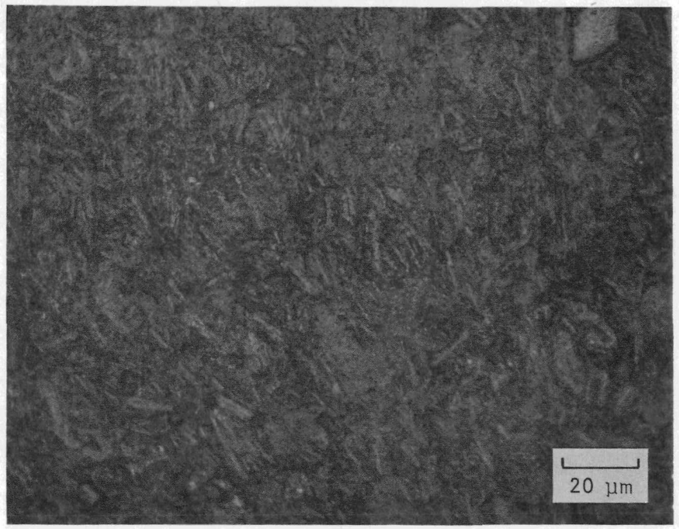

L7410-101 (a)

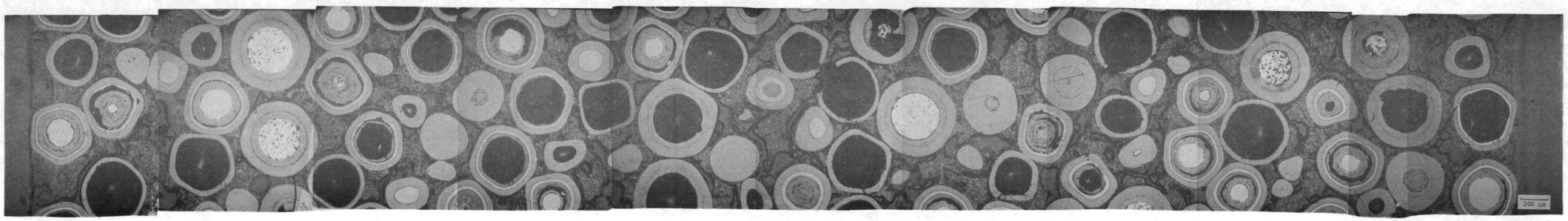

L7410 (89-99) (b)

Fig. 9-7. Photomicrographs of fuel rod 2-3-8 from FTE-4; irradiated to 1.87 x 10^{21} n/cm^2 (E > 0.18 MeV) at 1135°C: (a) typical graphite matrix and (b) composite radial cross section

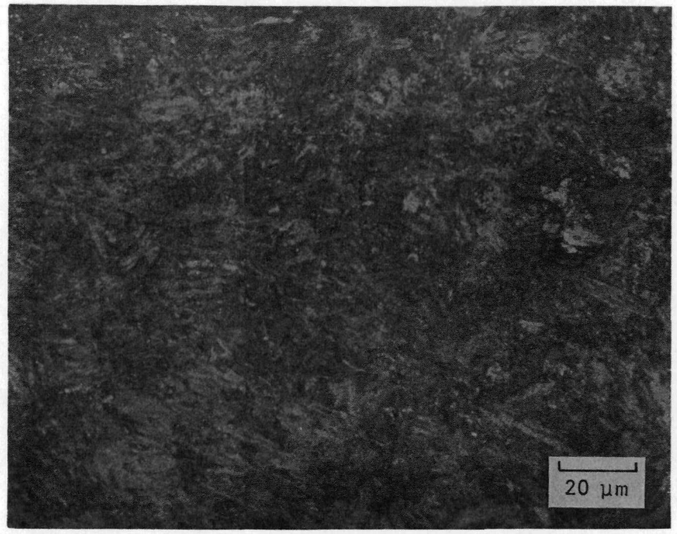

L7410-25 (a)

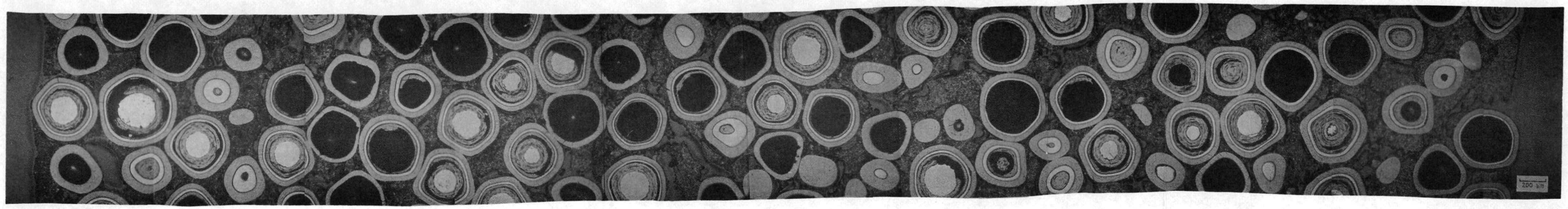

L7410 (13-23) (b)

Fig. 9-8. Photomicrographs of fuel rod 2-5-7 from FTE-4; irradiated to 1.87 x 10^{21} n/cm^2 (E > 0.18 MeV) at 1135°C: (a) typical graphite matrix and (b) composite radial cross section

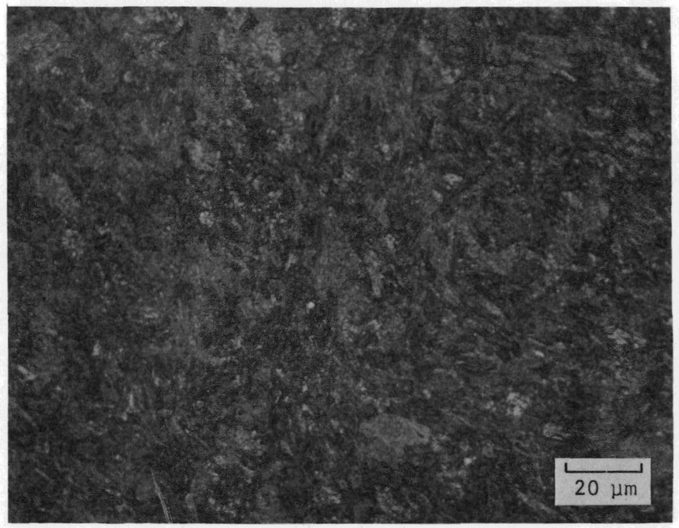

L7410-64 (a)

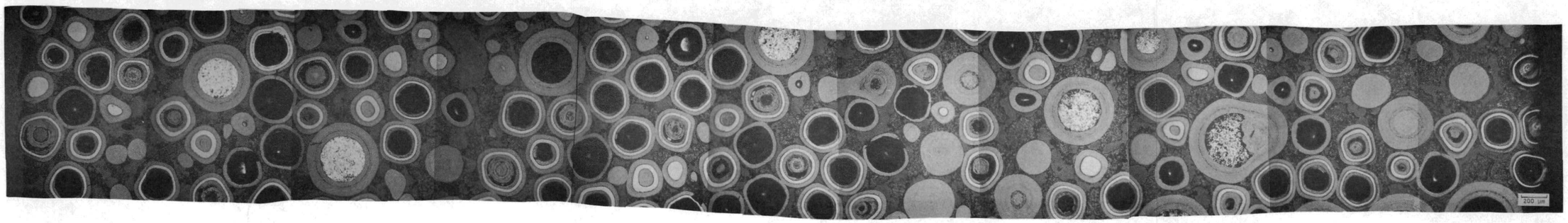

L7410 (52-62) (b)

Fig. 9-9. Photomicrographs of fuel rod 2-8-7 from FTE-4; irradiated to 1.87 x 10^{21} n/cm^2 (E > 0.18 MeV) at 1135°C: (a) typical graphite matrix and (b) composite radial cross section

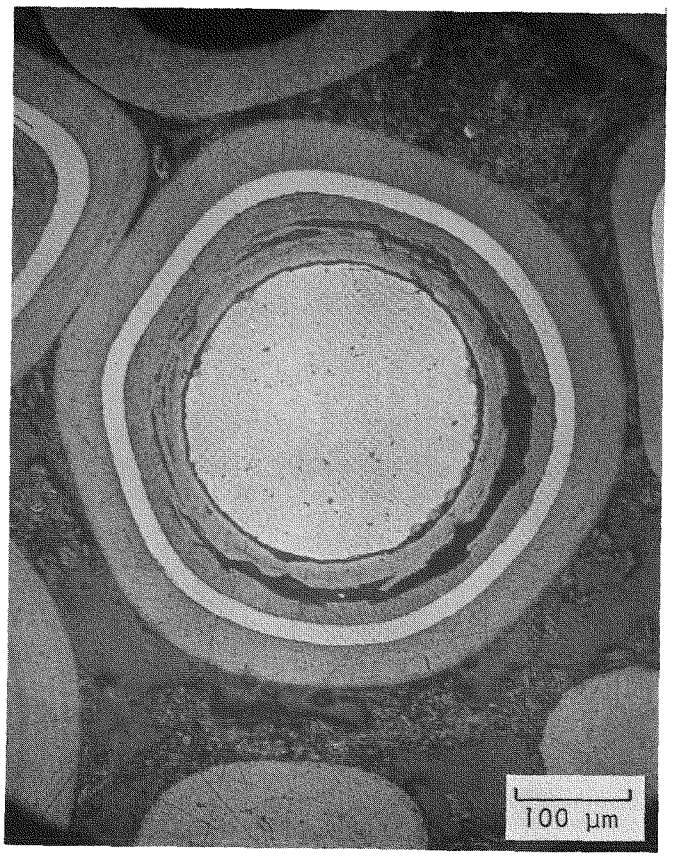

L7410-72 (a)

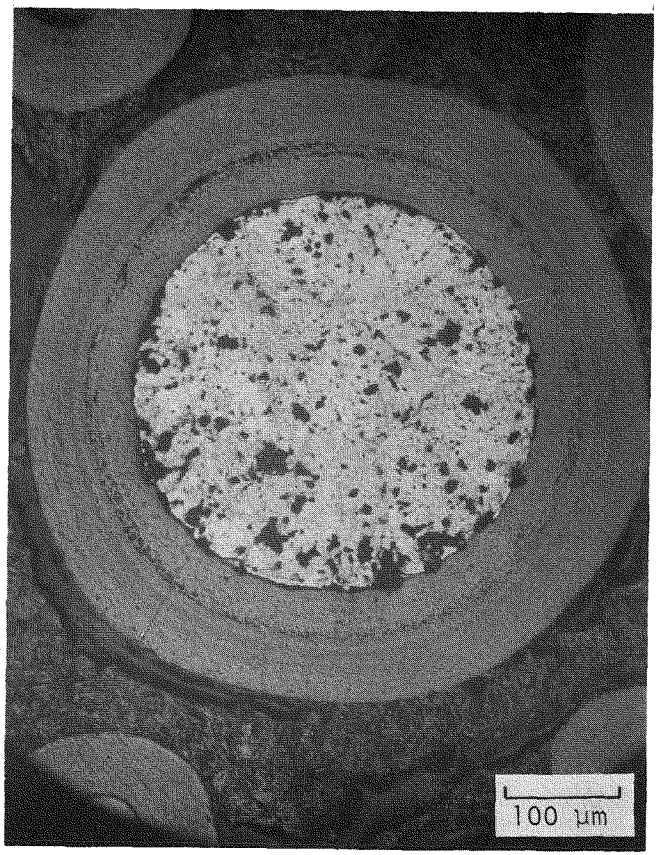

L7410-81 (b)

Fig. 9-10. Photomicrographs of representative particles from fuel rod 2-3-8 in FTE-4; irradiated to 1.87×10^{21} n/cm^2 (E > 0.18 MeV) at 1135°C: (a) (Th,U)C_2 TRISO and (b) ThC_2 BISO beginning to hydrolyze

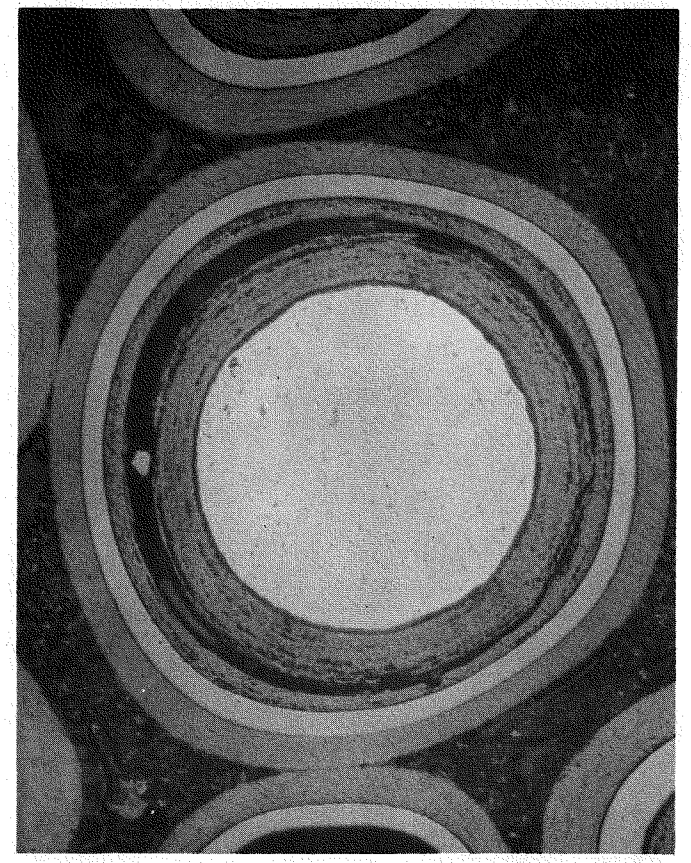

L7410-7 (a)

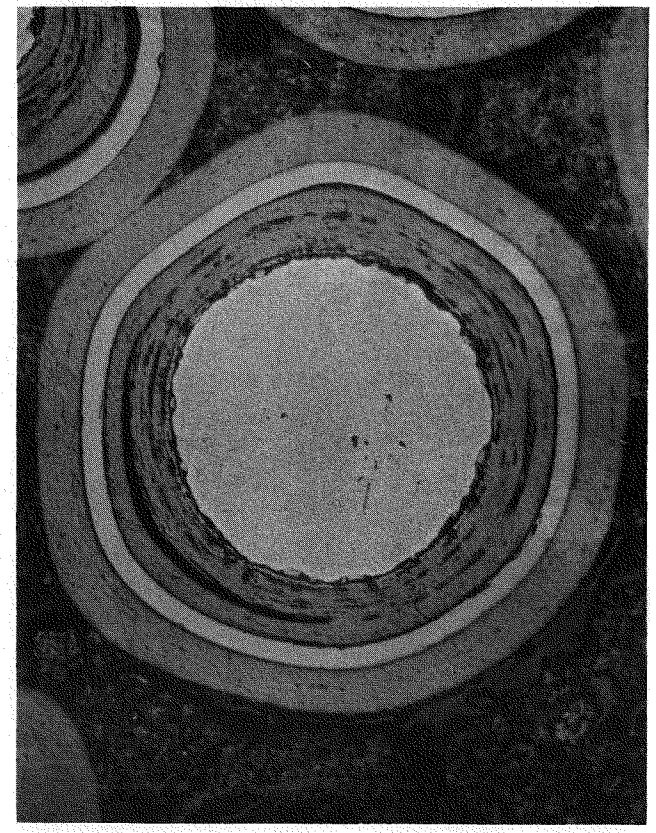

L7410-3 (b)

Fig. 9-11. Photomicrographs of representative particles from fuel rod 2-5-7 in FTE-4; irradiated to 1.87×10^{21} n/cm^2 (E > 0.18 MeV) at 1135°C: (a) ThC_2 TRISO and (b) $(Th,U)C_2$ TRISO

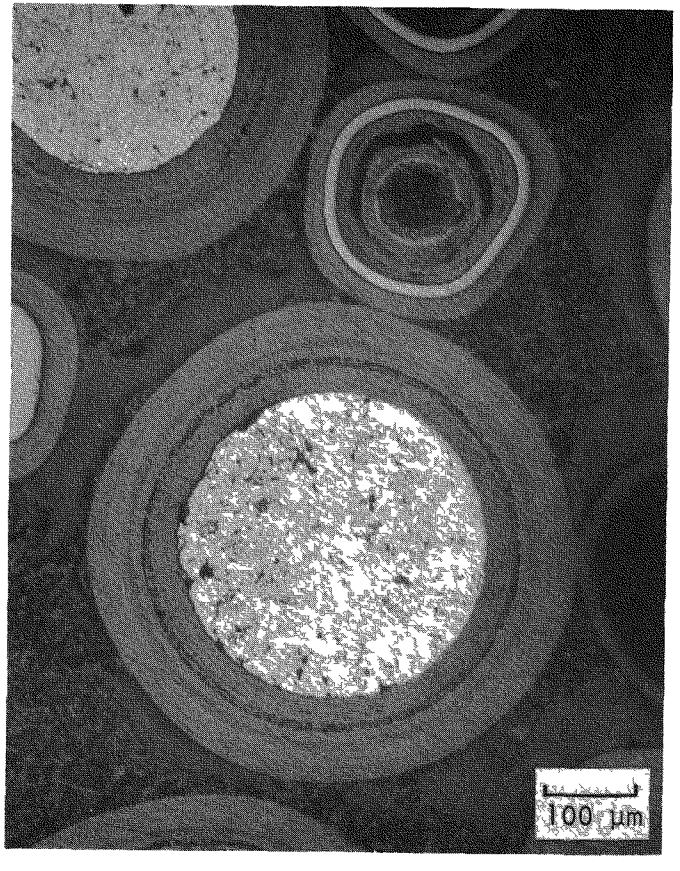

L7410-46 (a)

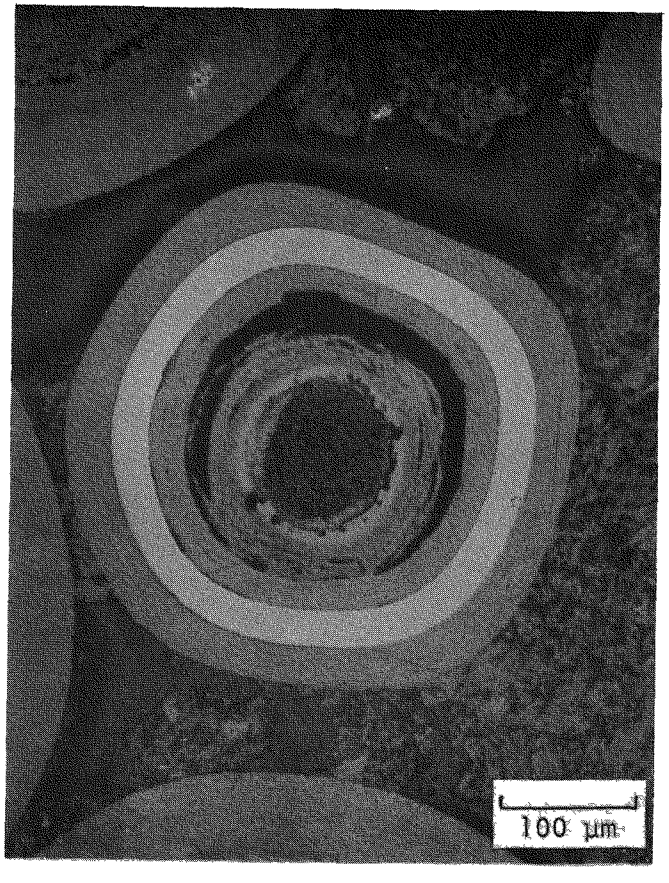

L7410-42 (b)

Fig. 9-12. Photomicrographs of representative particles from fuel rod 2-8-7 in FTE-4; irradiated to 1.87×10^{21} n/cm^2 (E > 0.18 MeV) at 1135°C: (a) ThC_2 BISO with UC_2 TRISO and (b) UC_2 TRISO

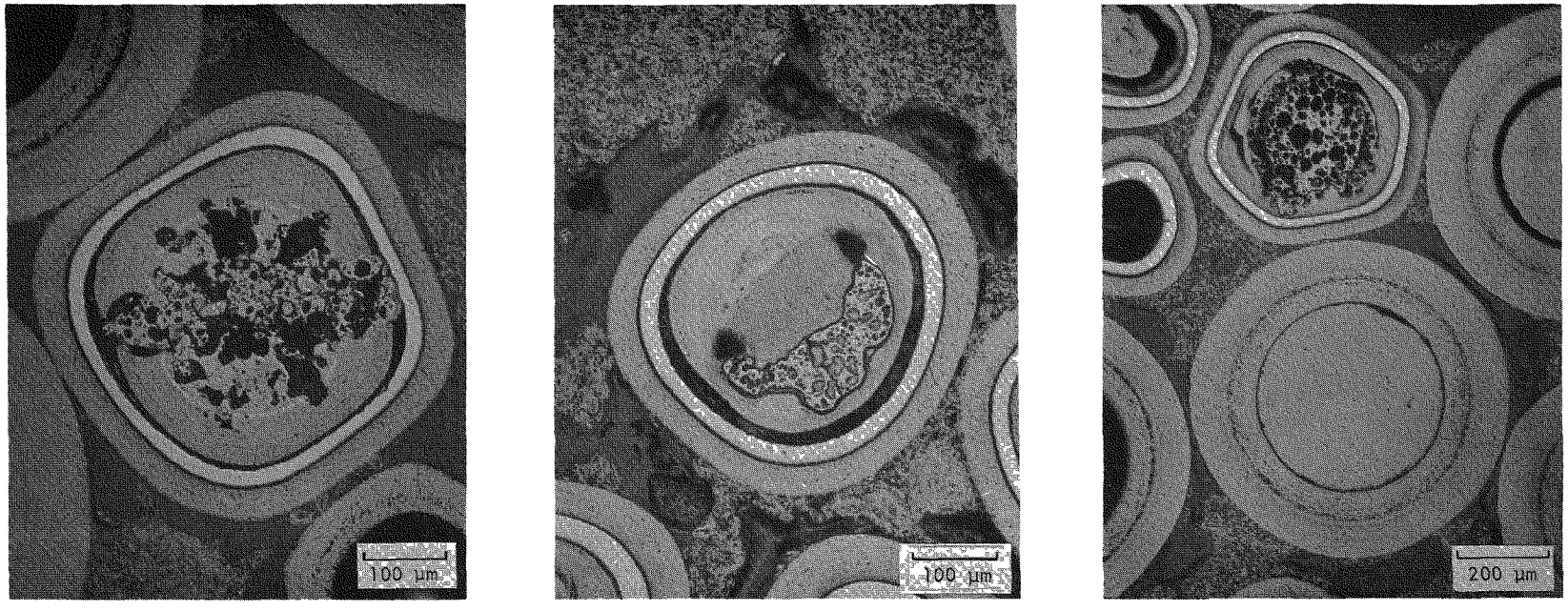

L7410-110 (a) L7410-142 (b) L7410-108 (c)

Fig. 9-13. Photomicrographs of representative particles from "hot spot" area of fuel rod 2-2-7 in FTE-4; irradiated to 1.87 x 10^{21} n/cm^2 (E > 0.18 MeV) at 1135°C: (a) UO_2 particle showing extrusion, (b) migrating UO_2 kernel, and (c) UO_2 kernel showing plasticity next to a ThO_2 BISO particle

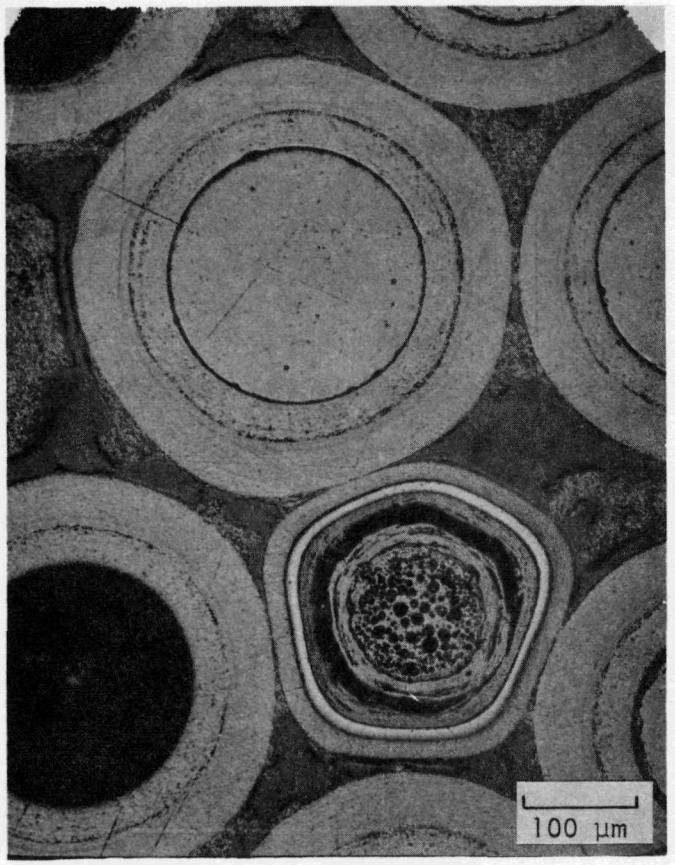

L7410-112

Fig. 9-14. Photomicrograph of representative particles from fuel rod 2-2-7 in FTE-4. These particles were from the "hot spot" area and showed good irradiation performance.

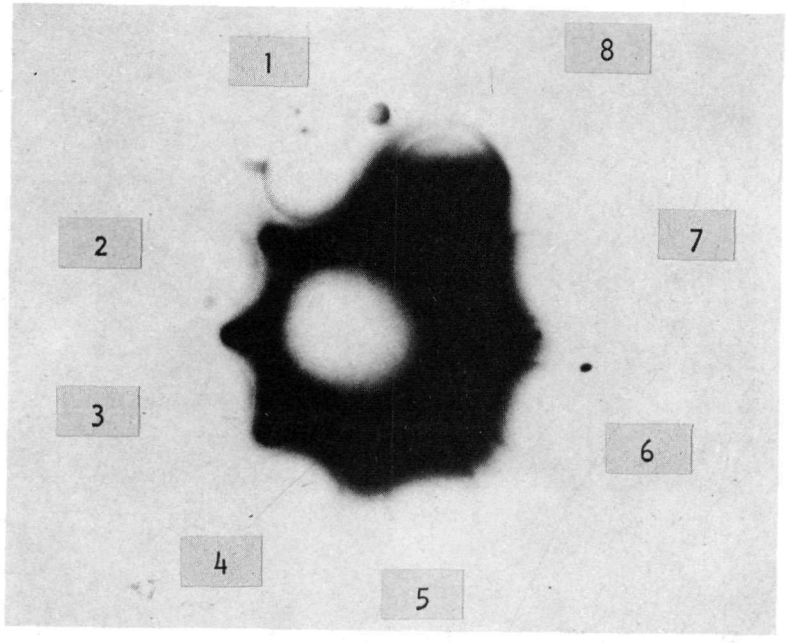

Fig. 9-15. Autoradiography of slice 1-3 from body 1 in FTE-4, located ∿18 in. from top of active core

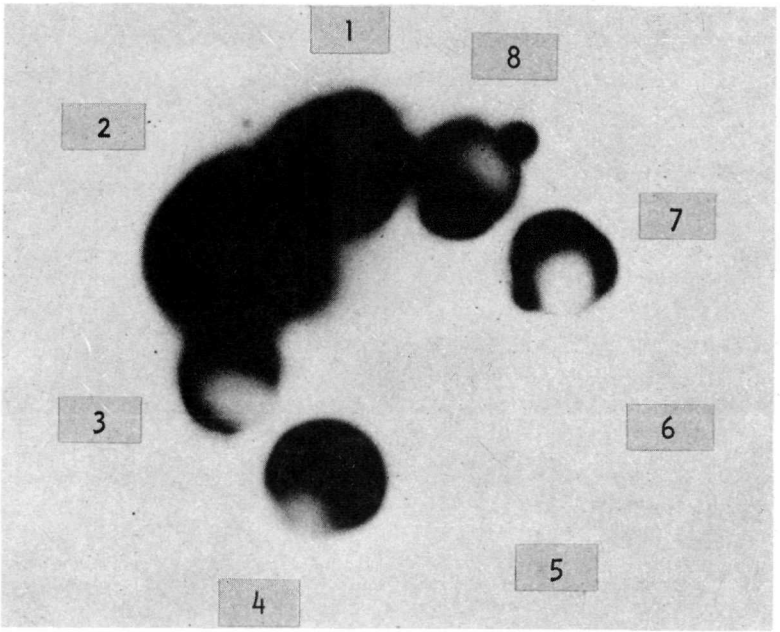

Fig. 9-16. Autoradiography of slice 2-2 from body 2 in FTE-4, located ∿34 in. from top of active core

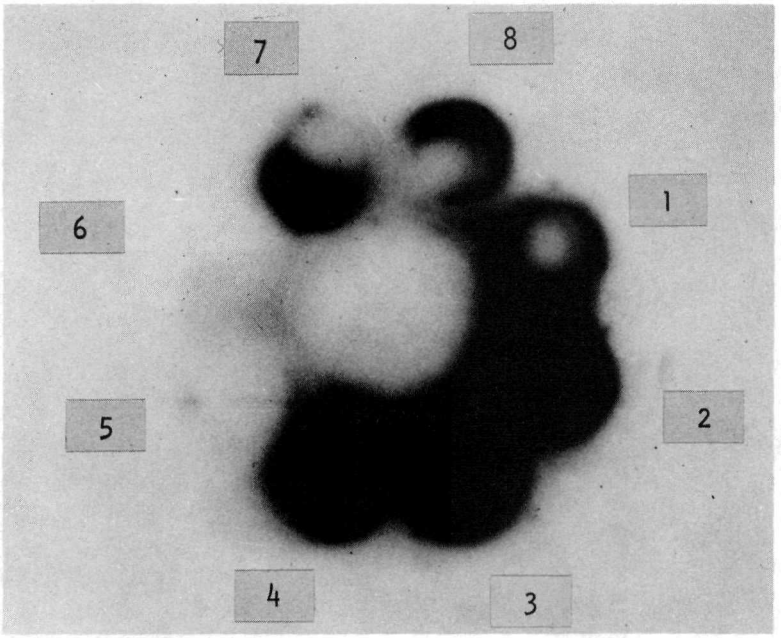

Fig. 9-17. Autoradiography of slice 3-2 from body 3 in FTE-4, located ∿75 in. from top of active core

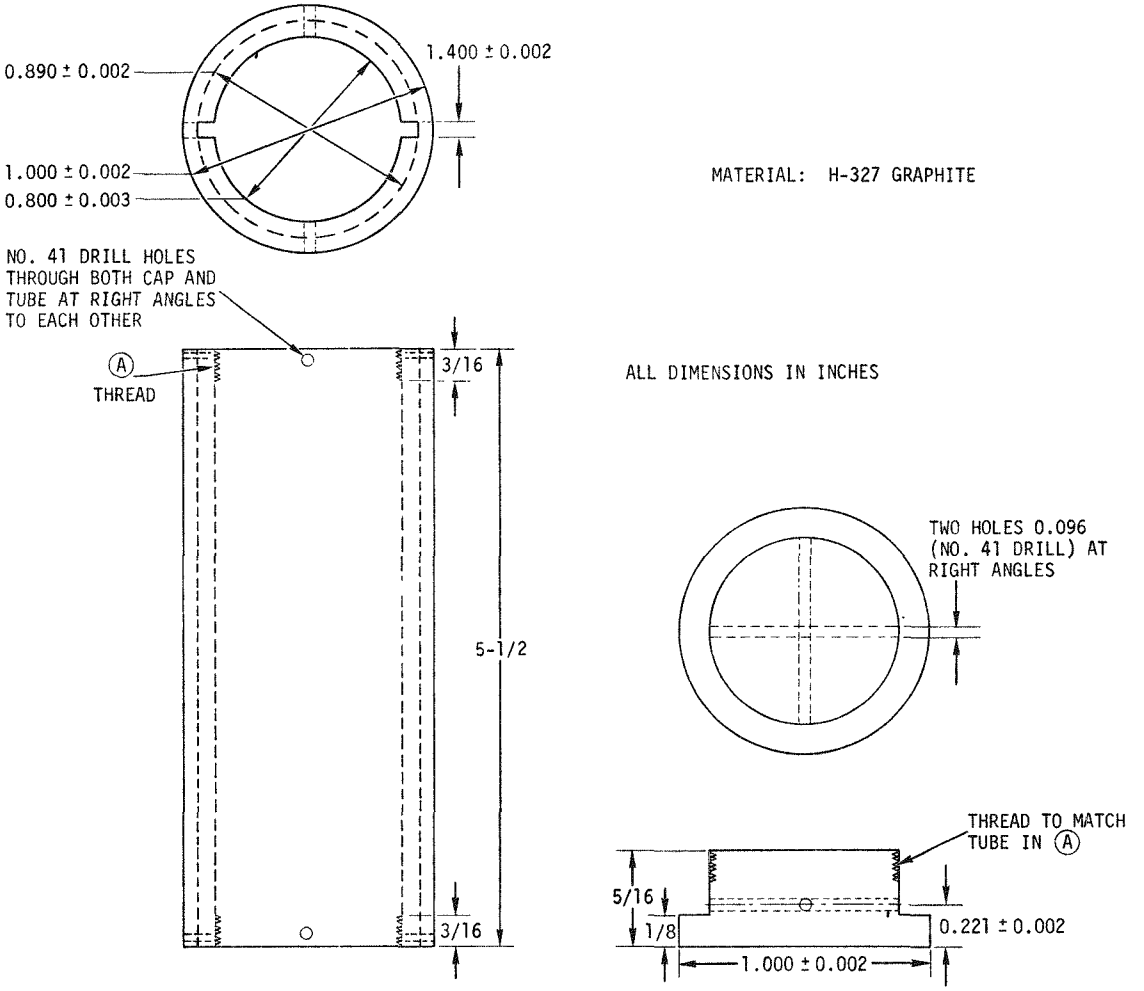

Fig. 9-18. Design of type 1 thermal stability outer crucibles

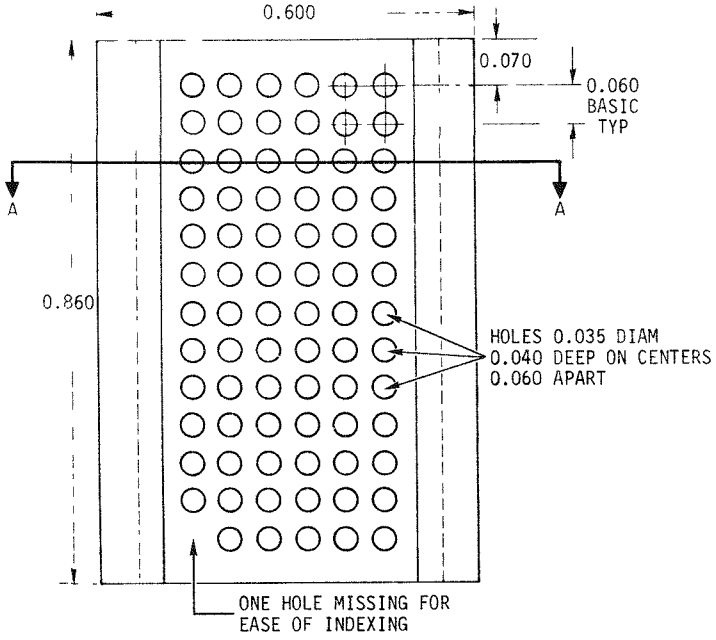

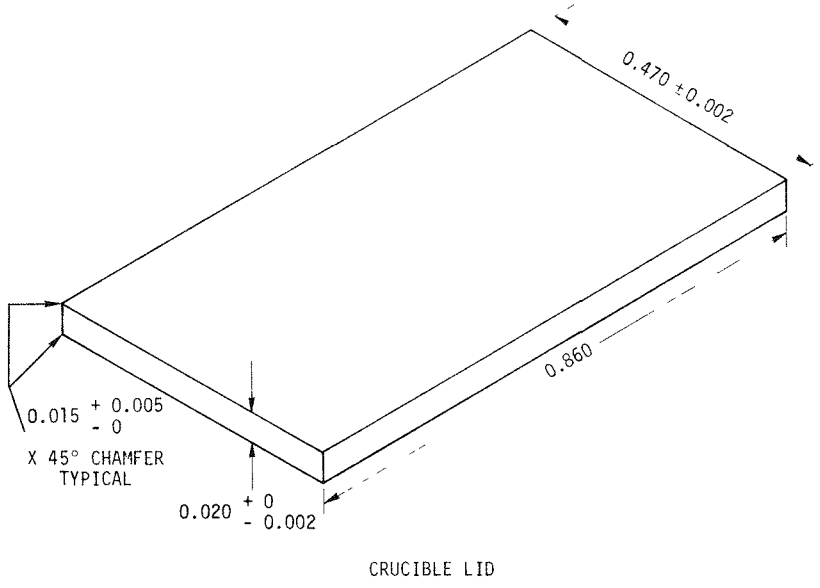

CRUCIBLE LID

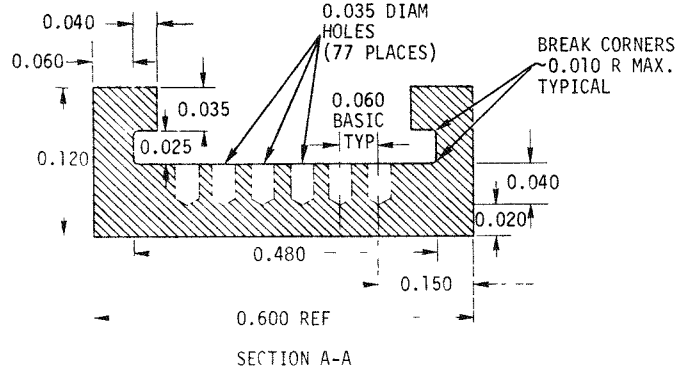

SECTION A-A

NOTES:
MATERIAL: HLM-85 OR ATJ GRAPHITE FOR ALL PARTS.
LINEAR DIMENSIONS < 0.050 ± 0.002.
LINEAR DIMENSIONS > 0.050 ± 0.005 EXCEPT WHERE STATED.
ALL DIMENSIONS IN INCHES.

Fig. 9-19. Design of type 1 thermal stability inner crucibles

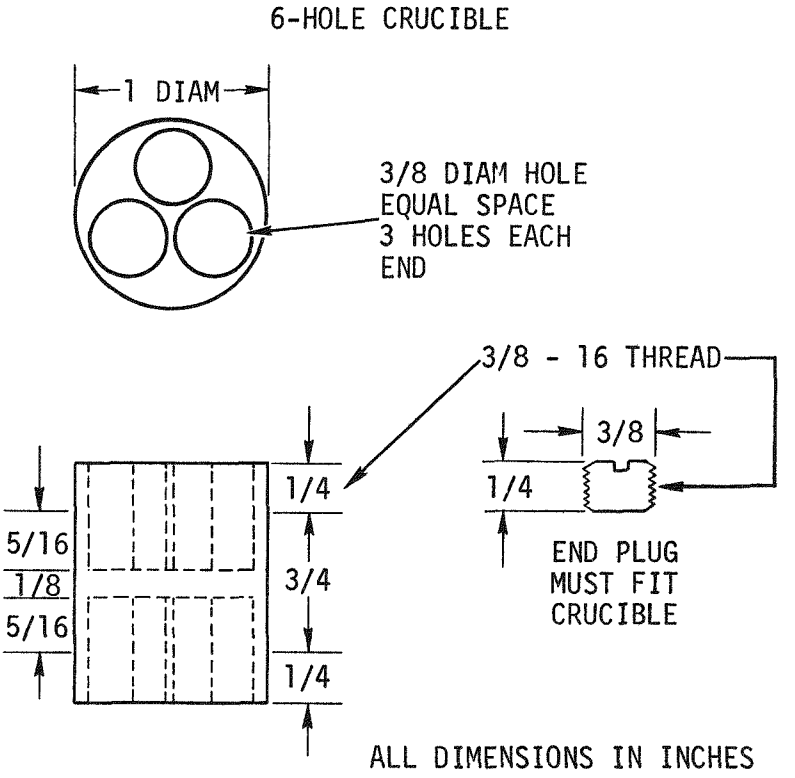

Fig. 9-20. Design of type 2 thermal stability crucibles

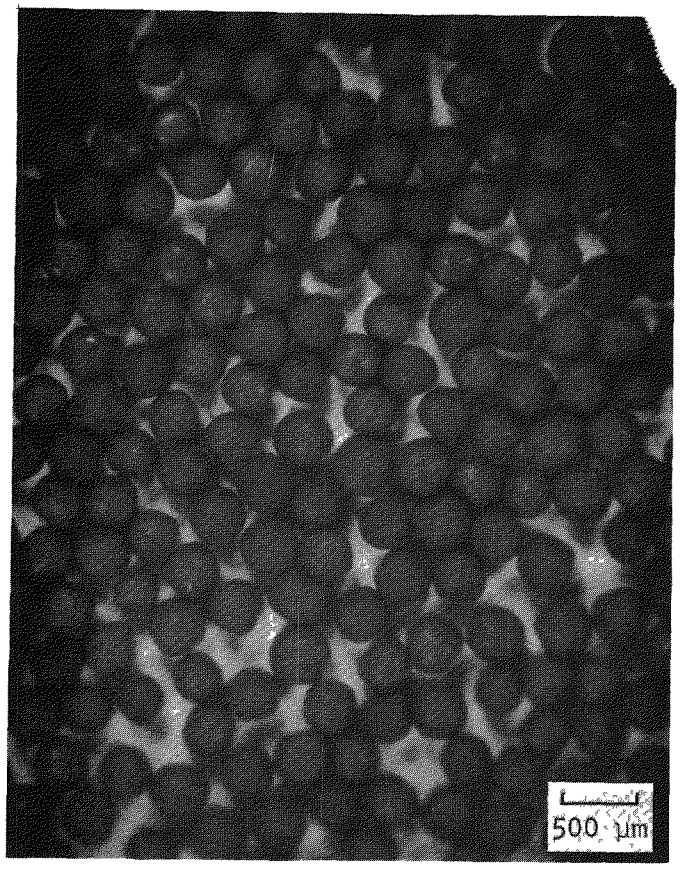

S7410-67

Fig. 9-21. Stereophotograph of UC_2 100-µm (VSM) particles from spine sample TS4-5 in FTE-4; irradiated to 1.1 x 10^{21} n/cm^2 (E > 0.18 MeV) at 918°C

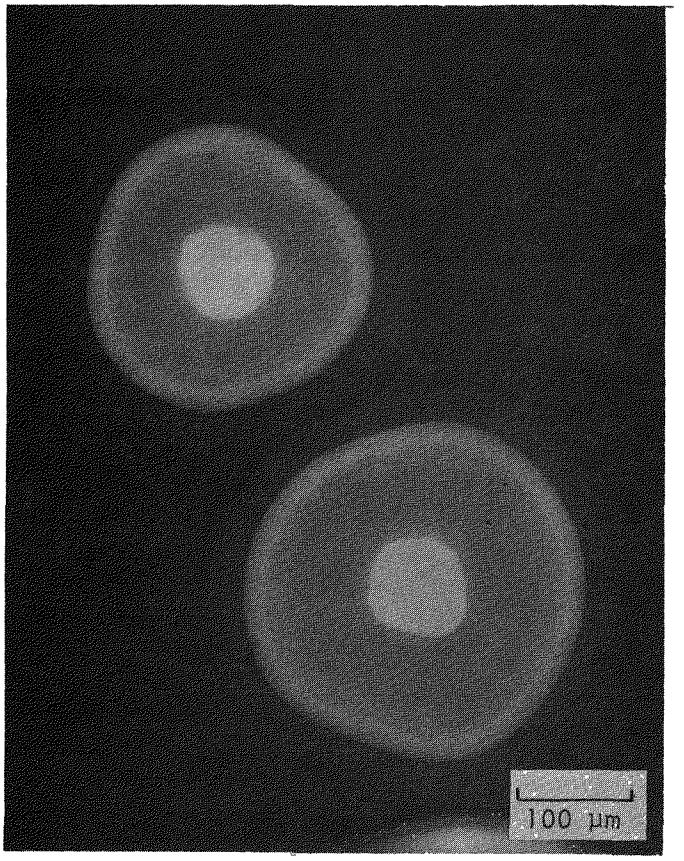

HA314

Fig. 9-22. Radiograph of representative UC_2 100-µm (VSM) particles from spine sample TS4-5 in FTE-4; irradiated to 1.1 x 10^{21} n/cm^2 (E > 0.18 MeV) at 918°C

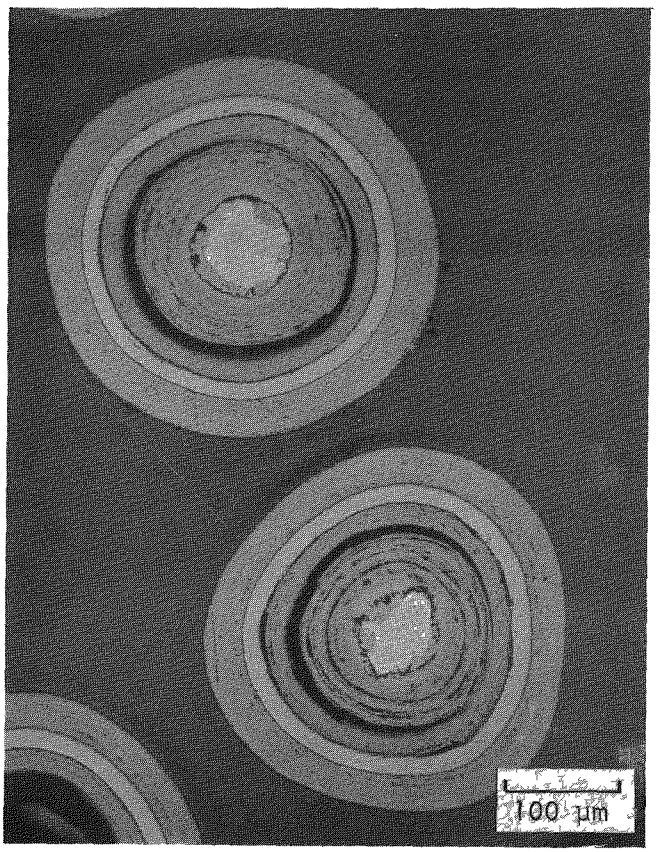

L7410-147

Fig. 9-23. Typical microstructure of UC_2 100-µm (VSM) particle from spine sample TS4-5 in FTE-4; irradiated to 1.1 x 10^{21} n/cm^2 (E > 0.18 MeV) at 918°C

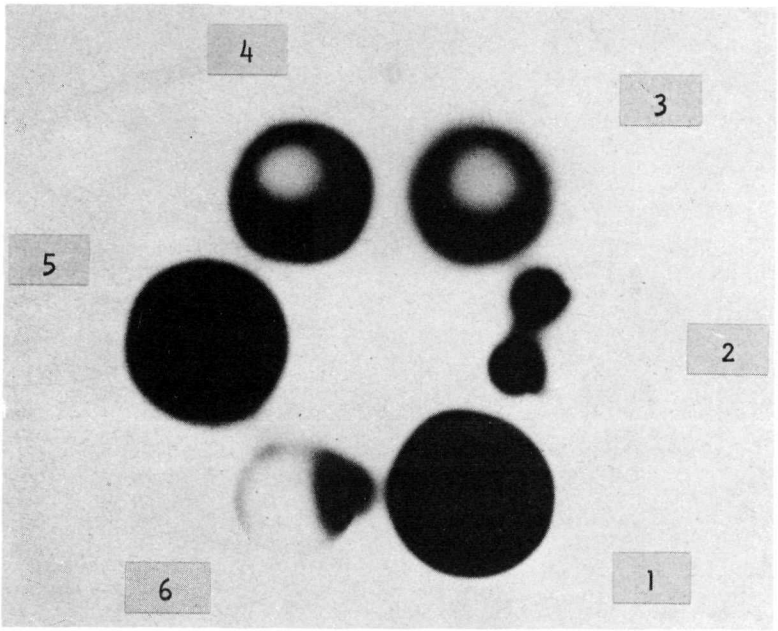

Fig. 9-24. Autoradiography of slice 2-2 from body 2 in FTE-14, located ~56 in. from bottom of active core

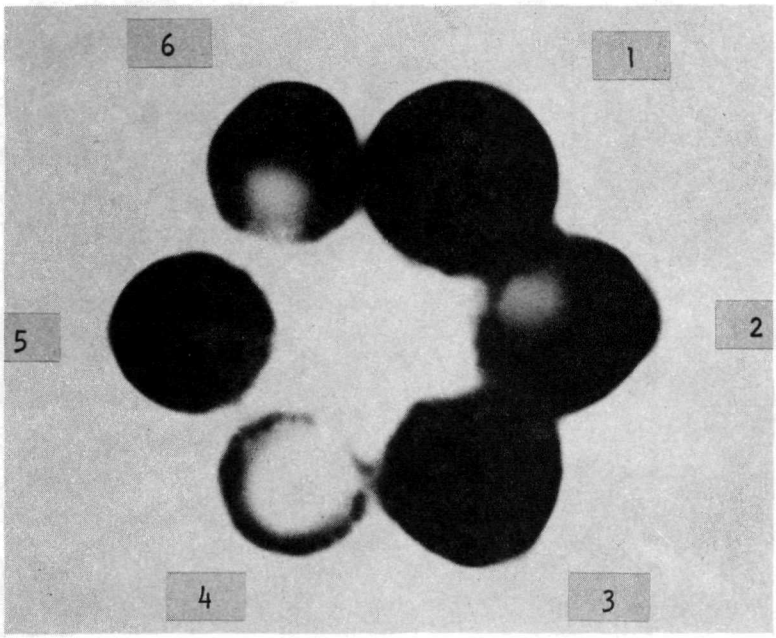

Fig. 9-25. Autoradiography of slice 3-2 from body 3 in FTE-14, located ∿15 in. from bottom of active core

TASK 11 (189a 13121)
GRAPHITE RESEARCH

INTRODUCTION

A program to characterize and irradiate near-isotropic graphite for HTGR fuel and reflector blocks is continuing. The graphites under investigation have been supplied by major carbon and graphite producers in the United States and Europe. The major emphasis is on the United States graphites, whereas a much smaller effort is devoted to the European materials. The work on the European graphites is to provide confimatory and comparative data with European HTGR programs where United States graphites are also being evaluated.

The Great Lakes Carbon Company (GLCC) has produced grade H-429, a prototype of H-451 which is their standard full-scale grade for HTGR core components. Grade H-429 has been under irradiation for approximately 4 yr, whereas Grade H-451 has been under a more extensive evaluation for about 3 yr. Great Lakes Carbon Company has produced six lots of H-451, consisting of a total of approximately 210 logs for which GLCC has reported strength, density, and purity data. Table 11-1 shows the disposition of material received from GLCC. Test data from GLCC are used for initial selection of logs for use in Task 11 programs. The selection of logs is made jointly by GLCC and GA personnel.

Union Carbide Corporation has produced approximately 48 production-size logs of TS-1240 of which 15 were delivered to GA in August 1973. Characterization is under way on these logs, and specimens from one log are under irradiation in capsule OG-2.

TABLE 11-1
DISPOSITION OF H-451 GRAPHITE LOGS

GLCC Lot No.	Approximate Number of Logs Tested by GLCC	Number of Logs Delivered to GA[a]	Approximate Date of Delivery	Disposition of Logs Under Task 11
266	8	2	Aug. 1972	Preliminary characterization completed on 2 logs. Specimens from one log irradiated in OG-1 and OG-2.
255	22	22[b]	Aug. 1973	Characterization under way on 3 logs. Specimens from one log irradiated in OG-2.
424	11	3	March 1974	No evaluation work under way.
426	127	73	March 1974	Characterization under way on 3 logs. Specimens from 3 logs will be irradiated in OG-3.
438	26	0	--	No evaluation work planned.
440	26	0	April 1975	Characterization work planned on 3 logs. Specimens from 3 logs will be irradiated in OG-4.

[a] Many of the logs delivered to GA will be used for programs other than Task 11; however, Task 11 coordinates the deliveries.

[b] Five logs delivered to ORNL for their HTGR program work.

Two lots of production-size SO-818 have been manufactured by AirCo Speer. Four logs from the first lot were delivered to GA in September 1974. Characterization will be started on SO-818 in May 1975. Specimens from one log of SO-818 will be included in capsule OG-3. The second lot of SO-818 will be delivered in April 1975.

Two logs, one of AS2-F-500 and one of AS2-F-I-500 have been received from Sigri in West Germany. These two graphites are possible candidates for inclusion in capsule OG-3.

Two logs, one P_3JHAN and one of P_3JHA_2N have been received from Pechiney in France. Specimens from P_3JHAN have been irradiated in capsules OG-1 and OG-2. Specimens of P_3JHA_2N will be included in capsule OG-3.

GRAPHITE CHARACTERIZATION

Characterization of grades TS-1240 and H-451, manufactured by Union Carbide Corporation and Great Lakes Carbon Company, respectively, is continuing. Initial characterization data (density, impurities, tensile properties, thermal expansion, and thermal conductivity) were reported previously (Refs 11-1 through 11-5). Additional tensile property data for grade H-451 are given in Table 11-2. Additional thermal expansivity data for both grades are given in Tables 11-3 through 11-5. Additional conductivity data for grade H-451 are given in Table 11-6.

The tensile property data presented in Table 11-2 were obtained on specimens 0.250-in. in diameter by 0.9 in. long. Each specimen was loaded to 1000 psi, unloaded to zero stress, and reloaded to fracture while recording the stress-strain curve. The eleastic modulus for each loading was taken as the chord modulus between 100 and 1000 psi. Values of ultimate strength, strain to fracture, and permanent deformation in the specimens after the first loading cycle were also obtained from the stress-strain curve.

TABLE 11-2
TENSILE PROPERTIES OF H-451 GRAPHITE
Log 5651-86, density = 1.74 g/cm^3, 0.25-in.-diameter by 0.90-in.-long samples

Specimen No.	Position and Orientation[a]	Elastic Modulus x 10^{-6} (psi) First Loading	Elastic Modulus x 10^{-6} (psi) Second Loading	Permanent Set After First Loading (%)	Fracture Strain (%)	Ultimate Strength (psi)
5651-86-3A-006B	MLC(||)	0.90	1.06	0.020	0.280	2095
-007B		0.90	1.125	0.020	0.260	1993
-012B		1.125	1.125	0.035	0.325	2199
-013B		0.75	--	--	0.360	1789
-018B		0.78	0.86	0.030	0.295	1710
-019B		0.86	1.06	0.025	0.325	2192
-024B		0.78	0.90	0.030	0.325	2075
-025B		0.95	1.06	0.020	0.185	1486
-027B		0.98	1.06	0.015	0.375	2153
-028B		0.86	1.00	0.026	0.190	1564
3B-006B		1.00	1.15	0.025	0.210	1587
-007B		0.95	1.29	0.027	0.300	2034
-012B		0.86	1.125	0.030	0.370	1931
-013B		0.90	1.125	0.030	0.250	1671
-018B		0.82	0.98	0.030	0.265	1626
-019B		1.00	1.20	0.025	0.285	1585
-024B		0.95	1.125	0.017	0.295	2138
-025B		1.00	1.20	0.020	0.255	2092
-027B		1.125	1.125	0.010	0.280	1730
-028B		0.86	1.00	0.020	0.250	1787
Mean		0.92	1.08	0.024	0.279	1872
Std. Dev.		0.103	0.104	0.006	0.047	242
-86-3A-036B	MLC(⊥)	0.86	1.06	0.030	0.255	1730
-037B		0.86	1.02	0.027	0.295	1889
-042B		0.95	1.10	0.020	0.280	2034
-043B		0.90	1.10	0.025	0.275	1953
-048B		0.84	0.95	0.020	0.225	1588
-049B		0.90	1.00	0.015	0.230	1711
-054B		0.82	0.95	0.025	0.305	1909
-055B		0.78	0.90	0.035	0.320	2029
-060A		0.95	1.00	0.020	0.205	1671
-060B		0.95	1.20	0.025	0.175	1361
-3B-036B		0.86	1.125	0.025	0.225	1564
-037B		0.90	1.125	0.025	0.295	1603
-042B		0.64	0.86	0.040	0.350	1915
-043B		0.64	0.82	0.040	0.265	2015
-048B		1.06	1.29	0.020	0.285	2162
-049B		0.90	1.06	0.030	0.200	1858
-054B		1.20	1.125	0.020	0.225	1565
-055B		0.72	1.00	0.035	0.245	1221
-060A		0.86	1.125	0.030	0.240	1810
-060B		0.90	1.06	0.020	0.285	1848
Mean		0.87	1.04	0.026	0.259	1772
Std. Dev.		0.127	0.114	0.007	0.044	239

TABLE 11-2 (Continued)

Specimen No.	Position and Orientation[a]	Elastic Modulus x 10^{-6} (psi) First Loading	Elastic Modulus x 10^{-6} (psi) Second Loading	Permanent Set After First Loading (%)	Fracture Strain (%)	Ultimate Strength (psi)
5651-86-3A-106B	MLE(||)	1.20	1.38	0.030	0.255	2215
-107B		1.00	1.29	0.030	0.375	2825
-112B		1.06	1.20	0.020	0.365	2647
-113B		0.95	1.15	0.030	0.300	2339
-118B		1.125	1.20	0.017	0.305	2541
-119B		1.06	1.29	0.021	0.320	2545
-124B		0.90	1.00	0.025	0.325	2461
-125B		0.82	1.125	0.040	0.370	2604
-127B		0.90	1.125	0.030	0.315	2276
-128B		0.95	1.125	0.035	0.335	2524
3B-106B		1.125	1.20	0.007	0.285	2520
-107B		1.20	1.20	0.015	0.350	2805
-112B		1.06	1.20	0.020	0.310	2504
-113B		1.06	1.125	0.025	0.335	2524
-118B		0.90	1.29	0.020	0.240	2117
-119B		1.06	1.50	0.020	0.320	2620
-124B		0.90	1.20	0.035	0.400	2746
-125B		1.00	1.20	0.025	0.360	2782
-127B		1.06	1.29	0.025	0.350	2785
-128B		1.00	1.20	0.027	0.240	2114
Mean		1.02	1.21	0.025	0.323	2525
Std. Dev.		0.104	0.106	0.008	0.044	219
5651-86-3A-136B	MLE(⊥)	0.82	1.125	0.030	0.335	2271
-137B		0.86	1.06	0.035	0.345	2256
-142B		0.78	1.08	0.050	0.395	2343
-143B		0.90	1.00	0.020	0.245	1648
-148B		0.86	1.00	0.037	0.310	2073
-149B		0.90	1.08	0.030	0.305	2132
-154B		0.72	0.82	0.025	0.295	1560
-155B		0.86	1.06	0.030	0.260	1865
-160A		0.78	0.86	0.025	0.295	1732
-160B		0.90	1.06	0.032	0.295	2138
3B-136B		0.86	1.00	0.025	0.335	2313
-137B		0.82	1.00	0.030	0.370	2099
-142B		1.00	1.125	0.030	0.320	2439
-143B		1.00	1.125	0.020	0.240	2012
-148B		0.72	0.82	0.040	0.450	2285
-149B		0.75	0.86	0.025	0.345	2040
-154B		0.95	1.06	0.015	0.300	2339
-155B		0.86	1.06	0.030	0.340	2234
-160A		0.95	1.125	0.020	0.260	2091
-160B		0.95	1.20	0.015	0.340	2293
Mean		0.86	1.03	0.028	0.319	2108
Std. Dev.		0.084	0.108	0.008	0.051	243

[a]MLC = midlength center, MLE = midlength edge.

TABLE 11-3
THERMAL EXPANSIVITY OF TS-1240 GRAPHITE
(Log 5651-73, density = 1.79 g/cm^3)

Specimen No.	Orientation	Location in Log	Mean Coefficient of Thermal Expansion,[a] $\alpha \times 10^6$ °C^{-1} (22°-500°C)
5651-73-3A-001B	Parallel	Midlength Center	4.17 (4.04)
-002B			4.22
-010B			4.20
-011B			4.46 (4.18)
-3B-001B			3.97 (4.22)
-002B			4.09
-010B			4.67
-011B			4.29 (3.99)
Mean			4.26
Std. Dev.			0.22
5651-73-3A-031B	Perpendicular	Midlength Center	4.81 (4.39)
-032B			4.81
-040B			4.96
-041B			4.89 (4.55)
3B-031B			4.85 (4.54)
-032B			4.64
-0408			4.86
-041B			4.89 (4.57)
Mean			4.84
Std. Dev.			0.09
5651-73-3A-101B	Parallel	Midlength Edge	4.29 (4.12)
-102B			4.61
-111A			3.86
-111B			4.04 (4.08)
-110B			4.51
3B-101A			4.05
-101B			4.15 (4.02)
-111A			4.27
-111B			4.25
-102B			4.63
-110B			4.45
Mean			4.28
Std. Dev.			0.25
5651-3A-131A	Perpendicular	Midlength Edge	4.28
131B			4.78 (4.57)
141A			4.56
141B			4.86 (4.45)
132B			4.70
140B			5.15
3B-131A			4.53
131B			4.83 (4.54)
141A			4.81
141B			4.70 (4.41)
132B			4.80
140B			4.78
Mean			4.73
Std. Dev.			0.21

[a] Numbers in parentheses are values for repeat measurements.

TABLE 11-4
THERMAL EXPANSIVITY OF TS-1240 GRAPHITE
(Log 5651-74, density = 1.79 g/cm^3)

Specimen No.	Orientation	Location in Log	Mean Coefficient of Thermal Expansion, $\alpha \times 10^6$ °C^{-1} (22°-500°C)
5651-74-1A-007A	Parallel	End Center	4.25
-007B	↓	↓	4.09
-010A			4.28
-010B			4.49
-1B-032A			4.25
-032B			4.55
-035A			4.25
-035B			4.15
Mean			4.29
Std. Dev.			0.16
5651-74-1A-063A	Perpendicular	End Center	4.45
-063B	↓	↓	4.52
-066A			4.75
-066B			4.75
-1B-073A			4.56
-073B			4.67
-076A			4.71
-076B			4.71
Mean			4.63
Std. Dev.			0.11
5651-74-1A-052A	Parallel	End Edge	4.45
-052B	↓	↓	4.68
-054A			4.23
-054B			4.16
-1B-057A			4.20
-057B			4.17
-059A			4.20
-059B			4.16
Mean			4.28
Std. Dev.			0.19
5651-74-1A-081A	Perpendicular	End Edge	4.75
-081B	↓	↓	4.86
-083A			4.94
-083B			4.65
-1B-085A			4.83
-085B			4.85
-087A			5.01
-087B			4.83
Mean			4.84
Std. Dev.			0.11

TABLE 11-4 (Continued)

Specimen No.	Orientation	Location in Log	Mean Coefficient of Thermal Expansion, $\alpha \times 10^6$ °C^{-1} (22°-500°C)
5651-74-3A-107A	Parallel	Midlength Center	4.38
-107B	↓	↓	4.22
-110A			4.39
-110B			4.27
3B-132A			4.33
-132B			4.33
-135A			4.31
-135B			4.41
Mean			4.33
Std. Dev.			0.06
5651-74-3A-163A	Perpendicular	Midlength Center	4.79
-163B	↓	↓	4.61
-166A			4.70
-166B			4.51
-3B-173A			4.16
-173B			4.59
-176A			4.60
-176B			4.57
Mean			4.57
Std. Dev.			0.18
5651-74-3A-152A	Parallel	Midlength Edge	4.33
-152B	↓	↓	4.27
-154A			4.28
-154B			4.13
-3B-157A			4.22
-157B			4.27
-159A			4.34
-159B			4.24
Mean			4.26
Std. Dev.			0.07
5651-74-3A-181A	Perpendicular	Midlength Edge	4.66
-181B	↓	↓	4.71
-183A			4.75
-183B			4.74
3B-185A			4.52
-185B			4.68
-187A			4.41
-187B			4.52
Mean			4.62
Std. Dev.			0.12

TABLE 11-5
THERMAL EXPANSIVITY OF H-451 GRAPHITE
(Log 5651-86, density = 1.74 g/cm^3)

Specimen No.	Orientation	Location in Log	Mean Coefficient of Thermal Expansion,(a) $\alpha \times 10^6$ °C^{-1} (22°-500°C)
5651-86-3A-001B	Parallel	Midlength Center	4.00 (4.36)
-002B			4.35 (4.26)
-010B			4.41
-011B			4.14
-3B-001B			4.08 (4.44)
-002B			4.27 (4.35)
-010B			4.04
-011B			4.16
Mean			4.18
Std. Dev.			0.15
5651-86-3A-031B	Perpendicular	Midlength Center	4.53 (4.73)
-032B			4.81 (4.77)
-040B			4.62
-041B			4.82
-3B-031B			4.37 (4.66)
-032B			4.47 (4.44)
-040B			4.72
-041B			4.64
-031A			4.83
-041A			4.46
Mean			4.63
Std. Dev.			0.17
5651-86-3A-101B	Parallel	Midlength Edge	4.20 (4.39)
-102B			4.36
-110B			4.21
-111B			4.11 (4.19)
-3B-101A			4.10
-101B			4.11 (4.31)
-111A			4.10
-111B			4.05 (4.31)
-102B			4.34
-110B			4.28
Mean			4.19
Std. Dev.			0.11
5651-86-3A-131A	Perpendicular	Midlength Edge	4.62
-131B			4.16 (4.40)
-141A			4.80
-141B			4.35 (4.64)
-132B			4.66
-140B			4.62
3B-131A			4.84
-131B			4.65 (4.77)
-141A			4.69
-141B			4.27 (4.40)
-132B			4.72
-140B			4.43
Mean			4.57
Std. Dev.			0.21

(a) Numbers in parentheses are values for repeat measurements.

TABLE 11-6
THERMAL CONDUCTIVITY OF H-451 GRAPHITE
(Log 5651-86, density = 1.74 gm/cm^3)

Specimen Number	Orientation	Location in Log	Thermal Conductivity (cal/cm-sec-°C)				
			22°C	200°C	400°C	600°C	800°C
5651-86-3A-L1M	Parallel	Midlength	0.288	0.273	0.242	0.196	0.177
-L1N	↓	Center	0.252	0.245	0.218	0.183	0.141
-L1O	↓	↓	0.242	0.238	0.205	0.176	0.150
-L1P	↓	↓	0.244	0.236	0.203	0.174	0.155
-L1Q	↓	↓	0.253	0.235	0.203	0.174	0.155
-L1R	↓	↓	0.253	0.219	0.182	0.163	0.144
-L1S	↓	↓	0.242	0.215	0.195	0.173	0.147
-L1T	↓	↓	0.248	0.246	0.209	0.173	0.151
Mean	↓	↓	0.253	0.238	0.207	0.176	0.152
Std. Dev.	↓	↓	0.015	0.018	0.017	0.010	0.011
5651-86-3A-L8A	Perpendicular	Midlength	0.249	0.221	0.188	0.160	0.145
-L8B	↓	Center	0.253	0.216	0.190	0.156	0.133
-L8C	↓	↓	0.242	0.234	0.201	0.173	0.144
-L8D	↓	↓	0.253	0.233	0.203	0.169	0.148
-L8E	↓	↓	0.266	0.236	0.210	0.178	0.152
-L8F	↓	↓	0.247	0.233	0.199	0.166	0.150
-L8G	↓	↓	0.251	0.228	0.192	0.166	0.147
-L8H	↓	↓	0.248	0.224	0.189	0.164	0.141
Mean	↓	↓	0.251	0.228	0.196	0.166	0.145
Std. Dev.	↓	↓	0.007	0.007	0.008	0.007	0.006

Patterns of property variations within individual logs and from log to log are starting to develop. This subject will be addressed in the next quarterly report.

GRAPHITE IRRADIATIONS

Capsule OG-2

Capsule OG-2 operated according to design for the final irradiation period. A minor gas leak in the crucible containment of cell 1 was detected on December 3, 1974, but design temperatures could still be maintained and no corrective action was needed. The capsule was removed from the Oak Ridge Reactor (ORR) at the end of cycle 122 on January 8, 1975. The capsule was disassembled in the GA hot cell, and the dosimeter wires and graphite sample crucibles were recovered without incident. The cause of the gas leak in cell 1 was determined to be a hairline crack originating at an end-cap weld.

The dosimeter wires have been transferred to the radiochemical laboratory and the graphite sample crucibles have been transferred to the graphite laboratory for physical property measurements. Dimensional changes will be measured on all cylindrical samples. The thermal diffusivity of 87 disc samples encapsulated in crucibles 1, 5, and 7 will be measured by the heat-pulse method. Ninety-eight cylindrical samples from a total of seven crucibles will be measured for thermal expansivity. Destructive tensile tests will be performed on a total of 120 samples of H-451, H-327, and TS-1240 graphites, and 216 tensile samples will be re-encapsulated in capsule OG-3 for further irradiation.

Capsule OG-3

An irradiation test plan for the OG-3 capsule irradiation (TP-325-004) was written and has received Approval in Principle from RRD. The capsule will be similar in design to capsule OG-2, with the exception of minor

changes in the sample holes in the graphite crucibles and the addition of two thermocouples. The design temperatures and fluences will be identical to those of capsule OG-2. The following samples will be included:

H-451 graphite:	102 dimensional change and CTE samples from OG-1 and OG-2
	24 thermal diffisivity samples from OG-1 and OG-2
	21 fatigue samples from OG-1 and OG-2
	34 tensile samples from OG-1 and OG-2
	96 tensile samples from OG-2
	36 virgin dimensional change and CTE samples
	24 virgin thermal diffusivity samples
	102 virgin tensile samples
H-429 graphite:	24 dimensional change and CTE samples from GEH-13-422, OG-1, and OG-2
TS-1240 graphite:	52 tensile samples from OG-2
	24 thermal diffusivity samples from OG-2
	126 virgin tensile samples
	16 virgin dimensional change and CTE samples
H-327 graphite:	42 dimensional change and CTE samples from OG-1 and OG-2
	10 tensile samples from OG-1 and OG-2
	26 tensile samples from OG-2
P_3JHAN graphite:	30 dimensional change samples from OG-1 and Og-2
P_3JHA_2N graphite:	22 virgin dimensional change samples
AS2-I-500 graphite:	22 virgin dimensional change samples

SO-818 graphite:	16 virgin dimensional change samples
	18 virgin thermal diffusivity samples
2020 graphite:	100 small dimensional change samples from OG-1 and OG-2
Boronated graphite:	16 dimensional change samples from OG-1 and OG-2
	8 dimensional change samples from OG-2
Glassy carbon:	18 small crucibles of miscellaneous samples
Pyrocarbon:	12 crucibles of miscellaneous samples
Matrix carbon:	1 thermal conductivity rod
	10 thermal diffusivity discs

The schedule for capsule OG-3 calls for sample loading on March 28, assembly complete by May 13, and insertion in the ORR on June 15.

Capsule OG-4

It is anticipated that the graphite irradiation program will be accelerated in FY-76 by the addition of a second capsule series which will use the same irradiation facility and "leap frog" the current capsules. The next OG capsule, OG-4, will therefore be loaded with all virgin samples and will be shipped to ORNL in time to replace capsule OG-3 in the C-3 test position when OG-3 is removed in December 1975.

In order to provide better coverage of the lower temperature in an HTGR, the thermal design of capsule OG-4 and subsequent even-numbered capsules will be modified. The odd-numbered capsules will continue to duplicate the thermal design of capsules OG-1 through OG-3. The modified thermal design for the even-numbered capsules will have as its goal the centerline temperatures given in Table 11-7.

TABLE 11-7
CENTERLINE TEMPERATURES FOR EVEN-NUMBERED CAPSULES

Cell Number	Crucible Number	Design Centerline Temperature (°C)
1	1	700
1	2	800
1	3	900 (control)
2	4	1100
2	5	1200
2	6	1000
2	7	900 (control)
2	8	600
2	9	500
2	10	400

GRAPHITE STANDARD

A revised draft of the proposed RDT standard E6-1 "Near-Isotropic Petroleum-Coke-Based Graphites for High-Temperature Gas-Cooled Reactor Core Components," has been written and released for review by the major carbon companies and RRD. The revised draft includes comments given by the major carbon companies during an August 1974 meeting with RRD personnel. The revised draft will be sent to RRD for approval in March 1975.

REFERENCES

11-1. "HTGR Base Program Quarterly Progress Report for the Period Ending February 28, 1974," USAEC Report GA-A12916, General Atomic Company, March 29, 1974.

11-2. "HTGR Base Program Quarterly Progress Report for the Period Ending May 31, 1974," USAEC Report GA-A13030, General Atomic Company, June 28, 1974.

11-3. "HTGR Fuels and Core Development Program Quarterly Progress Report for the Period Ending August 30, 1974," USAEC Report GA-A13126, General Atomic Company, September 30, 1974.

11-4. Engle, G. B., R. J. Price, W. R. Johnson, and L. A. Beavan, "Development Status of Near-Isotropic Graphites for Large HTGRs," USAEC Report GA-A12944, General Atomic Company, June 1, 1974.

11-5. "HTGR Fuels and Core Development Program Quarterly Progress Report for the Period Ending November 30, 1974," USAEC Report GA-A13253, General Atomic Company, January 31, 1975.

APPENDIX

PROJECT REPORTS PUBLISHED DURING THE QUARTER

Smith, P. D., "An Approximate Closed Form Solution to the Fission Product Diffusion Equation in One-Dimensional Slab Geometry," USAEC Report GA-A13196, November 1, 1974.

Myers, B. F., and W. E. Bell, "Strontium Transport Data for HTGR Systems," USAEC Report GA-A13168 (GA-LTR-16), December 6, 1974.